

Elucidating Water Sources and Interaction with Hydrogeologic Systems: Enthalpy,  
Radon, and Rare Earth Elements as Naturally Occurring Tracers

A Dissertation

Presented in Partial Fulfillment of the Requirements for the

Degree of Doctorate of Philosophy

with a

Major in Geology

in the

College of Graduate Studies

University of Idaho

by

Travis Lynn McLing

Major Professor: Robert W. Smith, Ph.D.

Scott A. Wood, Ph.D.; Dennis J. Geist, Ph.D.; Karen S. Humes, Ph.D.

Department Administrator: Leslie L. Baker, Ph.D.

August 2017

**Authorization to Submit Dissertation**

This dissertation of Travis Lynn McLing, submitted for the degree of Doctorate of Philosophy with a Major in Geology and titled “Elucidating Water Sources and Interaction with Hydrogeologic Systems: Enthalpy, Radon, and Rare Earth Elements as Naturally Occurring Tracers,” has been reviewed in final form. Permission, as indicated by the signatures and dates below, is now granted to submit final copies to the College of Graduate Studies for approval.

Major Professor: \_\_\_\_\_ Date: \_\_\_\_\_  
Robert W. Smith, Ph.D.

Committee Members: \_\_\_\_\_ Date: \_\_\_\_\_  
Scott A. Wood, Ph.D.

\_\_\_\_\_ Date: \_\_\_\_\_  
Dennis J. Geist, Ph.D.

\_\_\_\_\_ Date: \_\_\_\_\_  
Karen S. Humes, Ph.D.

Department Administrator: \_\_\_\_\_ Date: \_\_\_\_\_  
Leslie L. Baker, Ph.D.

## Abstract

Presented are three studies that utilize three natural tracers (enthalpy, radon gas, and rare earth elements) to characterize hydrologic systems at three different scales. The scale of investigation ranges from 27,900 km<sup>2</sup> for the Eastern Snake River Plain (ESRP) regional aquifer to 0.34 km<sup>2</sup> for Shepley's Hill in West Central Massachusetts. In the first study, we use aquifer temperature and wellbore temperature profiles from the ESRP in an integrated effort to trace regional groundwater flow and aquifer thickness and identify zones of elevated geothermal potential under the ESRP. Understanding the hydrologic conditions of the ESRP aquifer is important to the residents of Eastern Idaho, as it is a soul source aquifer for the region. In our second application of natural tracers, we utilize <sup>222</sup>Rn to detect fluid-flow pathways in a fractured-rock-hosted vadose zone at Fort Devens, Massachusetts. The vadose zone is believed to be the source of meteoric water infiltrating a contaminated aquifer that underlies a contaminated landfill. Understanding the source of the meteoric water that flows into the contaminated aquifer is an important part of remediation of the contaminated site. Finally, we investigate and test procedures to preconcentrate trace rare earth elements (REEs) to improve detection by inductively coupled plasma mass spectrometry (ICP-MS) and apply these techniques to characterize a leaking CO<sub>2</sub> system in Soda Springs, Idaho. Here, we use groundwater REE chemistry as a tracer to track CO<sub>2</sub>-charged waters at a natural carbon capture and storage (CCS) analogue site. At this site, naturally leaking CO<sub>2</sub> and associated brines from depth are migrating into a shallow aquifer. These studies conducted at widely varying scales and using different tracers demonstrate the usefulness of natural tracers to elucidate conditions in the subsurface that cannot be directly measured by anthropogenic tracers.

## **Acknowledgements**

Earning an advanced degree is a culmination of efforts from the student, the academic institution, and the sponsor of research. All three of these have played a large role in completing this Ph.D. dissertation. First and most importantly, I would like to acknowledge Dr. Bob Smith, who for over 25 years has been a patient source of academic and scientific mentoring. Without his efforts, this degree would not be possible. Bob's contribution to this work cannot be overstated and is greatly appreciated. I also acknowledge my Ph.D. committee and co-authors for the significant and important contributions they made to these combined works.

This work was supported by a combination of funding organizations. Chapter 1, "Wellbore and Groundwater Temperature Distribution Eastern Snake River Plain, Idaho: Implications for Groundwater Flow and Geothermal Potential," was funded by an LDRD award from the Idaho National Laboratory. Chapter 2, "The Application of Radon for Mapping Open Fracture Networks in a Thin Vadose Zone Underlain by Granite Rock, Fort Devens, Massachusetts," was funded by the United States Environmental Protection Agency (contract WFO 14815). Chapters 3 and 4 were funded by grants from the United States Department of Energy through the Big Sky Carbon Sequestration Partnership (contract FWP 1210) and Royal Dutch Shell Exploration Technologies (contract CCN #216849). In addition, the Idaho National Laboratory's Energy & Environment Science and Technology Directorate provided funds to cover travel and editing of the final dissertation.

### **Dedication**

My parents raised me to believe that I was capable of accomplishing anything I put my mind to, even when there was significant evidence to the contrary. They instilled in me a belief in the theater of the possible with regard to my career and personal life. I want to dedicate this dissertation to my wife, Alane, who for more than 30 years has been the most influential person in my life. Laney, thank you for your patience, love, and support throughout this long process, I will forever be grateful. I also want to thank my children—Kylie, Alex, and Mallory—for believing in their dad.

I am grateful for the fine women you have become.

## Table of Contents

Authorization to Submit Dissertation .....	ii
Abstract.....	iii
Acknowledgements.....	iv
Dedication.....	v
Table of Contents.....	vi
List of Figures.....	viii
List of Tables .....	xi
Introduction.....	1
<b>CHAPTER 1: Wellbore and Groundwater Temperature Distribution Eastern Snake River Plain, Idaho: Implications for Groundwater Flow and Geothermal Potential .....</b>	<b>4</b>
Abstract .....	4
1.1 Introduction.....	5
1.2 Background.....	7
1.3 Methods .....	11
1.4 Temperature Profiles in Deep Wells Implications for Aquifer Geometry .....	11
1.5 Aquifer Temperature Distribution .....	15
1.6 Vertical Aquifer Temperature Distribution.....	16
1.7 Horizontal Temperature Distribution: Implications for Groundwater Flow.....	18
1.8 Comparison to Flow Regime Indicated by Groundwater Chemistry and Equilibration of Natural Isotopes.....	20
1.9 Geothermal Implications.....	22
1.10 Summary .....	23
Acknowledgments .....	24
References .....	24
<b>CHAPTER 2: The Application of Radon for Mapping Open Fracture Networks in a Thin Vadose Zone Underlain by Granite Rock, Fort Devens, Massachusetts.....</b>	<b>29</b>
Abstract .....	29
2.1 Introduction.....	30
2.2 Materials and Methods.....	37
2.3 Results and Discussion .....	42
2.4 Summary .....	47
Acknowledgements .....	48
References .....	48

CHAPTER 3: Utilizing Rare Earth Elements as Tracers in High TDS Reservoir Brines in CCS	
Applications .....	53
Abstract .....	53
3.1 Introduction.....	55
3.2 Methods .....	56
3.3 Results.....	59
3.4 Summary .....	65
Acknowledgements .....	65
References .....	66
CHAPTER 4: The Use of Rare Earth Elements as Natural Tracers to Characterize a Leaky CO <sub>2</sub> CCS Natural Analogue Site, Soda Springs, Idaho.....	68
Abstract .....	68
4.1 Introduction.....	69
4.2 Methods .....	76
4.3 Results.....	81
4.4 Discussion.....	92
4.5 Implications for CCS .....	103
References .....	104
Conclusion .....	114
APPENDIX A: Title .....	117

## List of Figures

Figure 1.1: Map of ESRP aquifer, showing hydraulic head contours, groundwater flow direction, and aquifer temperature distribution across the study area. Groundwater flow-direction arrows account for thermal plume shape (elongated in the direction of flow), including cold plumes originating in tributary valleys and apparent hotspot plumes near the centerline of the aquifer. ....	6
Figure 1.2: Vertical temperature profiles from nine deep boreholes analyzed in this study. For clarity, the temperature profiles from the nine deep boreholes are shown on two graphs. ....	10
Figure 1.3: Contours of aquifer thickness on INL based on nine deep wells for which temperature logs are available. ....	14
Figure 1.4: Aquifer temperature at water table for the ESRP within and near INL. ....	14
Figure 1.5: Simplified and idealized longitudinal section (not to scale) of Eastern Snake River Plain aquifer from its source in the Yellowstone area to its discharge in the Thousand Springs area, modified after Smith (2004). Approximate line of section is shown in Figure 1.1. ....	16
Figure 1.6: Detailed north-to-south cross-section showing aquifer temperature distribution beneath INL. Lightly shaded zones are sediment interbed layers within the basalt sequence. ....	18
Figure 1.7: Flow pathways deduced from uranium data. High ratios characteristic of mountain recharge source regions extend far into the aquifer in preferential flow zones. Low isotope ratios characterize surface recharge areas (after Roback et al. 2001). Note comparison of these flow pathways to those deduced from temperature data (Figure 1.1). ....	21
Figure 2.1: The study area is comprised of a highly fractured granite highland known as Shepley's Hill and is located immediately west of the Fort Devens Landfill. Shepley's Hill is a known recharge area for the aquifer recharging the Fort Devens Landfill. ....	33
Figure 2.2: The location of the major DGFZ and NSFZ and the contact between the Chelmsford and Ayer granites relative to the transects used to collect radon in this study. ....	34
Figure 2.3: The stylized relationship between an active fracture emitting radon and a detection network that can measure the emanation at the soil-bedrock interface. Areas of high radon emanation are associated with open or active flow pathways in the bedrock. ....	36
Figure 2.4: How the Rapidly Deployable CR-39 Measurement Port (RDMP) is installed in the soil column and its position relative to the soil-bedrock interface. ....	38
Figure 2.5: Plot of <sup>222</sup> Rn data from Transect B showing the relationship between concentration and proximity to the DGFZ, NSFZ, and the non-fracture zones. ....	40



- Figure 3.1: Results from test of the high-TDS Chelex resin extraction of REEs. The black trend shows the results of the chromatography of a 5-ppb REE solution using reagent grade salts. A clear contamination of the sample in LREE, especially La, is obvious. The red trend line shows the results of the same experiment after running the synthetic brine solution, through the extraction column, prior to spiking with REE. .... 61
- Figure 3.2: Graphs of ICP-MS-measured REE concentrations from water samples taken from Soda Springs, Idaho, normalized to chondrite composite (Wakita et al. 1971). The data show characteristic high-LREE, chondrite-normalized concentration and generally a slightly positive slope from Eu to Lu. .... 63
- Figure 3.3: Graphs of ICP-MS measured chondrite-normalized REE concentrations from water samples taken from Madison and Weber formations at the Rock Springs Uplift (Wakita et al. 1971). Both these brines exhibit prominent Gd spikes and enrichments in LREE and HREE. .... 64
- Figure 4.1: Map of major geologic and hydrologic features of the Blackfoot Valley and Sulphur Canyon. Also shown are the sample locations for this study. Most of the CO<sub>2</sub>-charged springs and wells are located on the southeast side of Blackfoot Valley and along the shores of Alexander Reservoir, which impounds water from the Bear River. .... 73
- Figure 4.2: Regional cross-section of the southern Blackfoot Valley E-E.' (Figure 4.1) (Link 1996; Lewis et al. 2012). Used with permission from the Idaho Geologic Survey. .... 74
- Figure 4.3: Photo of highly mineralized basalt collected from the subsurface near Hooper Springs. The heavily mineralized basalt is characteristic of basalt chips from wells drilled into the subsurface in the Southern Blackfoot Valley. The orange mineralization is hydrous ferric oxide (HFO), which commonly co-precipitates with calcite at springs and wells. .... 75
- Figure 4.4: Photographs of nine of the sample locations. The Geyser Well located in the center photograph is the most prominent feature in the area. This well erupts CO<sub>2</sub>-charged water more than 30 meters above ground level every hour. Note the greenish hue in the water at Sulphur Springs in the upper left photograph. This color is due to the precipitation of elemental sulfur in the highly CO<sub>2</sub> and H<sub>2</sub>S water. The ubiquitous iron staining is common at all locations where CO<sub>2</sub> is bubbling to the surface. .... 85
- Figure 4.5: Piper diagram (Piper 1944) of Blackfoot Valley region water chemistry. Type I waters are shown as filled black circles, Type II waters are shown as filled blue squares, Type III waters are shown as filled red stars, and Type IV waters are shown as filled green triangles. The three Type III water samples shown are all from Sulphur Springs at different times of the year. Water chemistry ranges from Ca-Mg-HCO<sub>3</sub>-dominated for most locations to Ca-SO<sub>4</sub>-dominated at Sulphur Springs. .... 87
- Figure 4.6: REE trends for Type I water, Paleozoic Limestone (Madhavaraju and González-León 2012), and brine from Madison Formation at the Rock Springs Uplift. .... 88
- Figure 4.7: REE trends for Type II waters analyzed for this study. .... 90

Figure 4.8: REE trends plotted for Type III water (Sulphur Springs) and brine from Madison Formation at the Rock Springs Uplift (McLing et al 2012).....	91
Figure 4.9: REE data trends for Type IV water, REE data from the ESRP aquifer (Nelson 2005), and travertine from the Blackfoot Valley. ....	92
Figure 4.10: Simplified hydrogeological conceptual model for the Southern Blackfoot Valley, showing the stylized relationship between the four water types, host rock, and the deep thermal source that drives the CO <sub>2</sub> system. Note the basalt aquitard that has been formed over time by the precipitation of calcite that fills conductive structure in the rock.....	93
Figure 4.11: Location of samples collected to evaluate water chemistry changes along the flow path from the Geyser Well to the spreading area 350 m downstream. The inset figure shows the concentration drop in dissolved REE from sample location SG0 (at the Geyser Well) downstream to SG6. ....	96
Figure 4.12: The top figure shows the changes in major element concentration for Soda Geyser outflow study. (Note the increase in Na <sup>+</sup> and decrease in Ca <sup>2+</sup> .) The bottom figure shows the changes in chondrite-normalized REE trends and concentration relative to distance from the Soda Geyser Well. ....	97

## List of Tables

Table 1.1: Aquifer thickness calculated from temperature logs collected in deep wells drilled into the ESRP.....	13
Table 2.1: The data at Fort Devens show a wide range of $^{222}\text{Rn}$ concentrations, ranging from a low of 6.6 pCi/L in Transect B to a maximum (valid) of 163 pCi/L in Transect A. 167 pCi/L is the maximum concentration that can be measured by a CR-39. Values of 167 pCi/L should be considered the minimum value measured at the location. Normalized mean = concentration measure value/pCi/L/6.6 (lowest measured value). .....	41
Table 2.2: Values for data grouping used for statistical analysis.....	45
Table 4.1: Heuristics used for water classification in this study. Three of the water types (Types I, II, and III) are waters that effuse $\text{CO}_2$ . Only Type I water is warm and is actively precipitating travertine.....	82
Table 4.2: Presented here are data from the 45 samples collected and analyzed for this study, including location, temperature, major element data, TDS, and calcite saturation index.....	83
Table 4.3: Rare earth element data for the 12 samples analyzed in this study. Also included are calculated $(\text{Eu}/\text{Eu}^*)_{\text{cn}}$ , $(\text{Ce}/\text{Ce}^*)_{\text{cn}}$ , and trend lines for data from La to Lu.).....	84

## Introduction

In approximately AD 80, the historian Josephus Flavius describes what may be the first attempt at a tracers test in a geologic system. In *The Jewish War*, his account describes an attempt by Philip the Tetrarch of Trachonitis to identify the source of the Banias Spring at Panium, a major source of the Jordan River in the Golan Heights, by throwing chaff into Phiala (Lake Ram) (Flavius 1980). Lake Ram was at the time assumed to be the source of the spring through ground leakage. In Josephus' account, Philip observed chaff flowing out of Paninto (Banias Spring), thereby confirming the source of its water as Lake Ram. While it is unlikely that chaff could be transported through the porous media that lies between the lake and the spring, the concept of a tracer test proposed by Philip remains valid to the current day. Nearly 1,900 years later, Mazor (1976) demonstrated used hydrogen and oxygen isotopes date to refute Philip's conclusion. Interestingly, the conclusion made by Philip around AD 80 stood for about 1,900 years, until a more effective tracer study was conducted in modern times. The story of Philip and his attempt at a tracer test is evidence of the persistent human need to identify the source and transport of water resources. The need to track the flow of geofluids in subsurface environments is even more pressing today than it was in the days of Philip.

There is a long history of utilizing tracers to elucidate subsurface conditions in subsurface environments, and a detailed discussion is beyond the scope of this dissertation. Tracers are used to characterize the subsurface and fall into two broad categories: anthropogenic (i.e., tracers that are introduced into the system) and environmental (i.e., tracers that are naturally occurring in the system). Anthropogenic tracers may be dyes (e.g., rhodamine, fluorescein), soluble salts (conservative or reactive), or manufactured chemicals (e.g., fluorocarbons, sulfur hexafluoride, difurobenzoic acid), all of which can be detected at extremely low concentrations. Environmental tracers have traditionally been used less frequently but are becoming more common and are exceedingly powerful tools in elucidating subsurface conditions, especially at large-scale, such as the reservoir or aquifer scale. Some examples of commonly used environmental tracers are stable isotopes (e.g.,  $\delta^{18}\text{O}$ ,  $\delta\text{H}$ ,  $\delta^{34}\text{S}$ ,  $^{36}\text{Cl}$ ), radiogenic isotopes (e.g.,  $^{234/238}\text{U}$ ,  $^{222}\text{Rn}$ ,  $^{87/86}\text{Sr}$ ), temperature, and noble gases (e.g., He, Ar, Kr).

Presented in this volume are three studies that utilize three natural tracers (enthalpy, radon gas, and rare earth elements) to characterize three systems at very different scales. The scale of the systems varies significantly, with two studies in Southeastern Idaho—the 27,900-km<sup>2</sup> Eastern Snake River Plain regional aquifer (ESRP) and the 65-km<sup>2</sup> Southern Blackfoot Valley—and finally the 0.34-km<sup>2</sup> Shepley's Hill in West Central Massachusetts. A fourth method's development study associated with the Blackfoot Valley project is also presented.

## **Chapter 1: Wellbore and Groundwater Temperature Distribution Eastern Snake River Plain, Idaho: Implications for Groundwater Flow and Geothermal Potential**

This study uses aquifer temperature and wellbore temperature profiles from the Eastern Snake River Plain (ESRP) to trace regional groundwater flow and aquifer thickness and identify zones of elevated geothermal potential under the plain. At the regional scale, large connected zones of relatively cooler water in the aquifer correlates with the large-scale preferential flow corridors previously identified. In contrast, regions where water temperature is warmer generally correlate with the slower flow regions, providing support for the conclusion that in areas where water temperature is higher, groundwater flow is slow enough that the thermal gradient of the ESRP overwhelms flow velocity.

## **Chapter 2: The Application of Radon for Mapping Open Fracture Networks in a Thin Vadose Zone Underlain by Granite Rock, Fort Devens, Massachusetts**

This study uses  $^{222}\text{Rn}$  to detect pathways in fractured rock that conduct meteoric water from the surface into an underlying contaminated aquifer at Shepley's Hill site, located at Fort Devens, Massachusetts. We used standard CR-39-particle track  $^{222}\text{Rn}$  detectors with a specially designed sample deployment portal to measure the  $^{222}\text{Rn}$  at or near the bedrock soil contact. The results of this study offer a promising method for accurately locating zones of interconnected permeability in fractured vadose zones.

## **Chapter 3: Utilizing Rare Earth Elements as Tracers in High TDS Reservoir Brines in CCS Applications**

This chapter describes an improved method for preconcentrating trace rare earth elements (REEs) to improve detection by inductively coupled plasma mass spectrometry (ICP-MS). Trace elements, particularly REEs, can serve as natural tracers for monitoring in situ geochemical conditions and the migration of  $\text{CO}_2$ -charged brines in geologic carbon capture and storage (CCS). Here, we apply REEs to characterize geofluids at CCS analogue sites in Soda Springs, Idaho, and at a proposed CCS reservoir at the Rock Springs Uplift, Wyoming. In this study, we evaluate and modify established procedures that preconcentrate trace metals, including REEs, up to 100 $\times$  while eliminating interfering ions (e.g., Ba, Cl). The processes are straightforward and inexpensive and require little infrastructure, using only a single chromatography column with inexpensive, reusable, commercially available resins and wash chemicals. The procedure has been tested with synthetic brines (215,000 ppm TDS) and field water samples (up to 5,000 ppm TDS). Testing has produced data of high quality with REE capture efficiency exceeding 95%, while reducing interfering elements by >99%. Results have been encouraging and show that REEs may be effective tracers in CCS systems and overlying aquifers.

## **Chapter 4: The Use of Rare Earth Elements as Natural Tracers to Characterize a Leaky CO<sub>2</sub> CCS Natural Analogue Site, Soda Springs, Idaho**

The study uses groundwater REE chemistry tracers to track CO<sub>2</sub>-charged waters at a location near Soda Springs in Caribou County, Idaho. Here, we utilize a naturally leaking CO<sub>2</sub> system located at Soda Springs, Idaho, as a natural analogue site for CCS deployment. Analogue sites are particularly relevant and useful to the study of geologic CO<sub>2</sub> sequestration because they offer the chance to examine a geologic system on a time scale that laboratory and field experimentation cannot. At Soda Springs, a CO<sub>2</sub> formation fluid generated by the dissolution of Paleozoic carbonates and shale at-depth is migrating into the shallow subsurface, where it interacts with shallow groundwater. The vertically rising waters also degas significant amounts of CO<sub>2</sub>, which causes calcite to precipitate in the capping basalt, sealing much of the permeability.

### **References**

- Flavius, Josephus, 1980, *The Jewish War*, Israel: Steimatzky, p. 382.
- Mazor, R., 1976, "The Ram Crater Lake: A Note on the Revival of a 2000-Year-Old Groundwater Tracing Experiment," *Interpretation of Environmental Isotope and Hydrochemical Data in Groundwater Hydrology*, Vienna, Austria: International Atomic Energy Agency, pp. 179–181.

## CHAPTER 1: Wellbore and Groundwater Temperature Distribution Eastern Snake River Plain, Idaho: Implications for Groundwater Flow and Geothermal Potential

“Wellbore and Groundwater Temperature Distribution Eastern Snake River Plain, Idaho: Implications for Groundwater Flow and Geothermal Potential,” *Journal of Volcanology and Geothermal Research*, Vol. 320, June 2016, pp. 114–155.

Travis L. McLing,<sup>a,b,\*</sup> Richard P. Smith,<sup>c</sup> Robert W. Smith,<sup>d</sup> David D. Blackwell,<sup>d</sup> Robert C. Roback,<sup>f</sup> and Andrus J. Sondrup<sup>a</sup>

<sup>a</sup> Idaho National Laboratory, P.O. Box 1625, Idaho Falls, ID 83415-2107, USA

<sup>b</sup> The Center for Advanced Energy Studies, 995 University Blvd., Idaho Falls, ID 83401, USA

<sup>c</sup> Smith Geologic and Photographic Services, LLC, Nathrop, CO 81236, USA

<sup>d</sup> University of Idaho, Moscow, ID 83844, USA

<sup>e</sup> Department of Geological Sciences, Southern Methodist University, Dallas, TX 75275-0395, USA

<sup>f</sup> Earth and Environmental Sciences Division, Los Alamos National Laboratory, Los Alamos, NM 87545, USA

\* Corresponding author: Travis L. McLing; E-mail: [travis.mcling@inl.gov](mailto:travis.mcling@inl.gov); Telephone: 012085267269; Fax: 012085260875

### Abstract

A map of groundwater temperatures from the Eastern Snake River Plain (ESRP) regional aquifer can be used to identify and interpret important features of the aquifer, including aquifer flow direction, aquifer thickness, and potential geothermal anomalies. The ESRP is an area of high heat flow, yet most of this thermal energy fails to reach the surface due to the heat being swept downgradient by the aquifer to the major spring complexes near Thousand Springs, Idaho—a distance of 300 km. Nine deep boreholes that fully penetrate the regional aquifer display three common features: (1) high thermal gradients beneath the aquifer, corresponding to high conductive-heat flow in low-permeability, hydrothermally altered rocks; (2) isothermal temperature profiles within the aquifer, characteristic of an actively flowing groundwater; and (3) moderate thermal gradients in the vadose zone with values that indicate that over half of the geothermal heat flow is removed by advective transport in the regional aquifer system. This study utilized temperature data from 250 ESRP aquifer wells to evaluate regional aquifer flow direction, aquifer thickness, and potential geothermal anomalies. Because the thermal gradients are typically low in the aquifer, any measurement of groundwater temperature is a reasonable estimate of temperature throughout the aquifer thickness, allowing the construction of a regional aquifer temperature map for the ESRP. Mapped temperatures

are used to identify cold thermal plumes associated with recharge from tributary valleys and adjacent uplands, and warm zones associated with geothermal input to the aquifer. Warm zones in the aquifer can have various causes, including: local circulation of groundwater through the deep, conductively dominated region; slow groundwater movement in low-permeability regions; or localized heat flow from deeper thermal features.

**Keywords:** Eastern Snake River Plain, thermal groundwater tracer, groundwater flow, temperature distribution

## 1.1 Introduction

Beneath the Eastern Snake River Plain (ESRP) in Idaho, United States of America, is the ESRP aquifer (Figure 1.1), one of the most productive and heavily used aquifers in the United States. Because of its association with tectonic and thermal features of the Yellowstone hotspot track (Whitehead 1986), the ESRP is recognized as the location for potential (and actual) geothermal resources. The ESRP was highlighted as one of six high-grade, enhanced geothermal system (EGS) regions within the United States, with 75% of the 27,900-km<sup>2</sup> area demonstrating temperatures >200°C at a depth of 4 km (MIT 2006).

The ESRP has long been a target for geothermal exploration and development, but the presence of the vast cold-water aquifer largely prevents direct characterization of the plain's geothermal potential. Previous aquifer studies have relied on hydraulic data (Robertson et al. 1974; Lewis and Goldstein 1982; Goode and Konikow 1990) and geochemical data (Wood and Low 1986; McLing et al. 2002), and focused primarily on the uppermost productive part of the aquifer. This study presents the results from the analysis of groundwater temperature data from 250 wells, including nine deep wells that penetrate the aquifer. These wells were evaluated to trace aquifer flow patterns in the uppermost part of the aquifer and elucidate the vertical structure of the aquifer and confining zone beneath the aquifer.

Because of an extensive groundwater monitoring program at the Idaho National Laboratory (INL) Site, more than half of the wells used for this study are located near the INL Site. Many additional wells are distributed across the entire ESRP (Brott et al. 1981; Ziagos and Blackwell 1986; Bartholomay et al. 1997), especially in the agricultural regions along the Snake River. Background temperatures for the aquifer generally range from approximately 11 to 13°C in the central part of the aquifer but are punctuated by several anomalously warm and cool areas (Figure 1.1). Figure 1.1 was developed from the integration of data from this study for the area proximal to INL, with data from Brott et al. (1981) and Bartholomay et al. (1997) for the larger ESRP.



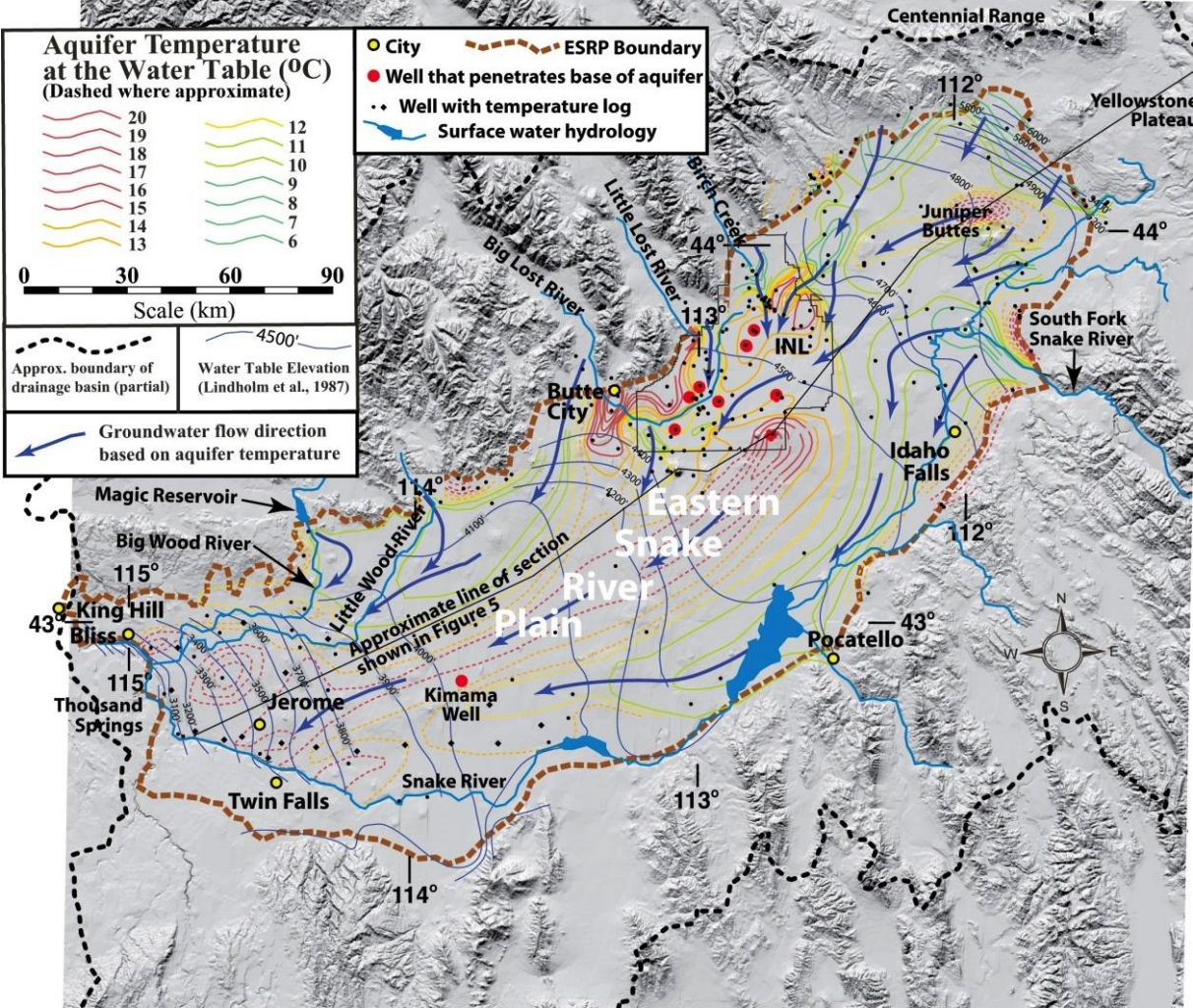


Figure 1.1: Map of ESRP aquifer, showing hydraulic head contours, groundwater flow direction, and aquifer temperature distribution across the study area. Groundwater flow-direction arrows account for thermal plume shape (elongated in the direction of flow), including cold plumes originating in tributary valleys and apparent hotspot plumes near the centerline of the aquifer.

The objective of this study is to demonstrate that aquifer temperature distribution, combined with other data sources, is a useful tool for revealing the groundwater flow patterns and determining the depth to which groundwater flow controls temperature in the ESRP. This study uses observed horizontal and vertical groundwater temperature profiles to infer the thickness of the aquifer. This approach is integrated with previously published isotopic studies (Johnson et al. 2000; Luo et al. 2000; Roback et al. 2001) to infer large-scale aquifer flow features and assess the relationship of the aquifer to the hydrothermal system at-depth.

## 1.2 Background

The ESRP is an arcuate, structural depression 50–100 km wide by 300 km long and encompasses approximately 27,900 km<sup>2</sup> of Southeastern Idaho (Figure 1.1). It is formed as a result of the passage of the Yellowstone hotspot. The plain rises from approximately 1,000 m above mean sea level, where it is bounded by the Western Snake River Plain, to >1,500 m at the Yellowstone Plateau, which marks its northeast boundary (Ackerman et al. 2006). The ESRP is bounded on the north and south by mountains rising >2,500 m above the plain. The mountain ranges are comprised of deformed Paleozoic and Mesozoic sedimentary rocks and silicic volcanics. The sedimentary rocks have been uplifted relative to the plain by northwesterly trending faults associated with the Basin and Range Province (Kuntz et al. 2002), through which the plain cuts a northeast-trending swath (Pierce and Morgan 2009).

More than 95% of the topography of the ESRP is covered by Quaternary, basaltic, eruptive centers and associated flows (Hackett and Smith 1992; Hughes et al. 2002). Surficial sedimentary deposits are largely thin and discontinuous, with loess mantling much of the plain, and quaternary fluvial deposits primarily along the Snake River and where tributary valleys join the plain (Bartholomay 1990). Individual basalt flows of relatively small volume were extruded primarily from northwest-trending fracture systems or numerous small monogenetic shield volcanoes (Greeley 1982; Kuntz et al. 2002; Hughes et al. 1999; Hughes et al. 2002). At-depth, the basalts are inter-layered with a variety of sediment, including carbonate; fluvial sands, gravels, and clays; carbonate-rich eolian silt; lacustrine deposits; and minor-reworked silicic tuffs (Bartholomay et al. 1997). Below approximately 1 km in depth, welded rhyolite tuff and tuffaceous sediments dominate the geology beneath the plain (Pierce and Morgan 1992). Recent (<16 Ma) volcanic activity on the plain has resulted in a very-high geothermal gradient (Blackwell 1989), as manifested by numerous thermal springs around the periphery of the plain, and high-measured heat flow.

### 1.2.1 Hydrogeology

The first comprehensive study of the ESRP aquifer system was conducted in the 1930s (Stearns 1936; Stearns et al. 1938). The aquifer is recharged by underflow (subsurface groundwater flow from outside the plain) and runoff from high mountains that surround the plain. The most prominent sources of recharge water to the aquifer are the result of precipitation in the highlands of the Yellowstone Plateau at the northeast margin of the plain, the Centennial Range north of the plain, the Basin and Range mountain ranges, which are on the northwest and southeast of the plain (Figure 1.1), and, to a lesser degree, the plain itself. Infiltration of irrigation water, derived primarily from the diversion of surface water sources on the plain, is also a locally important source of aquifer recharge in the vicinity

of large-scale irrigation projects (IDWR 2013). Regional groundwater flow is generally southwesterly, down the length of the ESRP from the Yellowstone Plateau to its discharge along the Snake River west of Twin Falls, Idaho (Figure 1.1). Because of low temperatures ( $<20^{\circ}\text{C}$ ), the short resident times of groundwater in the host rock (generally estimated to be less than a few hundred years), and the relative insolubility of the host rock, the productive aquifer is relatively inert geochemically (Wood and Low 1986; McLing 1994). Thus, the geochemical and isotopic signature of the recharge terrains is preserved in the groundwater tens of kilometers into the aquifer (Johnson et al. 2000; Luo et al. 2000; Roback et al. 2001). Groundwater moves through the host rocks of the ESRP in interflow rubble zones between lava flows, fractures within basalt flows, and coarse-grained, clastic interbeds at rates of 1.52–10.51 m/d in places (Fisher and Twining 2011). The deep, confining zone is much warmer ( $>30^{\circ}\text{C}$ ), characterized by greatly reduced hydraulic conductivity (0.0006 to 0.009 m/d), and has water chemistry that is enriched in sodium and potassium relative to the aquifer (Mann 1986; McLing et al. 2002).

Groundwater flow in the ESRP aquifer is dominated by fractures and rubble zones between basalt flows and is impeded by thick, relatively unfractured interior zones of lava flows; zones of fine-grained clastic interbeds; and perhaps vertical, northwest-trending basalt feeder dikes in volcanic rift zones (Kuntz et al. 2002). These geological heterogeneities lead to differences in saturated, hydraulic conductivity of several orders of magnitude (Welhan and Reed 1997), which render delineation of groundwater flow patterns difficult. Although it has been long recognized that the aquifer is highly heterogeneous, past investigators have used the assumption of an equivalent porous medium in their aquifer modeling efforts (Robertson et al. 1974; Lewis and Goldstein 1982; Goode and Konikow 1990). This assumption is based on the reasoning that a heterogeneous behavior observed at small scale is thought to average over a sufficiently large volume of the ESRP aquifer (Robertson et al. 1974; Robertson 1976; Garabedian 1986). However, previous investigations of groundwater chemistry and isotope content (Wood and Low 1986; McLing 1994; Johnson et al. 2000; Luo et al. 2000; Roback et al. 2001; McLing et al. 2002) suggest that an equivalent porous medium treatment does not adequately describe the complexities arising from the large-scale heterogeneities in aquifer properties at the scale of the ESRP aquifer or the observed interaction of cold-water recharge with high crustal heat.

### **1.2.2 Use of Heat as Groundwater Tracer**

Geothermal heat and borehole temperature logs have a long history of use for defining aquifer flow direction and quantifying aquifer hydraulic parameters (Bredenhoeft and Papadopoulos 1965; Smith and Chapman 1983; Forster and Smith 1988a; Forster and Smith 1988b; Ge 1998; Anderson 2005;

Saar 2011; Burns et al. 2015). In most of these applications, the aquifers that were studied have a large variability in horizontal and vertical permeability or are regionally confined. Burns et al. (2015) successfully used aquifer temperature to model regional aquifer behavior in the confined Columbia Plateau aquifer. Saar (2011) showed that using geothermal heat in an aquifer, combined with multiple diverse data sets, is useful in elucidating large-scale groundwater behavior. Also, well temperature profiles have been used in computational models to identify large-scale fracture flow zones within an aquifer system (Ingebritsen et al. 1992; Ge 1998).

Heat flow in the ESRP averages 110 mW/m (Blackwell 1989), one of the highest in North America (Blackwell and Steele 1992), and is highest along the margins of the plain (80–110 mW/m<sup>2</sup>) and lowest along the central plain (approximately 30 mW/m<sup>2</sup>). The low heat-flow values in the central plain are largely based on shallow wells, which are strongly influenced by the presence of the fast-flowing aquifer. When heat flow is measured in deep wells that penetrate below the base of the aquifer, the values are more consistent with the regional heat flow of 110 mW/m<sup>2</sup>-s (Blackwell 1989). However, even for the deepest boreholes drilled into the ESRP, there is significant variability in heat flow depending on location. For example, heat flow measured in well INEL-1 is up to 110 mW/m<sup>2</sup>, while heat flow in well CH-1, 15 km southeast, is 65 mW/m<sup>2</sup>.

### **1.2.3 Groundwater Temperature**

Water recharging the ESRP aquifer from the Yellowstone Plateau and mountain valleys surrounding the plain is mostly snowmelt from high elevation and, therefore, cold (6–9°C). As groundwater flows to the southwest, the depth to the water table generally deepens, and aquifer water intercepts the high, regional, crustal heat flow. The aquifer water gradually warms until its temperature is approximately 11–12°C at INL, and approximately 16°C at its discharge in the Thousand Springs area (Figure 1.1). The southwestward warming of groundwater (Blackwell 1989) is complicated by the addition of cold water recharging the aquifer from the high mountains along its northwest margin and from the infiltration of diverted Snake River irrigation water along its southeastern margin (Figure 1.1). As a result, local groundwater temperature is strongly influenced by large-scale aquifer permeability distribution. In addition, there are zones of deeper, warmer, groundwater recharge from the higher-temperature areas (>16°C) on the margins of the plain (e.g., Butte City, Idaho, area [Figure 1.1]), especially in places where cold groundwater recharge sources are absent.

### **1.2.4 Well Temperature Profiles**

In the ESRP, typical shallow aquifer wells have isothermal temperature profiles throughout the penetration depth of the well. In the case of the ESRP, in deep wells that penetrate the upper

permeable aquifer system, the base of the productive aquifer is marked by a break in slope from an isothermal gradient to a steep conductive gradient at-depth (Figure 1.2). The temperature inflection marks the point where this transition takes place in the borehole.

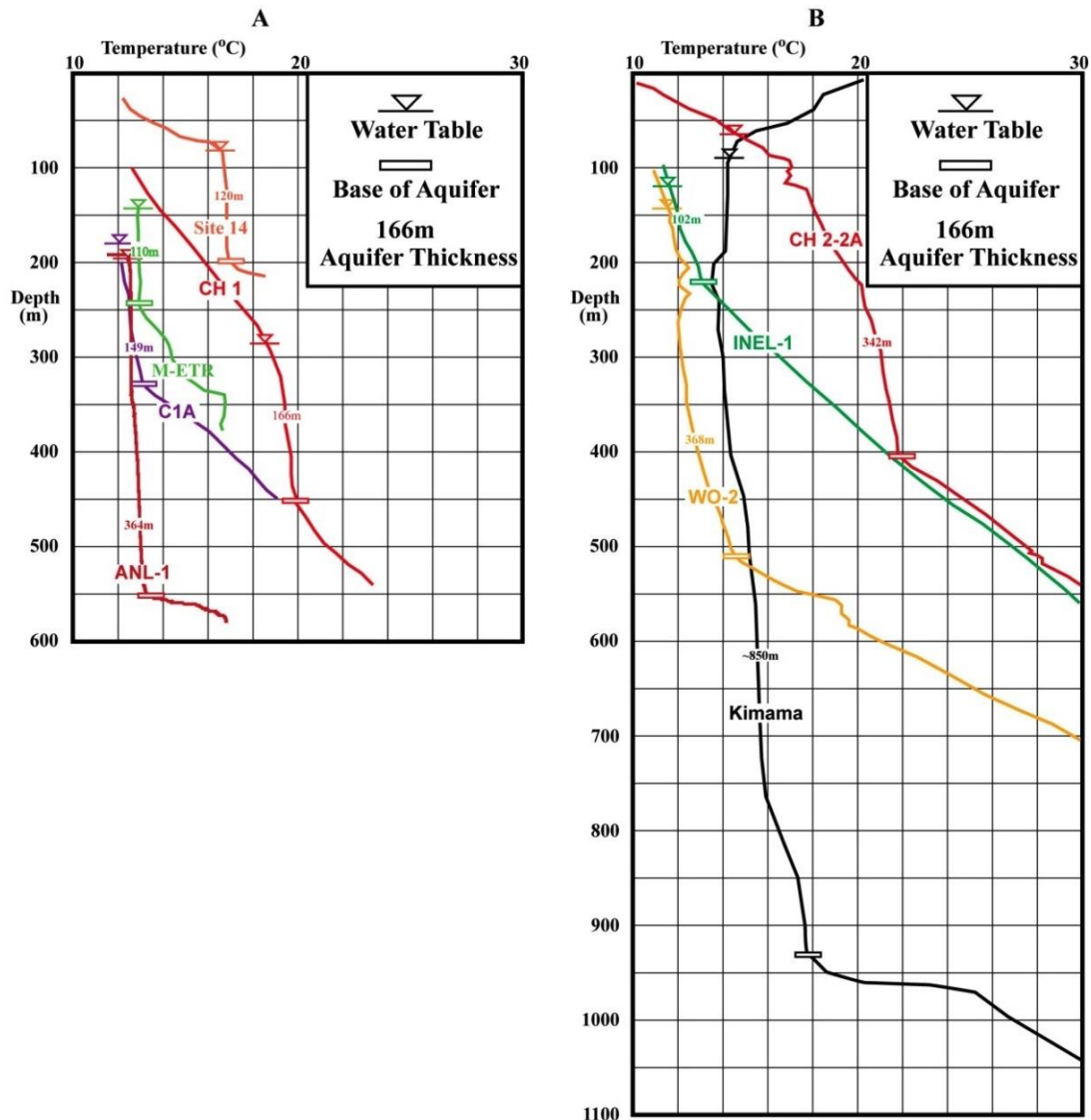


Figure 1.2: Vertical temperature profiles from nine deep boreholes analyzed in this study. For clarity, the temperature profiles from the nine deep boreholes are shown on two graphs.

The nine deep wells (Figure 1.2) evaluated in this study are of particular importance, as they fully penetrate the entire thickness of the ESRP aquifer and continue into the geothermal-confining zone below. These wells are important not only because of their depth but because they have also had multiple high-quality temperature profiles collected at multiple times (not shown). The resulting profiles were virtually identical to those shown in Figure 1.2, indicating that the aquifer temperatures and borehole temperature profiles have remained remarkably stable over time. Analyses of the

temperature profiles from these nine boreholes show that temperature profiles within the aquifer are nearly isothermal compared to the conductive gradients above and below the aquifer (Figure 1.2). As illustrated in Figure 1.2, thermal gradients within the aquifer are very small; therefore, temperature measurements from any part of the aquifer's saturated thickness can be used to analyze variations in groundwater temperature along the length of the ESRP. For decades, the United States Geological Survey (USGS) has collected and recorded temperature data from across the ESRP aquifer.

### **1.3 Methods**

It has been recognized that available hydraulic head data may lack the resolution to fully characterize groundwater flow in regional aquifers such as the ESRP aquifer (Blackwell and Priest 1996; Anderson 2005). Therefore, it is important that other sources of data be used to refine conclusions drawn from the water-table elevation measurements alone. Synthesis of multiple sources of data, such as temperature, chemistry, hydraulic head, and environmental isotopes, can offer a better understanding of the aquifer flow characteristics than any single data source considered in isolation. This study summarizes borehole temperature data from 241 shallow and nine deep wells across the ESRP to construct a map of groundwater temperature variation (Figure 1.1).

Because of the regional coverage and quality of the data, aquifer temperature can be used as a groundwater tracer to reveal medium- and larger-scale aquifer characteristics. A more detailed analysis was possible in the vicinity of INL, where groundwater chemistry was also used for comparison with groundwater flow and temperature contours to examine both the horizontal and vertical distributions of groundwater flow. Overlaying temperature profiles and inferred groundwater flow directions show elongation of thermal plumes in the direction of groundwater flow used to construct a regional aquifer temperature map (Figure 1.1). Regional aquifer temperature profiles also reveal additional characteristics of the aquifer, such as the influence of irrigation and recharge water entering the aquifer.

### **1.4 Temperature Profiles in Deep Wells Implications for Aquifer Geometry**

The ESRP aquifer provides the opportunity to use temperature logs in numerous wells to define aquifer flow in an exceptionally large, fractured, volcanic aquifer. It is also a well suited to test the validity of using groundwater temperature to determine the effective thickness of a regional aquifer. Prior to availability of drill core, water chemistry, and temperature data from deep boreholes on the ESRP, there was not an accurate method for determining the position of the effective base of the productive aquifer. Because little was known regarding the deep subsurface, an early approach was to assume that Tertiary volcanic rocks and sediments that lie beneath the Quaternary lavas and sediments



of the ESRP were so old that they were hydrothermally altered and relatively impermeable, thus defining the base for the aquifer (Robertson et al. 1974; Robertson 1976; Garabedian 1986). Whitehead (1986) used electrical resistivity surveys to define the thickness of the Quaternary section, estimating the thickness of the aquifer. Alternatively, Anderson and Bowers (1995) and Anderson et al. (1997) argued that the effective base of the aquifer coincides with the top of “a thick widespread layer of clay, silt, sand, and altered basalt that is older than about 1.8 million years and equivalent in age to the Glenns Ferry Formation.”

In 1979, well INEL-1 (3,160 m deep) was drilled and showed that, at least locally, the position of the aquifer base is related to the inception of secondary mineralization, which seals conductive structure in the aquifer host rock (Mann 1986). Mann (1986) noted that in well INEL-1, where the water table is approximately 120 m below land surface, temperature, groundwater chemistry, and permeability changed dramatically in the borehole approximately 250 m below land surface. Aquifer properties (i.e., temperature, chemistry, and permeability) above the 250-m transition are consistent with the regional aquifer system; however, below 250 m, temperatures are higher, groundwater chemistry is more sodium- and potassium-rich, and matrix permeability is dramatically reduced and heat increased (Mann 1986). The change in aquifer properties with depth is further confirmed by studies conducted on other deep boreholes by Morse and McCurry (2002). In this study, the authors propose that the effective thickness of the productive aquifer, while variable depending on where it is observed, is consistent with the lower boundary defined by a hydrothermally altered confining unit. Water chemistry is also different in the aquifer and the lower confining unit, which transitions from Ca-Mg-HCO<sub>3</sub> in the productive aquifer to N-K-HCO<sub>3</sub>-type groundwater in the deep thermal-confining unit (McLing et al. 2002; Mann 1986).

Temperature profiles for individual wells completed in the ESRP aquifer illustrate the regional and local three-dimensional character of the aquifer temperature. Across most of the study area, temperature in the vadose zone increases with increasing depth, though in areas with cold recharge to the aquifer, the gradient may be reversed (Brott et al. 1981). Below the water table, the profiles are either isothermal or show minimal temperature change with depth (Figure 1.2). This lack of vertical variation in temperature is interpreted to be the result of fast-flowing groundwater in the highly transmissive upper aquifer (Anderson 2005). As shown in Figure 1.2, the bottom of the isothermal section is usually abrupt, and below that depth the gradient increases to reflect the vertical transfer of heat from the deep crust and upper mantle. These types of abrupt vertical changes in thermal regime are also seen in other volcanic terrains, such as the Cascade Range and Columbia River Plateau (Blackwell and Priest 1996; Burns et al. 2015).

The temperature profiles of the nine deep wells for which quality temperature logs are available (Figure 1.2) provide important insights regarding geometry and flow dynamics of the ESRP aquifer (Table 1.1). First, the depth to the base of the aquifer (the inflection from isothermal to regional geothermal gradient) ranges from 100 to 860 m beneath the water table. Second, the aerial distribution of aquifer thickness contoured from these nine deep wells shows that a deep, east-to-northeast-trending “channel” crosses through INL in a northeast-southwest direction (Figure 1.3). Six of the nine deep-well logs reveal a water-table temperature of approximately 12–13°C, but three of them (wells CH-1, Site 14, and CH2-2A) have aquifer temperatures of approximately 18°C, defining a warm zone in the aquifer (Figure 1.2). Vertical profiles for these wells show increasing groundwater temperatures with depth to the base of the aquifer. These observations refute the suggestion by Robertson et al. (1974) that warm groundwater rests above colder groundwater due to infiltrating irrigation water or playa lake settings. Rather, temperature profiles in these deep wells show that heat from depth through the upwelling of geothermally heated water entering the upper productive aquifer is the cause of the warm zones. The likely cause of the thermal anomalies in these areas is a geothermal flux large enough to affect aquifer temperature at the water table, either because of slow groundwater flow in the aquifer or vigorous input of geothermally heated water from below the base of the aquifer.

Table 1.1: Aquifer thickness calculated from temperature logs collected in deep wells drilled into the ESRP.

<b>Well Name</b>	<b>Aquifer Thickness (m)</b>	<b>Depth to Aquifer Base (m)</b>	<b>Gradient (°C/km) Below Confining Zone</b>
INEL-1	100	220	44
Site 14	120	200	14
CH2-2A	342	405	60
CH-1	166	450	39
C1A	149	330	49
WO-2	368	510	72
ANL-1	364	550	120
M-ETR	110	245	39
Kimama	860	>860	75



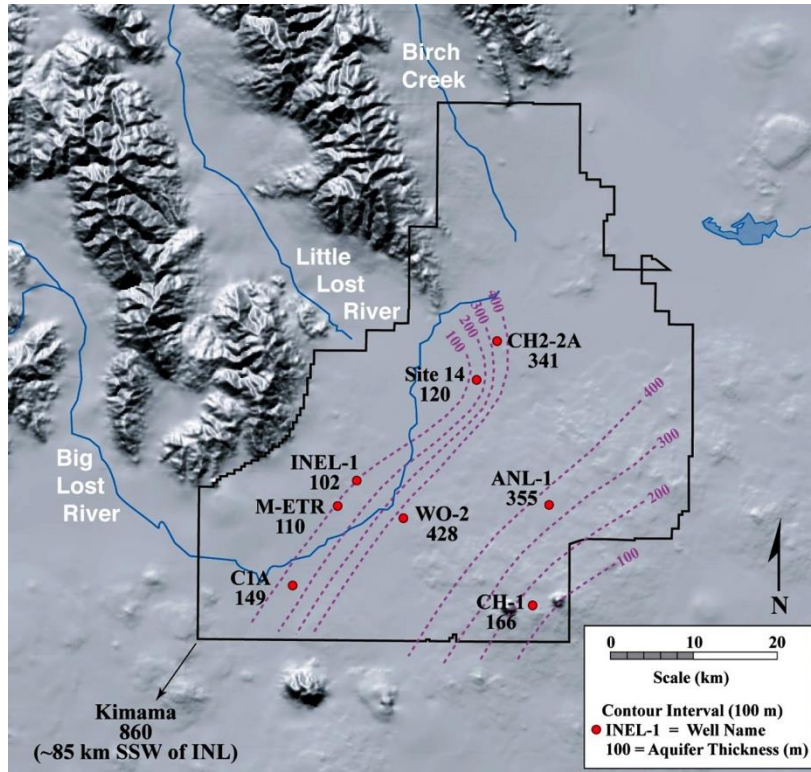


Figure 1.3: Contours of aquifer thickness on INL based on nine deep wells for which temperature logs are available.

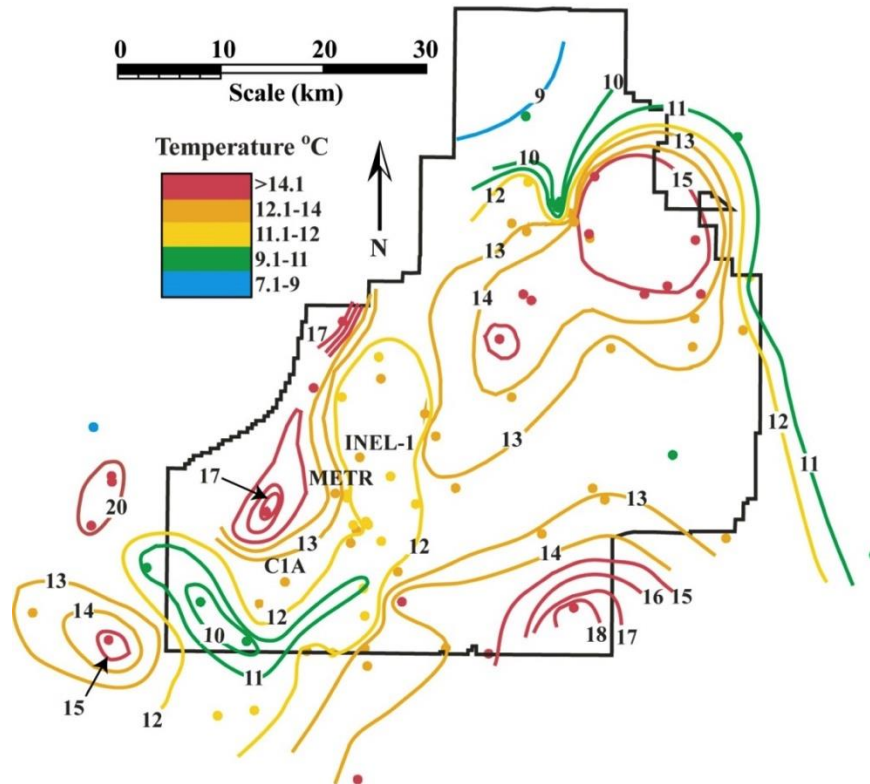


Figure 1.4: Aquifer temperature at water table for the ESRP within and near INL.

## 1.5 Aquifer Temperature Distribution

The ESRP aquifer temperature distribution at the water table (Figure 1.1) was mapped using temperature-logging data from more than 250 wells in the ESRP, showing temperature distribution of the aquifer is not uniform across the plain, but rather varies as a function of distance from recharge areas, aquifer flow velocity, and geothermal upwelling from depth. Figure 1.4 shows the aquifer temperature distribution at and near INL. Because data density is much greater near INL due to the large number of monitoring wells, it is possible to observe aquifer temperature in much greater detail. The areal aquifer temperature distribution in this area provides information about aquifer flow directions at the local scale. An example of local-scale flow structure is illustrated in the north-central part of INL (Figure 1.4). Here, a narrow plume of cool recharge water penetrates the large, warm zone in the central part of INL. Additionally, there are two other areas of anomalously cool water—one in the southwest corner of INL and the other at the mouth of the Little Lost River in the northern part of INL. The southwest cool zone, with temperatures of 10–11°C, is located in a region of INL where water from the Big Lost River (Figure 1.1) is diverted (for flood-control purposes) into large infiltration basins in high-precipitation years. This water infiltrates rapidly through the vadose zone to the aquifer, where it forms an anomalously cool zone in this area of INL. The northern cool zone is the result of cold-water recharge entering the aquifer from the Little Lost River Valley (Figure 1.1). Zones of higher aquifer temperatures exist at a number of places along the margins of the narrow plume of cold recharge water penetrating the central area of INL. The warm zone located on the western boundary of INL is of particular interest due to its proximity to the proposed range-bounding faults that could potentially act as conduits for upwell of thermal water from depth.

Additional support for these interpretations of aquifer character and groundwater flow comes from multiple sources, including tracer tests in which tracers break through to distant observation wells long before breaking through to nearer wells that are not within the preferential pathway indicated by the temperature data (Arnett 2002). Likewise, the contamination plume from INL's Test Area North injection well located proximal to CH2-2A has the same overall shape and direction as the narrow, cold plume (Whitmire 2003).

As illustrated in Figure 1.5, a longitudinal cross-section of the aquifer shows the warming of the aquifer from recharge to discharge zones. Groundwater flow shown in Figure 1.5 is generally parallel to the section, but there is considerable lateral infiltration from the highlands surrounding the ESRP. Only the fast-flowing upper productive aquifer is colored to indicate that vertical variation in aquifer temperature is negligible compared to horizontal temperature variation. The indicated temperature distribution illustrates the overall warming from approximately 5°C in the source areas to

approximately 16°C at the discharge area and effect of two “hotspots,” one at Juniper Buttes (18°C) and one in the southeastern corner of INL (Figure 1.1). Basal heat flux is the average annual heat flux estimated by Blackwell (1989). Burns et al. (2016) attributes the zone of anomalous, cool groundwater downgradient of Juniper Butte (Figure 1.5) to the presence of an anomalously thin vadose zone and the addition of cool recharge water (Figure 1.1). The cool zone downgradient of the INL (Figure 1.1), where the vadose zone is very thick (>200 m), can only be explained by the addition of cool recharge water from the basins along the margin of the plain.

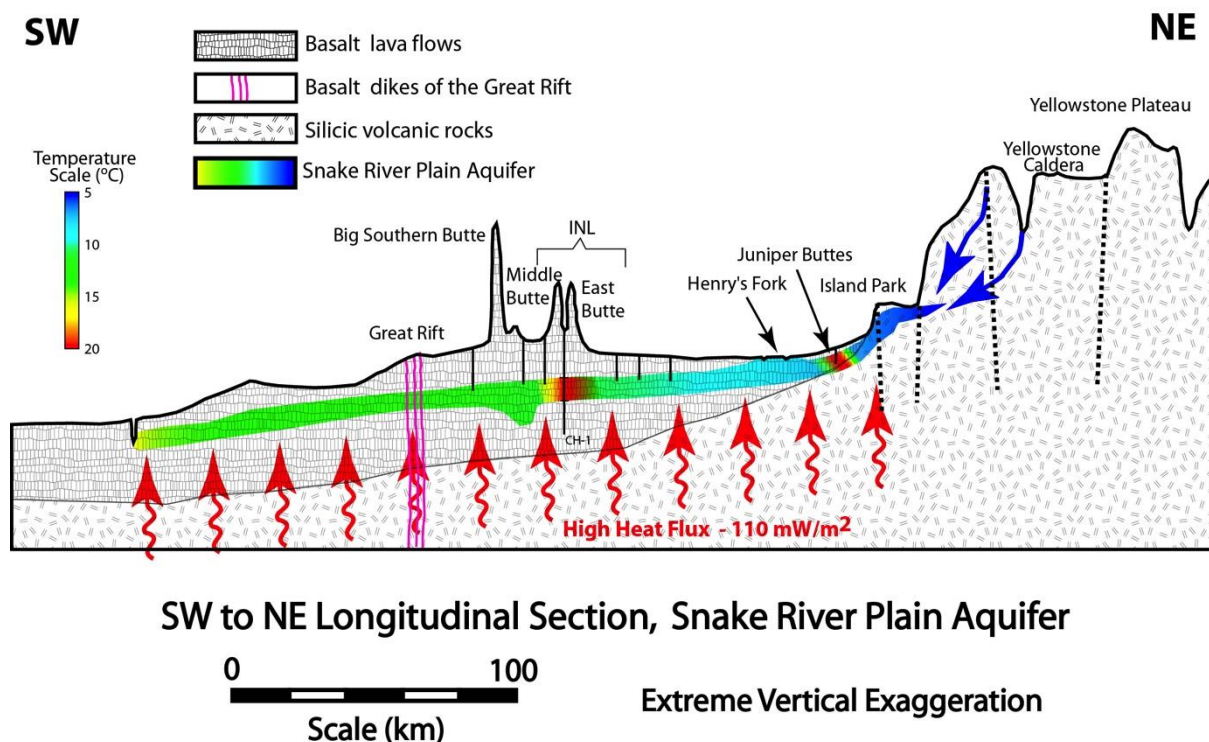


Figure 1.5: Simplified and idealized longitudinal section (not to scale) of Eastern Snake River Plain aquifer from its source in the Yellowstone area to its discharge in the Thousand Springs area, modified after Smith (2004). Approximate line of section is shown in Figure 1.1.

## 1.6 Vertical Aquifer Temperature Distribution

The temperature profiles in the ESRP-aquifer wells are similar to those of some wells in the Cascade Range in Oregon, where fractured dacitic-to-basaltic volcanic rocks host cold-water aquifers that lie above altered and mineralized rocks at-depth (Blackwell 1990; Burns et al. 2015). Because erosion has exhumed, altered, and mineralized rocks in the Cascade Range, the presence of alteration and mineralization at the surface is a good indicator that permeabilities are low in the subsurface and that conductive temperature gradients will prevail. In contrast, the continuing subsidence history of the ESRP (Kuntz et al. 2002; Hughes et al. 1999; Hughes et al. 2002) precludes deep erosion, and the surface rocks and those in the vadose zone and aquifer have never

experienced hydrothermal alteration. The vigorous flow of cold groundwater in the plain controls the geothermal gradient to the base of the aquifer and produces the observed isothermal zones in the temperature profiles.

The earliest aquifer temperature logging (Olmsted 1962) was done by USGS personnel working at what was then the National Reactor Testing Station (now INL), and since the 1970s, many temperature-logging campaigns have been conducted in the ESRP (Brott et al. 1978; Ziagos and Blackwell 1986; Blackwell 1989; Blackwell 1990; Blackwell et al. 1992). These campaigns were mainly aimed at determining crustal heat flow through the ESRP (Blackwell and Steele 1992) and evaluating the geothermal potential of the area beneath the ESRP aquifer. The goals of these studies were to (1) measure crustal heat flow beneath the ESRP aquifer, (2) determine the temperature distribution in the aquifer water itself (Blackwell and Steele 1992), and (3) evaluate the geothermal potential beneath the aquifer. However, because most of the logged wells were drilled to monitor water levels and collect water samples, they generally extend only a few meters below the water table and provide only limited information on sub-aquifer geothermal characteristics. In addition to the shallow aquifer and monitoring wells, a number of deep wells were drilled that penetrate the base of the aquifer (see Section 1.4).

Vertical aquifer temperature distribution at INL, where a number of deep wells have been drilled and logged, is illustrated by a northeast-to-southwest cross-section shown in Figure 1.6. This cross-section shows the profound differences in aquifer temperature distribution and temperature gradients for different areas at INL. The south-central part of INL, represented by well ANL-1, is characterized by a thick channel of relatively cool groundwater that extends to a depth of approximately 400 m below the water table, below which a sharp inflection to the regional conductive gradient occurs (Figures 1.1, 1.3, and 1.6). In contrast, the north-central part of INL, represented by wells CH2-2A, Site 14, and USGS-7 (identified as 7 on the map in Figure 1.6), is characterized by relatively warm temperatures at the water table (i.e., temperatures up to 16 to 17°C), gradual warming with depth below the water table, and a less-abrupt transition to the regional geothermal gradient. Because this warm zone occurs in an area where sediment interbeds within the basalt sequence are numerous and thick (Helm-Clark et al. 2004), we speculate that transmissivities are lower here than elsewhere in the aquifer and that groundwater is moving sufficiently slowly, allowing geothermal heat from below to affect aquifer temperature throughout the entire thickness of the aquifer.

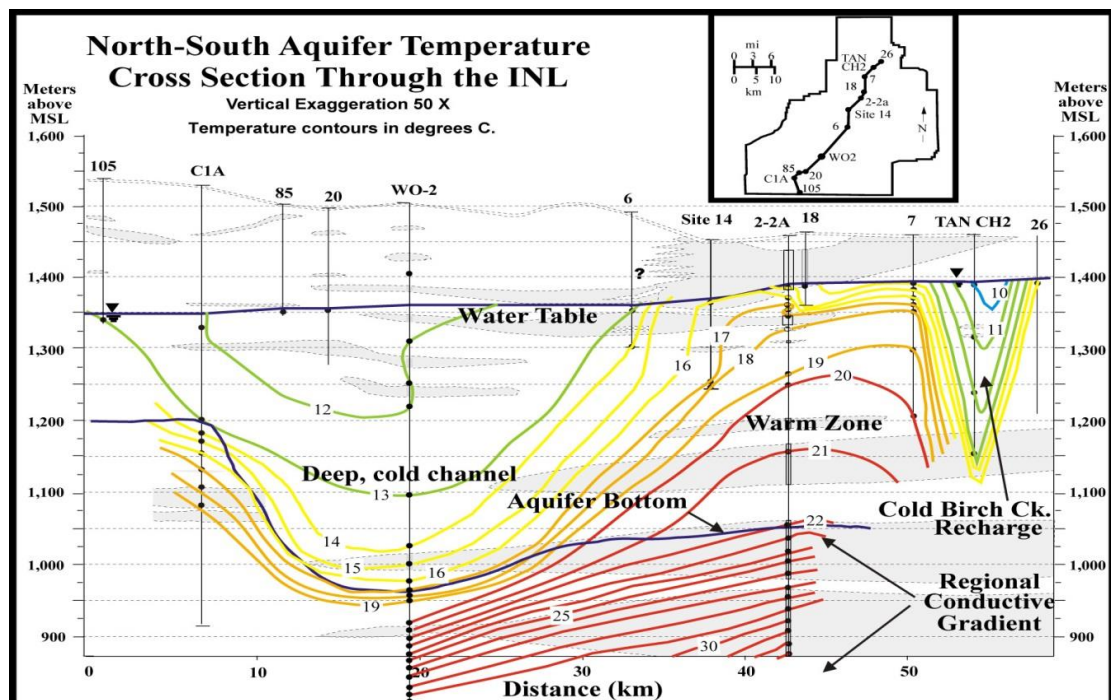


Figure 1.6: Detailed north-to-south cross-section showing aquifer temperature distribution beneath INL. Lightly shaded zones are sediment interbeds layers within the basalt sequence.

The warm zone at the southeast corner of INL (Figure 1.4) requires an alternate explanation. It occurs along the axis of the ESRP, where interbeds are few but where volcanic source areas with porous near-vent facies are abundant (Hackett and Smith 1992). In this instance, ESRP aquifer temperatures may reflect longer residence times, coupled with the presence of a geothermal circulation system of sufficient size that is able to overwhelm the cooler, productive aquifer. The interpretation that this thermal anomaly is caused by the presence of a strong geothermal circulation may imply that this area is a good target for geothermal exploration.

### 1.7 Horizontal Temperature Distribution: Implications for Groundwater Flow

ESRP aquifer-temperature variation along and across the plain provides useful information for tracing aquifer flow paths because of the interaction of cold recharge waters (mostly snowmelt) with exceptionally high heat flow (Blackwell 1989; Blackwell et al. 1992) from the crust beneath the plain. Cold recharge water derived along the margins of the plain and from surface recharge, and plumes of warm groundwater created by the upwelling of geothermal water, act as long-term, large-scale tracer tests that elucidate the flow paths within the aquifer. The size, shape, and continuity of these cold and warm plumes are influenced by preferential pathways in the aquifer and provide information about flow direction, relative flow velocities, and lateral dispersivity of the aquifer.

An example of local-scale aquifer flow structure is shown in the north-central part of INL (Figure 1.4). Here, a narrow plume of cold recharge groundwater penetrates the large, warm zone in the central part of INL. This narrow cold plume is not just a surface feature, where cold recharge water is riding on top of the regional aquifer. Rather, this cold channel penetrates the aquifer as shown in Figures 1.1, 1.3, and 1.6. This cold channel results from aquifer recharge water moving along strong, preferential pathways (probably fracture zones), aligned with the regional stress field (Welhan and Reed 1997). In this portion of the aquifer, groundwater flows with sufficient velocity to counter the effects of geothermal heat from below. The addition of the Kimama well data in 2011 (Twining and Bartholomay 2011; Shervais et al. 2013) may support the existence of a thick, cold, preferential channel for groundwater flow along the central axis of the ESRP, as the well is aligned with the cold, thick aquifer channel at INL and has an aquifer thickness of 860 m. However, given the paucity of data and distance between INL and the Kimama well, this speculation should be considered tenuous.

On the regional scale, the temperature distribution provides information about long-range ESRP aquifer flow. Throughout the aquifer, temperature distribution reveals the numerous flow paths that are defined by warm and cold groundwater moving through the aquifer (Figures 1.1 and 1.4). For example, in the northeast portion of the aquifer, a warm zone near Juniper Buttes is elongated to the west-southwest (Figure 1.1) at an oblique angle to the southwest-trending axis of the plain. The westerly elongation of this thermal anomaly may result from the large influx of cooler recharge water from the South Fork of the Snake River (Figure 1.1) as it emerges from the southeastern margin of the plain near Idaho Falls, Idaho. USGS data for the Lorenzo gauge on the South Fork of the Snake River north of Idaho Falls shows that water temperature during the irrigation season (May to September) is approximately 7–16°C and drops to <5°C from November to March. Another major contributor to this diversion to the west is the influx of large volumes of irrigation water diverted from the Snake River to support agriculture in the eastern region of the plain. This large volume of cold-water recharge causes a ridge in the water table (Ackerman et al. 2006), having the effect of forcing the flow from upgradient parts of the aquifer through INL, most of it through the deep, cool channel discussed in Section 1.6 (Figures 1.3 and 1.6).

The warm groundwater zone near the southeast corner of INL (Figure 1.1) appears to be a zone of high geothermal input to the aquifer, resulting in significant warming of groundwater in this area. The flow path defined by this warm groundwater zone remains intact throughout the reach of the aquifer, from INL downgradient to Butte City. Water from the cold channel at INL, from Birch Creek, and from the Little Lost River flows parallel to the warm plume but remains along its northwest margin. The apparent persistence of the warm flow path for >100 km downgradient suggests that lateral dispersion in this reach of the aquifer is limited.



Large-scale flow directions based on aquifer temperature distribution can be compared to previous interpretations characterization studies (for example, see Ackerman et al. 2006; Wood et al. 2005; Johnson et al. 2000; Roback et al. 2001; Garabedian 1986). Our flow-direction analysis is based on aquifer temperature and provides more details for the area within INL, where the data density is greater due to the large number of monitoring wells. The presence of a warm zone in the aquifer near the southeast corner of INL (Figure 1.1) defines the western boundary between the heat flow of the regional ESRP aquifer and the limit of influence that cold recharge from the South Fork of the Snake River has on aquifer temperature.

### **1.8 Comparison to Flow Regime Indicated by Groundwater Chemistry and Equilibration of Natural Isotopes**

Johnson et al. (2000) and Roback et al. (2001) used strontium-87/86 and uranium-234/238 isotope ratios to track groundwater flow paths through the ESRP aquifer at INL. The areal distribution of these isotopes provides a clear and detailed pattern of flow pathways that shows many similarities to that provided by temperature data; however, similar conclusions can be made on the basis of strontium isotopes and, to a lesser extent, the solute concentration data (Johnson et al. 2000; for brevity, only the uranium data are discussed in detail). Figure 1.7 shows the distribution of uranium isotope ratios in the aquifer beneath INL and reveals flow patterns at scales of tens of kilometers in length. These patterns reflect the fact that groundwater recharging the aquifer from drainages north of the ESRP and from surface water sources has isotopic signatures that are distinct from those of the main aquifer. This recharging groundwater, tagged with a unique, natural, isotopic signature, can be traced downgradient until the uniqueness of the isotopic signature is lost, due to water-rock reaction or mixing and dilution.

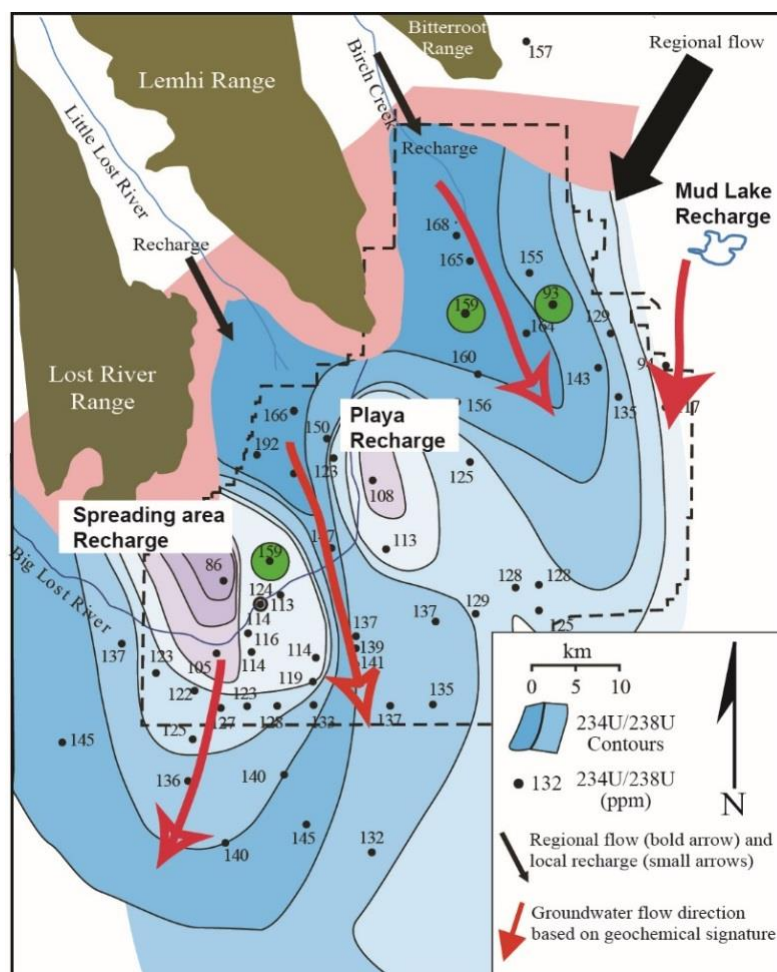


Figure 1.7: Flow pathways deduced from uranium data. High ratios characteristic of mountain recharge source regions extend far into the aquifer in preferential flow zones. Low isotope ratios characterize surface recharge areas (after Roback et al. 2001). Note comparison of these flow pathways to those deduced from temperature data (Figure 1.1).

Principal groundwater flow directions deduced from the two independent data sets (groundwater temperature and chemical signatures) are generally similar; however, there is not always a direct correlation between temperature and isotope ratios at a local scale. This is especially the case along the margins of the ESRP where geothermal input is highest. For example, groundwater with high uranium-isotope ratios emanate from the valleys of Birch Creek and Little Lost River; these zones generally correlate with the cold groundwater-recharge plumes defined by the thermal profiles (Figure 1.7). However, when compared in detail, samples with high uranium-234/238 isotope ratios at the mouths of the valleys of Birch Creek and Little Lost River span a wide range of temperatures. This is interpreted to indicate that groundwater originating from these recharge valleys is warmed as it enters the ESRP aquifer proper, which, along its northwest margin, is an area of high heat flow, without significantly changing the isotope ratios. This implies that in these particular areas, the flux of



recharge water is sufficiently high to overwhelm the chemical signature of deep-sourced geothermal water. In a second example, cool groundwater zones in the southwest part of INL and to the northeast of INL correspond to zones of lower uranium-234/238 isotope ratios. Both of these zones are interpreted to be zones of infiltration based on chemical, isotopic, and hydrologic data (Roback et al. 2001) and references therein, and based on temperature data from this study. Therefore, the fact that temperature and isotope ratios are not directly correlated is due to different mechanistic origins of the temperature and isotopic signatures. Because of the different mechanistic origins of the temperature and isotope signatures, the two data sets combined provide valuable information regarding the origin and evolution of the groundwater.

### **1.9 Geothermal Implications**

The many thermal springs along the margin of the ESRP (Cannon et al. 2014), high heat flow (Blackwell and Steele 1992) within the plain, and recent volcanic activity (Pierce and Morgan 2009) suggest the presence of a significant geothermal potential beneath the aquifer. However, the large volume of fast-moving, cold groundwater in the aquifer effectively blankets the ESRP geothermal system. The high, crustal, heat flow of the plain manifests itself in several geothermal springs and warm groundwater in domestic wells along the margins of the plain, where the aquifer is very thin. It is also apparent in the temperature logs of deep wells that penetrate to depths beneath the bottom of the aquifer on the plain as described in this study and Brott et al. (1981). In both of these cases, heat flow  $>100 \text{ mW/m}^2$  is observed. In contrast, heat flow estimates made above the aquifer average only  $\sim 25\text{--}30 \text{ mW/m}^2$  (Brott et al. 1981), illustrating the efficiency with which the aquifer intercepts heat before it reaches the near-surface environment.

Our analysis of temperature data adds valuable insight into the flow dynamics of the upper productive aquifer, which in turn helps identify several areas of high geothermal potential beneath the ESRP (Figures 1.1, 1.4, and 1.7). These results indicate that vigorous geothermal input from depth can be detected by anomalous temperature and chemical signatures in the upper aquifer. These areas of vigorous thermal input may represent targets for future geothermal exploration. Additionally, Mann (1986) conducted several hydraulic tests in well INEL-1 at the interval of 1.3 to 3.2 km below ground surface. A pumping test in this interval was conducted for seven days and yielded an average reservoir permeability of  $7.2 \times 10^{-16} \text{ m}^2$  for the interval. Permeability this low in the deep geothermal zone would require advanced engineered geothermal systems (EGS) reservoir technology (Tester et al. 2006) to allow for sufficient water movement to economically recover any geothermal energy resources (Evans et al. 1999) in the ESRP.

## 1.10 Summary

This study represents an integrated effort to apply ESRP aquifer temperature and wellbore temperature profiles, in conjunction with previously reported isotopic data (Johnson et al. 2000; Roback et al. 2001), to trace regional groundwater flow and aquifer thickness and identify zones of elevated geothermal potential under the plain. Evaluation of these combined data sets confirms the validity of using temperature to refine the aquifer conceptual model and gain insights into the geothermal potential of the ESRP.

By studying the thermal characteristics of the nine deep wells used for this study, combined with data from 241 shallow boreholes, we have been able to elucidate details of the ESRP aquifer that have not been seen by other techniques (e.g., hydraulic head and chemical tracers), including refinement of the nature of the lower boundary of the aquifer across a large area of the plain. One critical observation is that the boundary contact between the aquifer and lower confining zone is not uniform but varies significantly in depth across the plain. Depth to this boundary is shallower along the margins of the ESRP and significantly deeper down the central axis of the plain. The boundary is also relatively sharp and related to the first occurrence (with depth) of thermal alteration minerals (Morse and McCurry 2002) and is marked by a change in groundwater chemistry from Ca-Mg-HCO<sub>3</sub>-dominated aquifer to Na-K-HCO<sub>3</sub>-type water in the confining zone (Mann 1986; McLing et al. 2002). The occurrence of mineral alteration is important because it results in the sealing of conductive structure within the aquifer, causing permeability to dramatically decrease, and allowing high heat flow from below to dominate aquifer temperature below this horizon.

Depth to the water table in the aquifer occurs 60 m to >200 m below land surface, while the depth to the base of the aquifer (the inflection from isothermal to regional conductive gradients) ranges from 220 to 860 m below the surface.

Groundwater temperatures and borehole temperature profiles support the conclusions of the isotope-preferred groundwater flow-path studies (Johnson et al. 2000; Luo et al. 2000; Roback et al. 2001). For example, groundwater temperature at the top of the aquifer beneath INL ranges from <8°C to >18°C. At the regional scale, the coldest of this groundwater correlates with the large-scale, preferential flow corridors identified by these studies. As a result, it is concluded that these preferential flow corridors are associated with areas where groundwater moves rapidly through the aquifer system, allowing for minimal equilibration with the host rock. This is also consistent with the conclusions of the INL Site-wide Waste Area Group 10 Site-wide (Wood et al. 2005) and USGS (Ackerman et al. 2006) flow models. In contrast, regions where water temperature is warmer generally correlate with the slower flow regions identified by the previous studies (Ackerman et al. 2006; Wood et al. 2005;

Johnson et al. 2000; Roback et al. 2001; Garabedian 1986), providing support for the conclusion that in areas where water temperature is higher, groundwater flow is slow enough that the thermal gradient of the ESRP overwhelms flow velocity.

Overall, this study shows that using three-dimensional synthesis of new and existing aquifer temperature data can aid in constraining aquifer geometry, constraining groundwater flow paths, and identifying the location of potential shallow EGS resources.

### Acknowledgments

The authors would like to acknowledge the numerous past researchers who have contributed to increasing the understanding of the ESRP aquifer—specifically, USGS, Southern Methodist University, and INL. We also thank the reviewers of this manuscript for significant and meaningful recommendations that improved the final text.

### References

- Ackerman, D. J., G. W. Rattray, J. P. Rousseau, L. C. Davis, and B. R. Orr, 2006, *A Conceptual Model of Ground-Water Flow in the Eastern Snake River Plain Aquifer at the Idaho National Laboratory and Vicinity with Implications for Contaminant Transport*, DOE/ID-22198, U.S. Department of Energy Idaho Operations Office.
- Anderson, M. P., 2005, "Heat as a Ground Water Tracer," *Groundwater*, Vol. 43, No. 6, pp. 951–968, DOI: 10.1111/j.1745-6584.2005.00052.x.
- Anderson, S. R. and B. Bowers, 1995, *Stratigraphy of the Unsaturated Zone and Uppermost Part of the Snake River Plain Aquifer at Test Area North, Idaho National Engineering Laboratory, Idaho*, DOE/ID-22142, U.S. Department of Energy Idaho Operations Office.
- Anderson, S. R., M. J. Liszewski, and L. D. Cecil, 1997, *Geologic Ages and Accumulation Rates of Basalt-Flow Groups and Sedimentary Interbeds in Selected Wells at the Idaho National Engineering Laboratory, Idaho*, DOE/ID-22134, U.S. Department of Energy Idaho Operations Office.
- Arnett, R. C., 2002, *Test Area North Operable Unit 1-07B In-situ Bioremediation Groundwater Model Development and Initial Performance Simulation*, INEEL/EXT-02-00560, Idaho National Engineering and Environmental Laboratory, June 2002.
- Bartholomay, R. C., 1990, *Mineralogical Correlation of Surficial Sediment from Area Drainages with Selected Sedimentary Interbeds at the Idaho National Engineering Laboratory, Idaho*, DOE/ID-22092, U.S. Department of Energy Idaho Operations Office.
- Bartholomay, R. C., L. M. Williams, and L. J. Campbell, 1997, *Evaluation of Radionuclide, Inorganic Constituent, and Organic Compound Data from Selected Wells and Springs from the Southern Boundary of the Idaho National Engineering Laboratory to the Hagerman Area, Idaho*, 1996, DOE/ID-22141, U.S. Department of Energy Idaho Operations Office.
- Blackwell, D. D., 1989, "Regional Implications of Heat Flow of the Snake River Plain, Northwestern United States," *Tectonophysics*, Vol. 164, No. 2, August 1989, pp. 323–343, DOI: 10.1016/0040-1951(89)90025-5.

- Blackwell, D. D., 1990, *Temperatures and Heat Flow in the INEL-GT1 and WO-2 Boreholes, Snake River Plain, Idaho*, EGG-NPR-10690, November 1990.
- Blackwell, D. D. and G. R. Priest, 1996, "Comment [on 'Rates and Patterns of Groundwater Flow in the Cascade Range Volcanic Arc and the Effect on Subsurface Temperatures' by S. E. Ingebritsen, D. R. Sherrod, and R. H. Mariner]," *Journal of Geophysical Research: Solid Earth*, Vol. 101, No. B8, pp. 17561–17568, DOI: 10.1029/96JB01507.
- Blackwell, D. D. and J. L. Steele, 1992, "DNAG Geothermal Map of North America," Geological Society of America.
- Blackwell, D. D., S. Kelley, and J. L. Steele, 1992, *Heat Flow Modeling of the Snake River Plain, Idaho*, EGG-C91-103450, April 1992.
- Bredehoeft, J. D. and I. S. Papaopulos, 1965, "Rates of Vertical Groundwater Movement Estimated from the Earth's Thermal Profile," *Water Resources Research*, Vol. 1, No. 2, June 1965, pp. 325-328, DOI: 10.1029/WR001i002p00325.
- Brott, C. A., D. D. Blackwell, and J. C., Mitchell, 1978, "Tectonic Implications of the Heat Flow of the Western Snake River Plain, Idaho," *Bulletin of the Geological Society of America*, Vol. 89, No. 12, December 1978, pp. 1697–1707, DOI: 10.1130/0016-7606(1978)89<1697:TIOTHF>2.0.CO;2.
- Brott, C. A., D. D. Blackwell, and J. P., Ziagos, 1981, "Thermal and Tectonic Implications of Heat Flow in the Eastern Snake River Plain, Idaho," *Journal of Geophysical Research: Solid Earth*, Vol. 86, No. B12, December 1981, pp. 11709–11734, DOI: 10.1029/JB086iB12p11709.
- Burns, E. R., C. F. Williams, S. E. Ingebritsen, C. I. Voss, F. A. Spane, and J. DeAngelo, 2015, "Understanding Heat and Groundwater Flow Through Continental Flood Basalt Provinces: Insights Gained from Alternative Models of Permeability/depth Relationships for the Columbia Plateau, USA," *Geofluids*, Vol. 15, Nos. 1–2, February 2015, pp. 120–138, DOI: 10.1111/gfl.12095.
- Burns, E. R., S. E. Ingebritsen, M. Manga, and C. F. Williams, 2016, "Evaluating Geothermal and Hydrogeologic Controls on Regional Groundwater Temperature Distribution," *Water Resources Research*, Vol. 52, No. 2, February 2016, pp. 1328–1344, DOI: 10.1002/2015WR018204.
- Cannon, C., T. Wood, G. Neupane, T. McLing, E. Mattson, P. Dobson, and M. Conrad, 2014, "Geochemistry Sampling for Traditional and Multicomponent Equilibrium Geothermometry in Southeast Idaho," INL/CON-14-32242, Idaho National Laboratory, October 2014.
- Evans, K. F., F. H. Cornet, T. Hashida, K. Hayashi, T. Ito, K. Matsuki, and T. Wallroth, 1999, "Stress and Rock Mechanics Issues of Relevance to HDR/HWR Engineered Geothermal Systems: Review of Developments during the Past 15 Years," *Geothermics*, Vol. 28, Nos. 4–5, August-October 1999, pp. 455–474, DOI: 10.1016/S0375-6505(99)00023-1.
- Fisher, J. C. and B. V. Twining, 2011, *Multilevel Groundwater Monitoring of Hydraulic Head and Temperature in the Eastern Snake River Plain Aquifer, Idaho National Laboratory, Idaho, 2007-08*, DOE/ID-22213, U.S. Department of Energy Idaho Operations Office.
- Forster, C. and L. Smith, 1988a, "Groundwater Flow Systems in Mountainous Terrain: 1. Numerical Modeling Technique," *Water Resources Research*, Vol. 24, No. 7, July 1988, pp. 999–1010, DOI: 10.1029/WR024i007p00999.
- Forster, C. and L. Smith, 1988b, "Groundwater Flow Systems in Mountainous Terrain: 2. Controlling Factors," *Water Resources Research*, Vol. 24, No. 7, July 1988, pp. 1011–1023, DOI: 10.1029/WR024i007p01011.

- Garabedian, S. P., 1986, *Application of a Parameter-Estimation Technique to Modeling the Regional Aquifer Underlying the Eastern Snake River Plain, Idaho*, U.S. Geological Survey, Water Supply Paper 2278.
- Ge, S., 1998, "Estimation of Groundwater Velocity in Localized Fracture Zones from Well Temperature Profiles," *Journal of Volcanology and Geothermal Research*, Vol. 84, Nos. 1–2, August 1998, pp. 93–101, DOI: 10.1016/S0377-0273(98)00032-8.
- Goode, D. J. and L. F. Konikow, 1990, "Reevaluation of Large-Scale Dispersivities for a Waste Chloride Plume: Effects of Transient Flow," *ModelCARE 90: Calibration and Reliability in Groundwater Modelling, International Association of Hydrological Sciences, The Hague, The Netherlands, September 1990*.
- Greeley, R., 1982, "The Snake River Plain, Idaho: Representative of a New Category of Volcanism," *Journal of Geophysical Research*, Vol. 87, No. B4, April 1982, pp. 2705–2712, DOI: 10.1029/JB087iB04p02705.
- Hackett, W. R. and R. P. Smith, 1992, *Quaternary Volcanism, Tectonics, and Sedimentation in the Idaho National Engineering Laboratory Area*, EGG-M-92071.
- Helm-Clark, C. M., R. P. Smith, D. W. Rodgers, and C. F. Knutson, 2004, "Neutron Log Measurement of Moisture in Unsaturated Basalt," *Vadose Zone Journal*, Vol. 3, No. 2, May 2004, pp. 485–492, DOI: 10.2113/3.2.485.
- Hughes, S. S., P. H. Wetmore, and J. L. Casper, 2002, "Evolution of Quaternary Tholeiitic Basalt Eruptive Centers on the Eastern Snake River Plain, Idaho," *Tectonic and Magmatic Evolution of the Snake River Plain Volcanic Province*, Idaho Geological Survey Bulletin 30, pp. 363–385.
- Hughes, S. S., R. P. Smith, W. R. Hackett, and S. R. Anderson, 1999, "Mafic Volcanism and Environmental Geology of the Eastern Snake River Plain, Idaho," *Guidebook to the Geology of Eastern Idaho*, Pocatello: Idaho Museum of Natural History, pp. 143–168.
- IDWR, *Enhanced Snake Plain Aquifer Model Version 2.1 Final Report*, [http://www.idwr.idaho.gov/Browse/WaterInfo/ESPAM/ESPAM\\_2\\_Final\\_Report/ESPAM21FinalReport.pdf](http://www.idwr.idaho.gov/Browse/WaterInfo/ESPAM/ESPAM_2_Final_Report/ESPAM21FinalReport.pdf), published January 2013, website visited March 2017.
- Ingebritsen, S. E., D. R. Sherrod, and R. H. Mariner, 1992, "Rates and Patterns of Groundwater Flow in the Cascade Range Volcanic Arc, and the Effect of Subsurface Temperatures," *Journal of Geophysical Research: Solid Earth*, Vol. 97, No. B4, April 1992, pp. 4599–4627, DOI: 10.1029/91JB03064.
- Johnson, T. M., R. C. Roback, T. L. McLing, T. D. Bullen, D. J. DePaolo, C. Doughty, R. J. Hunt, R. W. Smith, L. D. Cecil, and M. T. Murrell, 2000, "Groundwater 'Fast Paths' in the Snake River Plain Aquifer: Radiogenic Isotope Ratios as Natural Groundwater Tracers," *Geology*, Vol. 28, No. 10, June 2000, pp. 871–874, DOI: 10.1130/0091-7613(2000)28<871:GFPITS>2.0.CO;2.
- Kuntz, M. A., S. R. Anderson, D. E. Champion, M. A. Lanphere, and D. J. Grunwald, 2002, "Tension Cracks, Eruptive Fissures, Dikes, and Faults Related to Late Pleistocene-Holocene Basaltic Volcanism and Implications for the Distribution of Hydraulic Conductivity in the Eastern Snake River Plain, Idaho," *Geology, Hydrogeology, and Environmental Remediation: Idaho National Engineering and Environmental Laboratory, Eastern Snake River Plain, Idaho*, Geological Society of America Special Paper 353, January 2002, pp. 111–133, DOI: 10.1130/0-8137-2353-1.111.
- Lewis, B. D. and F. J. Goldstein, 1982, *Evaluation of a Predictive Ground-Water Solute-Transport Model at the Idaho National Engineering Laboratory, Idaho*, U.S. Geological Survey, Water-Resources Investigations Report 82-25, March 1982.

- Luo, S., T. L. Ku, R. Roback, M. Murrell, and T. L. McLing, 2000, "In-situ Radionuclide Transport and Preferential Groundwater Flows at INEEL (Idaho): Decay-Series Disequilibrium Studies," *Geochimica et Cosmochimica Acta*, Vol. 64, No. 5, March 2000, pp. 867–881, DOI: 10.1016/S0016-7037(99)00373-7.
- Mann, L. J., 1986, *Hydraulic Properties of Rock Units and Chemical Quality of Water for INEL-1: a 10,365-foot-deep Test Hole Drilled at the Idaho National Engineering Laboratory, Idaho*, IDO-22070, February 1986.
- McLing, T. L., 1994, *The Pre-anthropogenic Groundwater Evolution at the Idaho National Engineering Laboratory, Idaho*, M. S. Thesis: Idaho State University, Pocatello, Idaho.
- McLing, T. L., R. W. Smith, and T. M. Johnson, 2002, "Chemical Characteristics of Thermal Water Beneath the Eastern Snake River Plain," *Geology, Hydrogeology, and Environmental Remediation: Idaho National Engineering and Environmental Laboratory, Eastern Snake River Plain, Idaho*, Geological Society of America Special Paper 353-13, pp. 205–211, DOI: 10.1130/0-8137-2353-1.205.
- MIT, 2006, *The Future of Geothermal Energy: Impact of Enhanced Geothermal Systems (EGS) on the United States in the 21st Century*, INL/EXT-06-11746, Idaho National Laboratory, November 2006.
- Morse, L. H. and M. McCurry, 2002, "Genesis of Alteration of Quaternary Basalts within a Portion of the Eastern Snake River Plain Aquifer," *Geology, Hydrogeology, and Environmental Remediation: Idaho National Engineering and Environmental Laboratory, Eastern Snake River Plain, Idaho*, Geological Society of America Special Paper 353.
- Olmsted, F. H., 1962, *Chemical and Physical Character of Ground Water in the National Reactor Testing Station, Idaho*, IDO-22043-USGS, May 1962.
- Pierce, K. L. and L. A. Morgan, 1992, "The Track of the Yellowstone Hotspot: Volcanism, Faulting and Uplift," *Regional Geology of Eastern Idaho and Western Wyoming, Geological Society of America Memoir 179*.
- Pierce, K. L. and L. A. Morgan, 2009, "Is the Track of the Yellowstone Hotspot Driven by a Deep Mantle Plume? — Review of Volcanism, Faulting, and Uplift in Light of New Data," *Journal of Volcanology and Geothermal Research*, Vol. 188, Nos. 1–3, November 2009, pp. 1–25, DOI: 10.1016/j.jvolgeores.2009.07.009.
- Roback, R. C., T. M. Johnson, T. L. McLing, M. T. Murrell, S. Luo, and T. L. Ku, 2001, "Uranium Isotopic Evidence for Groundwater Chemical Evolution and Flow Patterns in the Eastern Snake River Plain Aquifer, Idaho," *Bulletin of the Geological Society of America*, Vol. 113, No. 9, September 2001, pp. 1133–1141, DOI: 10.1130/0016-7606(2001)113<1133:UIEFGC>2.0.CO;2.
- Robertson, J. B., 1976, *Numerical Modeling of Subsurface Radioactive Solute Transport from Waste Seepage Ponds at the Idaho National Engineering Laboratory*, IDO-22057-C3.
- Robertson, J. B., R. Schoen, and J. T. Barraclough, 1974, *The Influence of Liquid Waste Disposal on the Geochemistry of Water at the National Reactor Testing Station, Idaho, 1952–1970*, IDO-22053.
- Saar, M. O., 2011, "Review: Geothermal Heat as a Tracer of Large-Scale Groundwater Flow and as a Means to Determine Permeability Fields, Special Theme Issue on Environmental Tracers and Groundwater Flow, Editor-Invited Peer-Reviewed Contribution," *Hydrogeology Journal*, Vol. 19, No. 1, pp. 31–52, DOI: 10.1007/s10040-010-0657-2.

- Shervais, J. W., D. R. Schmitt, D. Nielson, J. P. Evans, E. H. Christiansen, L. Morgan, W. C. Pat Shanks, A. A. Prokopenko, T. Lachmar, L. M. Liberty, D. D. Blackwell, J. M. Glen, L. D. Champion, K. E. Potter, and J. A. Kessler, 2013, "First Results from HOTSPOT: The Snake River Plain Scientific Drilling Project, Idaho, U.S.A.," *Scientific Drilling*, Vol. 15, March 2013, pp. 36–45, DOI: 10.2204/iodp.sd.15.06.2013.
- Smith, L. and D. S. Chapman, 1983, "On the Thermal Effects of Groundwater Flow: 1. Regional Scale Systems," *Journal of Geophysical Research: Solid Earth*, Vol. 88, No. B1, January 1983, pp. 593–608, DOI: 10.1029/JB088iB01p00593.
- Smith, R. P., 2004, "Geologic Setting of the Snake River Plain Aquifer and Vadose Zone," *Vadose Zone Journal*, Vol. 3, No. 1, February 2004, pp. 47–58, DOI: 10.2136/vzj2004.4700.
- Stearns, H. T., 1936, "Origin of the Large Springs and their Alcoves along the Snake River in Southern Idaho," *The Journal of Geology*, Vol. 44, No. 4, May/June 1936, pp. 429–450.
- Stearns, H. T., L. Crandall, and W. G. Steward, 1938, *Geology and Ground-Water Resources of the Snake River Plain in Southeastern Idaho*, U.S. Geological Survey, Water-Supply Paper 774.
- Twining, B. V. and R. C. Bartholomay, 2011, *Geophysical Logs and Water-Quality Data Collected for Boreholes Kimama-1A and -1B, and a Kimama Water Supply Well Near Kimama, Southern Idaho*, DOE/ID-22215, U.S. Department of Energy Idaho Operations Office.
- Welhan, J. A. and M. F. Reed, 1997, "Geostatistical Analysis of Regional Hydraulic Conductivity Variations in the Snake River Plain Aquifer, Eastern Idaho," *Bulletin of the Geological Society of America*, Vol. 109, No. 7, July 1997, pp. 855–868, DOI: 10.1130/0016-7606(1997)109<0855:GAORHC>2.3.CO;2.
- Whitehead, R. L., 1986, *Geohydrologic Framework of the Snake River Plain, Idaho and Eastern Oregon*, U.S. Geological Survey, Hydrologic Atlas 681.
- Whitmire, D. L., 2003, *2003 Update to the Test Area North Large-Scale Groundwater Flow and Transport Model for the Assessment of Monitored Natural Attenuation*, INEEL/INT-03-00709, Idaho National Engineering and Environmental Laboratory, November 2003.
- Wood, T. R., B. R. Orr, C. M. Helm-Clark, M. S. Roddy, H. Huang, M. J. Rohe, S. O. Magnuson, M. A. Plummer, T. McLing, and R. K. Podgorney, 2005, *Operable Unit (OU) 10-08 Summary Report on the Subregional Scale Two Dimensional Aquifer Model*, ICP/EXT-05-00979, Idaho Cleanup Project, October 2005.
- Wood, W. W. and W. H. Low, 1986, "Aqueous Geochemistry and Diagenesis in the Eastern Snake River Plain Aquifer System, Idaho," *Bulletin of the Geological Society of America*, Vol. 97, No. 12, December 1986, pp. 1456–1466, DOI: 10.1130/0016-7606(1986)97<1456:AGADIT>2.0.CO;2.
- Ziagos, J. P. and D. D. Blackwell, 1986, "A Model for the Transient Temperature Effects of Horizontal Fluid Flow in Geothermal Systems," *Journal of Volcanology and Geothermal Research*, Vol. 27, Nos. 3–4, March 1986, pp. 371–397, DOI: 10.1016/0377-0273(86)90021-1.

## CHAPTER 2: The Application of Radon for Mapping Open Fracture Networks in a Thin Vadose Zone Underlain by Granite Rock, Fort Devens, Massachusetts

“The Application of Radon for Mapping Open Fracture Networks in a Thin Vadose Zone Underlain by Granite Rock, Fort Devens, Massachusetts.” Accepted *Vadose Zone Journal*.

Travis L. McLing,<sup>a,b,\*</sup> William Brandon,<sup>c</sup> Bernie Zavala,<sup>d</sup> Robert W. Smith,<sup>e</sup> Casey Smith,<sup>a</sup> Trent Armstrong,<sup>a</sup> and Michael Carpenter<sup>a</sup>

<sup>a</sup> Idaho National Laboratory, P.O. Box 1625, Idaho Falls, ID 83415-2107, USA

<sup>b</sup> The Center for Advanced Energy Studies, 995 University Blvd., Idaho Falls, ID 83401, USA

<sup>c</sup> U.S. EPA Region 1, Suite 100, Boston, MA 02109, USA

<sup>d</sup> U.S. EPA Region 10, 1200 6th Avenue, Suite 900, Seattle, WA 98101, USA

<sup>e</sup> University of Idaho, Moscow, ID 83844, USA

\* Corresponding author: Travis L. McLing; E-mail: [travis.mcling@inl.gov](mailto:travis.mcling@inl.gov); Telephone: 012085267269; Fax: 012085260875

### Abstract

The use of naturally occurring tracers to elucidate subsurface flow and transport of water and gases through fractured vadose zones represents a powerful and inexpensive methodology for understanding geologic systems. Our study was conducted at Shepley’s Hill, a highly fractured granite highland at the former Fort Devens military base. This study evaluates the applicability of using cheap, readily available, passive radon detectors to identify conductive structures (e.g., fractures and fracture networks) in fracture-dominated vadose zones.

Results from the Shepley’s Hill study show a clear spatial correlation of elevated  $^{222}\text{Rn}$  concentrations emanating from fracture zones previously identified by independent geologic studies. At Shepley’s Hill, the  $^{222}\text{Rn}$  concentrations measured from detector locations directly above the major bedrock fractures, located within the Disc Golf Fracture Zone (DGFZ) and the Nona-Shep Fracture Zone (NSFZ), were almost exclusively the highest values measured in the study. Conversely, probes located above areas of less-fractured bedrock, although highly fractured, showed relatively low  $^{222}\text{Rn}$  concentrations. These two observations provide strong supporting evidence that not all fractures are equal when it comes to their ability to transmit gas and by-inference water into and out of the subsurface. Based on the results of this study,  $^{222}\text{Rn}$  is an environmental tracer capable of efficiently detecting major bedrock fracture sets in the vadose zone that readily transport gas and may be responsible for focusing water infiltration into contaminated aquifers.

**Keywords:** Radon, Fort Devens, vadose zone, fracture networks, CR-39



## 2.1 Introduction

It has long been recognized that preferential flow, primarily through interconnected fracture networks, dominates contaminant transport at many contaminated sites. The presence of these preferred transport pathways makes it extremely difficult to both model and remediate subsurface contamination. Therefore, the ability of scientists and engineers to locate conductive fracture networks (i.e., those responsible for the vast majority of the transport) is critical to successful remediation and monitoring of fracture-dominated sites. Measuring the distribution of  $^{222}\text{Rn}$  concentration at the soil-bedrock interface represents a fast, inexpensive way to identify these important open-fracture networks. This information can be used to create a more-accurate conceptual model for transport modeling and related cleanup activities. It may also allow for mitigation for fluid pathways by local capping or grouting of the most fractured pathways.

Studies conducted at sites with fractured-rock vadose zones have shown that the flow of water through the fractured rock into the underlying aquifer is generally rapid and focused to narrow zones of interconnected permeability (Wood et al. 2004; Faybishenko et al. 2000, 2001; NRC 2000; Fabryka-Martin et al. 1996; Davidson et al. 1998). These studies conclude that one of the major limitations to understanding contaminant transport is the ability to identify and characterize these preferential zones of interconnected permeability. In this study, we used the flux of  $^{222}\text{Rn}$  to locate fracture sets with relatively higher permeability than the rock matrix and other impermeable fractures, and by inference these same fractures may be able to more quickly transmit water to the aquifer.

The inability to effectively identify and characterize fractures and fracture networks has resulted in cleanup strategies that rely upon the use of an equivalent porous media (EPM) approach (Bear 1988) to model contaminant transport at fractured-rock-hosted sites (Hao et al. 2008). The EPM approach fails in that it cannot account for episodic and localized fracture flow within both the vadose zones and aquifers, which accounts for a significant amount of water and contaminant movement through these systems. As a result, dual-porosity approaches have been developed to account for matrix and fracture porosity (Gerke and van Genuchten 1993; Duguid and Lee 1977). Although dual-porosity approaches provide a better representation of the interactions between fracture and matrix permeability than does the EPM approach, a more robust and defensible approach is to identify the location and characteristics of the permeable fracture networks themselves.

Fracture network characterization, coupled with recent advances in discrete fracture network (DFN) modeling, has improved the ability to model real fracture networks (McClure and Horne 2013). However, at many sites, accurate mapping of fracture networks is difficult and expensive because of soil and vegetation cover and the sheer number of fractures. In addition, only a fraction of all fracture

networks at a given site are capable of transporting water and contaminants (Dershowitz et al. 2002; Wood et al. 2002); this poses additional characterization and modeling challenges. To partially address this characterization challenge, we have evaluated the effectiveness of using naturally occurring  $^{222}\text{Rn}$  to identify the locations of active fracture networks in near-surface fractured bedrock responsible for preferential water infiltration into the subsurface. We hypothesize that areas near the soil-bedrock interface, where open fractures exist, will exhibit elevated concentrations of  $^{222}\text{Rn}$  activity, due to the greater flux of gases within active fracture systems, and that these fluxes can be quantified by deploying inexpensive, off-the-shelf, CR-39 radon detectors.

Multiple studies report the use of radon emissions from natural systems to gain insight into faults and fractures associated with tectonic, volcanic, and geothermal systems (Abumuradet al. 1997; Zhang and King 1994; Akawwi 2014; King 2010; Richon et al. 2010; Manavhela 2007; Baixeras et al. 2001; Burton et. al 2004; Mazur et al. 1999; King et al. 1996; Zang and King 1994). Four of these studies are briefly described here; a more detailed discussion can be found in Manavhela (2007). Swakoń et al. (2004) successfully used CR-39 film to investigate elevated radon concentration in soils along active fault zones within the Krakow region of Poland and concluded that fractures in the underlying bedrock resulted in elevated radon concentrations in the overlying soil. İnceöz et al. (2006) investigated the seasonal variation in radon concentration associated with natural geothermal activity related to the Anatolian fault systems in Turkey. They concluded that radon anomaly near the fault zones is relatively high and decreases rapidly with distance from the fault trace. Moloney et al. (2010) used a suite of naturally occurring gases, including radon, to characterize the large volcanic system at Yellowstone National Park. Maloney concluded that, in that system, there is a weak correlation between  $\text{CO}_2$  and radon, indicating that  $\text{CO}_2$  emissions may be a carrier to get radon to the surface, and that the radon is sourced from the rocks in the shallow subsurface, not magmatic degassing. They were also able to conclude by comparing radon isotope data and major element chemistry that solute transport at Yellowstone is much longer than radon half-lives. Richon et al. (2010) studied the transport potential of  $^{222}\text{Rn}$  in a fault system in the Qinghai Province, China. In this study, the emanation of radon measured at the bedrock contact in a trench across a fault trace was two orders of magnitude higher than was measured in the soil horizon, illustrating the importance of understanding the influence of soil cover when interpreting environmental radon concentrations.

Here, we describe a study using CR-39 detectors at contaminated, fractured, granitic bedrock sites. The study was conducted over a 22-day period in August 2012, with rapidly deployable measurement ports (RDMP) being installed over a two-day period. CR-39 radon detectors were placed and allowed to monitor  $^{222}\text{Rn}$  flux over a 20-day period.

### 2.1.1 Site Description

The study site is located 35 miles west of Boston, near the towns of Ayer and Shirley in Middlesex County, Massachusetts, and is proximal to the Shepley's Hill Landfill (located on the former Fort Devens; Figure 2.1). The landfill was active from 1917 until 1992 and was closed and capped in 1993. Fort Devens was listed on the National Priorities List (NPL) in November 1989. A remedial investigation was conducted in 1995 (ABB-ES 1995) and identified arsenic in the aquifer beneath the landfill as the principal threat to human health and the environment.

Although the landfill is capped, there continues to be a significant influx of meteoric water entering the landfill, resulting in continued mobilization of contaminants. Based on rapid and large-amplitude changes in water levels in boreholes drilled into the hill, Shepley's Hill, located directly west of the landfill, is the suspected primary recharge area for groundwater entering the landfill (Harding ESE 2003). Harding ESE (2003) concludes that infiltration due to meteoric precipitation on Shepley's Hill is the dominant source of recharge to the landfill.

Shepley's Hill covers an area of approximately 0.34 km<sup>2</sup>, rising to 38 m above the rather-flat topography of the surrounding area. Nonacoicus Brook and the Nashua River cut the topography of Shepley's Hill to the north and west (Figure 2.1). Only a fraction of Shepley's Hill granitic bedrock is exposed; a layer of soil covers the remainder of the hill, ranging from a few cm to more than 1.5 m thick (as encountered in this study). The maximum soil cover encountered by Gannett Fleming, Inc. (2012) was more than 3.5 m.

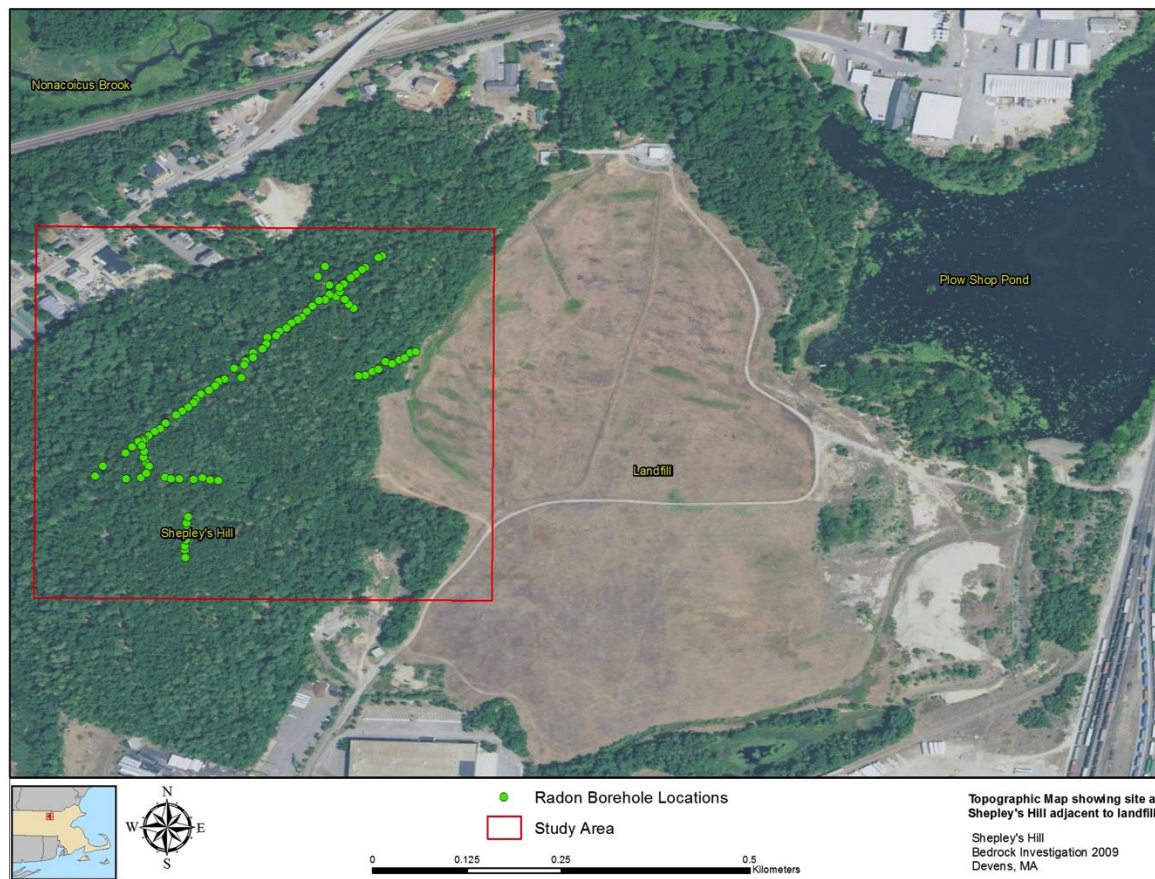


Figure 2.1: The study area is comprised of a highly fractured granite highland known as Shepley’s Hill and is located immediately west of the Fort Devens Landfill. Shepley’s Hill is a known recharge area for the aquifer recharging the Fort Devens Landfill.

A detailed description of the geology of Shepley’s Hill can be found in Koteas et al. (2010), Kopera (2008), and Robinson (1981), and is summarized here. Shepley’s Hill is entirely comprised of two granites: the early Silurian Ayer Granodiorite and early Devonian Chelmsford Granite. The Ayer Granodiorite underlies most of Shepley’s Hill, with the Chelmsford Granite occurring only in a narrow finger extending under the landfill along the eastern boundary of Shepley’s Hill (Figure 2.2). Faulting in the area immediately surrounding Shepley’s Hill is associated with the Late Devonian Clinton-Newbury Fault Zone. The intense fracturing that occurs at Shepley’s Hill site (gray lines, Figure 2.2) is the result of multiple generations of faulting and shearing over the past 320 Ma. The Shepley’s Hill scale fracture network and fault zones shown in Figure 2.2 have been located by a combination of direct measurement in the field and a combination of remote sensing techniques, including a high-resolution, ground-penetrating radar (GPR).



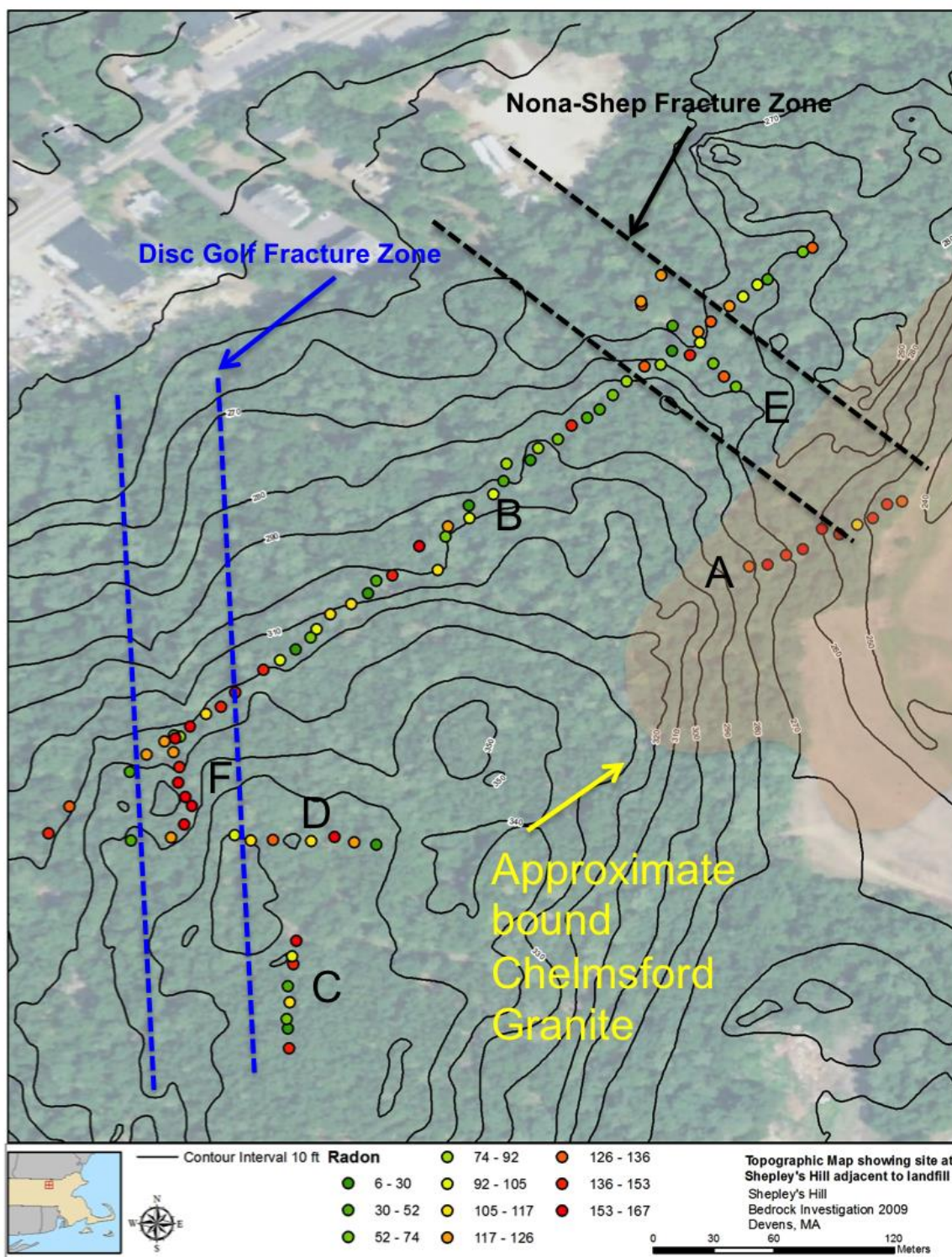


Figure 2.2: The location of the major DGFZ and NSFZ and the contact between the Chelmsford and Ayer granites relative to the transects used to collect radon data in this study.

Two prominent structural features are exposed at Shepley's Hill: (1) the Nona-Shep Fracture Zone (NSFZ), which cuts the hill from southeast to northwest, and (2) the Disc Golf Fracture Zone (DGFZ), which trends north to south (Gannett Fleming, Inc. 2012; Figure 2.2). These structural features are local manifestations of the regional fracture system that cuts the granitic basement rocks of the area. The DGFZ and the NSFZ express themselves in the surface topography as distinct linear valleys indicative of steeply dipping fracture zones within the granitic bedrock. Both of these major fracture zones are expressed as linear topographic depressions 30–35 meters wide, extending hundreds of meters laterally.

### **2.1.2 Fracture and Water Transport**

The goal of this study was to assess the relationship between radon emission and the presence of active fracture networks on Shepley's Hill that have been implicated as recharge pathways for water entering the Shepley's Hill Landfill. Critical to our conceptual model is that fractures that actively transport vadose zone gases are also able to preferentially transport water through the vadose zone. As discussed above, there is a wealth of studies that have shown that water is transmitted through the vadose via preferential flow paths. Whether or not these preferred pathways are also the primary conduits for gas transport is not clear; however, previous researchers (Gannett Fleming, Inc. 2012) have concluded that recharge from the 0.34 km<sup>2</sup> is the dominant source of recharge to the landfill. This conclusion is based on water level response to precipitation events in monitoring wells located along the contact between Shepley's Hill and the landfill. Therefore, it is not unreasonable to conclude that same zone of interconnected permeability that preferentially transports a vadose zone gas is also implicated in the transport of water into the landfill.

Figure 2.3 shows the stylized relationship between active fractures and the flux of <sup>222</sup>Rn (a decay product of <sup>238</sup>U) released from minerals in the rock and transported through the vadose zone by a conductive fracture network. We hypothesize that, even in a heavily fractured system, only a small subset of fractures preferentially dominate vadose recharge, and that these fractures will exhibit higher <sup>222</sup>Rn emission relative to other less-communicative fractures (fractures where gas flow is significantly restricted). To evaluate this hypothesis, CR-39 detectors were used to measure radon along a series of transects on Shepley's Hill that encompassed the DGFZ and NSFZ, as well as areas not identified as fracture zones.

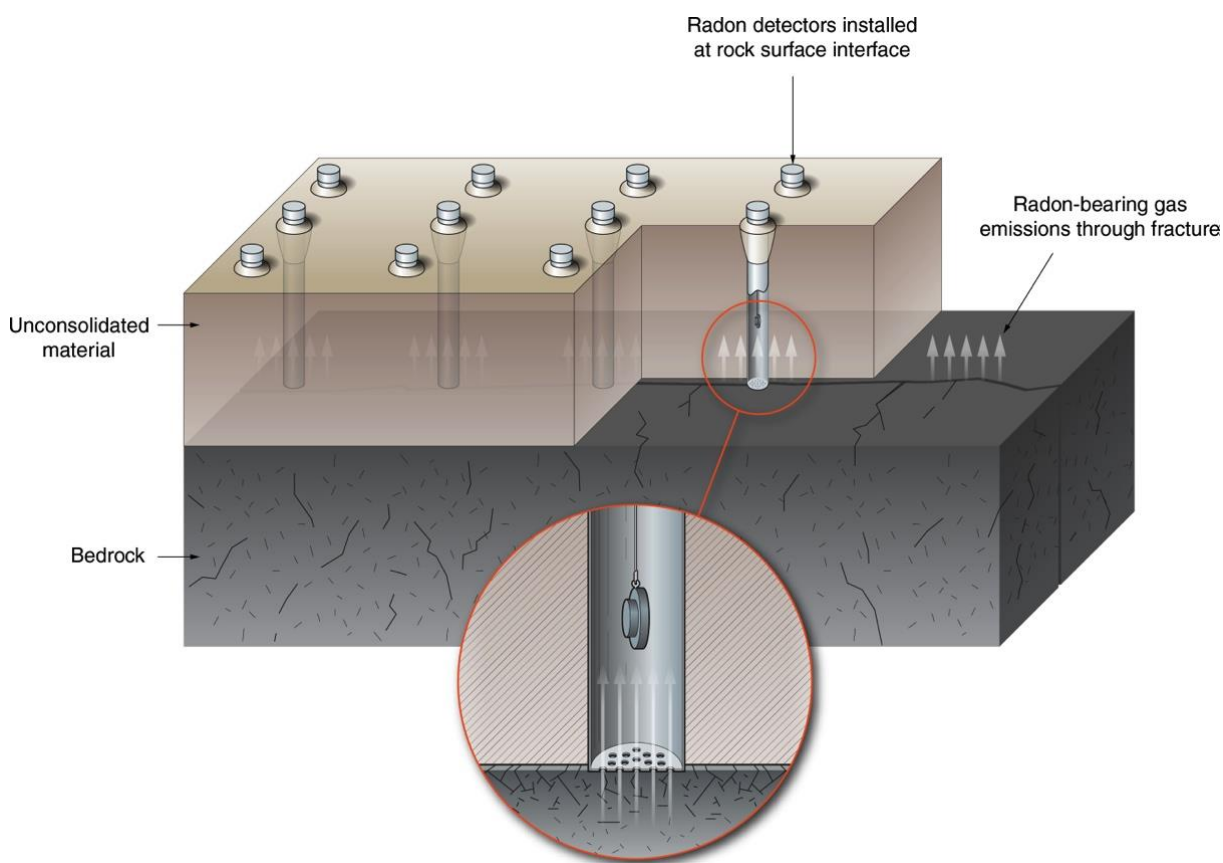


Figure 2.3: The stylized relationship between an active fracture emitting radon and a detection network that can measure the emanation at the soil-bedrock interface. Areas of high radon emanation are associated with open or active flow pathways in the bedrock.

### 2.1.3 Radon

Radon is a naturally occurring radioactive noble gas that is ubiquitously distributed in the earth's crust as a result of the radioactive decay series of uranium and thorium isotopes. In the environment, radon exists primarily as three isotopes:  $^{219}\text{Rn}$  progeny (half-life 3.96s),  $^{220}\text{Rn}$  (half-life 55.6s), and  $^{222}\text{Rn}$  (half-life 3.83d). These radon isotopes are produced as a decay product of  $^{235}\text{U}$  ( $^{219}\text{Rn}$ ),  $^{238}\text{U}$  ( $^{222}\text{Rn}$ ), and  $^{232}\text{Th}$  ( $^{220}\text{Rn}$  thoron) (Cecil and Green 2000).  $^{222}\text{Rn}$  is distributed in the crust as a function of the concentration of uranium in bedrock and the resulting alluvium. We focused our study on  $^{222}\text{Rn}$ ; other isotopes of radon (e.g.,  $^{219}\text{Rn}$  and  $^{220}\text{Rn}$ ) were not considered in this study due to their decay properties.  $^{219}\text{Rn}$ , with its 3.96s half-life, is excluded from detection as it decays to an insignificant level before it can be transported to the detector.  $^{220}\text{Rn}$ , with its 55.6s half-life, is excluded from detection by the RDMP, which is an effective diffusion barrier (Figure 2.3) that increases travel time, allowing the  $^{220}\text{Rn}$  to decay to an insignificant level before reaching the CR-39 detector. The CR-39 detectors are configured to allow ambient soil gas to diffuse through a filter into a detection chamber where the CR-39 film is located.

Radon is enriched at mineral surfaces and in porewater due to preferential dissolution from crystallographic defects created by alpha recoil during the decay of  $^{226}\text{Ra}$  (Kigoshi 1971). The ~100 keV alpha-recoil kinetic energy released when  $^{226}\text{Ra}$  decays to  $^{222}\text{Rn}$  (Cecil and Green 2000; Sun and Furbish 1995) ejects the progeny  $^{222}\text{Rn}$  atom out of the host mineral from the region within 63  $\mu\text{m}$  of the mineral surface (Kigoshi 1971). Once in the pore region, some of the newly formed radon atoms, which originate in or on the surface of mineral grains, escape into the pore space, where they diffuse within the groundwater or the vadose zone gas. Some of the radon atoms find their way to the surface, where they enter the atmosphere. In most vadose zone systems, only 10–50% of the radon produced actually escapes from the mineral grains and enters the pore space or fracture aperture (Otton 1992). Radon transport can be facilitated by barometric pumping in vadose zones (Abbas 2011; Auer 1996). Because the vadose zone at Shepley's Hill is not very thick, gaseous diffusion is not considered important in this study. A study by Fukui (1987) found a strong correlation between vadose-zone radon concentration and barometric-pressure fluctuations due to barometric pumping.

Another factor that can influence the transport of  $^{222}\text{Rn}$  is humidity (Porstendörfer, J., and Mercer 1978; Yamanishi et al 1991). Although humidity can have a large impact on the transport of  $^{222}\text{Rn}$ , this impact is only observed across wide humidity ranges. For example, Porstendörfer, J., and Mercer (1978) found that in moist air (30% < relative humidity < 90%), the diffusivity of the positively charged  $^{222}\text{Rn}$  atoms was 0.068 and 0.004  $\text{cm}^2/\text{sec}$ , respectively, while it was about 0.024  $\text{cm}^2/\text{sec}$  in exceptionally dry air. At Shepley's Hill, the humidity stayed at approximately 90% in the vadose throughout the study; therefore, the effect of humidity was not considered. Because of the short duration of our study (21 days), the vadose zone humidity was assumed to be constant.

## 2.2 Materials and Methods

### 2.2.1 Passive Radon Detection

Radon concentrations were determined using a Rapidly Deployable CR-39 Measurement Port (RDMP) (Figure 2.4) system that was designed for this study. The RDMP allowed for rapid installation of numerous CR-39 detectors while protecting detectors from impact and from potential sources of atmospheric contamination. Individual RDMPs were readily adaptable to variations in soil thickness, and because they were constructed using materials readily available at hardware stores, cost less than \$20 each in 2012, including the CR-39 detector.



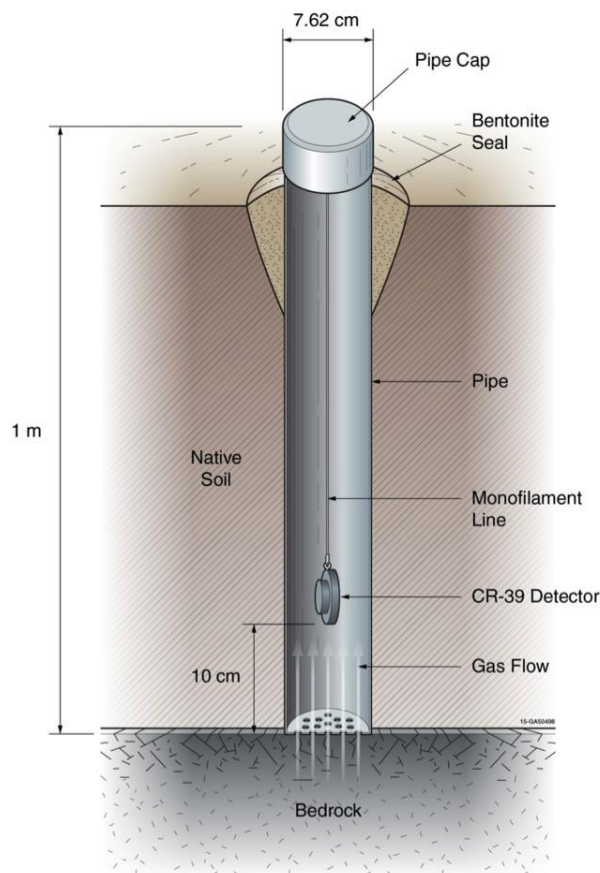


Figure 2.4: How the Rapidly Deployable CR-39 Measurement Port (RDMP) is installed in the soil column and its position relative to the soil-bedrock interface.

Standard off-the-shelf CR-39 detectors were purchased in bulk from AccuStar in Medway, Massachusetts. The CR-39 detectors were made of Columbia Resin #39 (CR-39), an allyl diglycol carbonate, which is a plastic polymer commonly used to manufacture lenses for eyeglasses. When used as an alpha radiation detection medium, the CR-39 film is exposed directly to the radiation source (Mishra et al. 2005). As the radon decays, the resulting energetic alpha particles create submicroscopic damage tracks across the surface of the CR-39 film, much like bullets passing through ballistic media. After deployment for a fixed period of time (in the case of this study, 21 days) the CR-39 detectors were returned to the manufacturer for their evaluation and quantification. The damage tracks are accentuated by placing the CR-39 film into a caustic etching bath with a voltage applied. The accentuated tracks are then counted by a computer-controlled video imaging system. The number of tracks per unit of analyzed detector area produced per unit of time (minus the background) is converted to an equivalent radon concentration, based on a manufacture-proprietary protocol. Because the CR-39 detector measures the total number of alpha tracks per unit area of the detector over the sensor deployment time, the resulting concentrations do not represent the concentration of  $^{222}\text{Rn}$  in the

soil gas at any specific time, but rather the average concentration of  $^{222}\text{Rn}$  that would yield the equivalent number of background-corrected tracks over the time of the deployment. As a result, the reported concentrations are averaged over the deployment time and important to this study, proportional to the  $^{222}\text{Rn}$  flux through the detection chamber.

CR-39 detectors are routinely capable of a lower limit of detection (LLD), calculated using methods described by Altshuler and Pasternack (1963) of 1.0 picocurie per liter (pCi/L) or less. AccuStar reports an LLD of  $0.4 \text{ pCi L}^{-1}$ , with a relative standard deviation (RSD) of less than 10% at  $4 \text{ pCi L}^{-1}$  or greater. AccuStar's quality-assurance program followed the protocol outlined in EPA 520-402-R-92-004 (U.S. EPA 1992c) and included the following four parts: (1) calibration of optical counter, (2) background measurements, (3) repeated measurements, and (4) routine instrument checks (<http://www.accustarlabs.com/support/testing-protocols/dprotocols2.aspx#2.2>).

In this study, the concentration of  $^{222}\text{Rn}$  in soil gas was a major concern because the project was not afforded the opportunity to conduct background concentration measurements. Therefore, we took great care in developing a methodology that would shield the detectors from  $^{222}\text{Rn}$ -contaminated dust and dirt, and especially radon that originates from elsewhere in the study area. Additionally, we needed to be able to deploy the detectors near the soil-rock interface to ensure that the measurement point was representative of the underlying rock, not from elsewhere. To address these concerns, our team designed a deployment methodology that would allow for rapid installation of numerous detectors within a short period of time while protecting them from potential sources of contamination.

The RDMP (Figure 2.5) was designed and employed for this study. This port could easily be adapted to variations in soil thickness and could be constructed using materials readily available at local hardware stores. Additionally, the low cost for each detector and RDMP allowed for more to be deployed at the study site, effectively increasing our survey size significantly. Initially, the study had called for 35 detectors to be deployed, but because the cost of detectors and RDMPs were inexpensive the team was able to install 92 ports across Shepley's Hill.

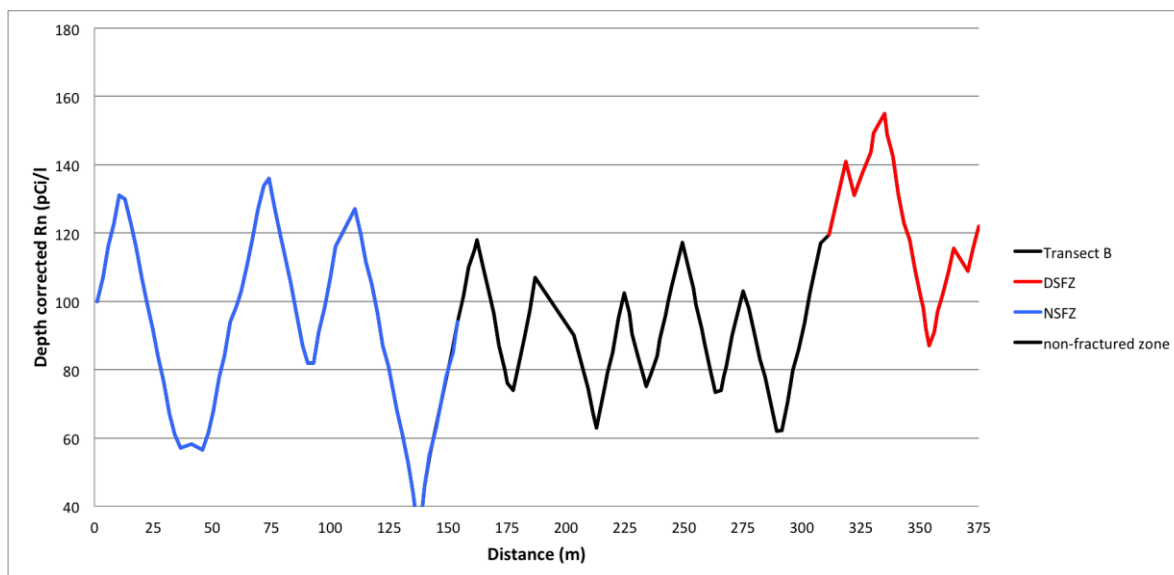


Figure 2.5: Plot of  $^{222}\text{Rn}$  data from Transect B showing the relationship between concentration and proximity to the DGFZ, NSFZ, and the non-fracture zones.

### 2.2.2 Transect Design

Transect locations and individual RDMP positions were surveyed using GPS with the RDMPs' sample positions marked with colored flags. At each RDMP location, a 0.1-m-diameter hole was augured through the soil to the soil-bedrock interface using a hand-held motorized auger operated by two of the field crew. The RDMP ports were placed in bored holes at the soil-bedrock interface. The soil-bedrock contact was defined as the point where the auger was stopped by large chunks of granite that could not easily be removed. In each case the hole was further cleaned using a handheld clamshell posthole digger and by hand excavating chunks of regolith to allow for the RDMP to be deployed as near the bedrock soil contact as possible. The annulus area around the RDMP was backfilled with native soil to within 0.15 m of ground surface, which was sealed with wetted bentonite to prevent water flow down the annulus of the probe (Figure 2.4). The CR-39 detectors were placed in the RDMP near the bottom, suspended by heavy-gauge monofilament. Each detector came with two identification tags: one was left on the detector and the other was recorded and then placed in the field book next to the RDMP number.

### 2.2.3 Transect Design and Deployment

Ninety-two RDMPs were deployed at 7.5-m intervals in transect lines. Transect alignments were selected to evaluate the major fracture systems (DGFZ and NSFZ) as well as less-fractured area on Shepley's Hill (Figure 2.2). Transects A, B, C, and F are generally aligned orthogonal to the DGFZ and NSFZ. Two shorter transect lines, D and E, were positioned within and parallel to the strike of the

fracture zones. The southernmost transect (Transect C) was located in an area of relatively fewer fractures in the bedrock (Gannett Fleming, Inc. 2012). At some RDMP deployment locations, placement was complicated by the presence of large rocks and thick roots. Great care was taken to place each of the RDMPs at their preselected and mapped locations. Except for a few cases, each RDMP was emplaced within a few centimeters of its flagged position. The conditions at each RDMP location, such as the difficulty with installation, presence of roots, and any off-transect axis installation that resulted, were recorded in the master field book.

#### 2.2.4 Detector Deployment

The CR-39 detectors were deployed for 21 days, resulting in sufficient  $^{222}\text{Rn}$  exposure (Table 2.1). The goal of this study was not to quantify the exact  $^{222}\text{Rn}$  flux of the area, but rather to find areas of Shepley's Hill where the flux of radon is higher, relative to other areas, as a proxy for high-water infiltration zones.

Table 2.1: The data at Fort Devens show a wide range of  $^{222}\text{Rn}$  concentrations, ranging from a low of 6.6 pCi/L in Transect B to a maximum (valid) of 163 pCi/L in Transect A. 167 pCi/L is the maximum concentration that can be measured by a CR-39. Values of 167 pCi/L should be considered the minimum value measured at the location. Normalized mean = concentration measure value/pCi/L/6.6 (lowest measured value).

Transect	Number of Probes	Concentration			
		Minimum	Maximum	Mean	Normalized Mean
A	9	117.0	163	144.9	21.95
B	51	6.6	167	91.9	13.66
C	8	30.0	147	100.5	15.20
D	10	26.0	157	107.0	16.20
E	8	43.0	153	105.5	16.00
F	6	122.0	>167	115.3	23.54

Originally we had planned to deploy the detectors for 10 days; however, due to unforeseen personnel complications, the deployment time was increased to 21 days. In retrospect, the additional 11 days was beneficial to our study in that it is likely the originally planned 10-day deployment would have resulted in a large number of detectors being reported as below detection limits. Although it was fortuitous that the deployment was longer than planned, it does illustrate the importance of conducting a pre-study survey of the  $^{222}\text{Rn}$  flux. A pre-study survey was a luxury this study was not afforded, due to the short period of performance for the project and the distance from the team's home base.

Analytical results obtained for the 92 CR-39 detectors are presented in Table 2.1. The results were reported as concentrations of  $^{222}\text{Rn}$  in soil-gas units of picocuries per liter (pCi/L). Of the 92 detectors,

six had analytical results flagged by the AccuStar Laboratory as “oversaturated,” due to the reported concentration exceeding the maximum calibration range at 167 pCi/L. While these overexposed detectors did not yield a precise measure, the data does provide information that the exposure at the RDMP location is greater than 167pCi/L, thereby indicating that at that sample location the detector was located in a high-flux area, which can then be compared to neighboring detectors. The data in Table 2.1 show a wide range of  $^{222}\text{Rn}$  concentrations, ranging from a low of 6.6 pCi/L in Transect B to a high of greater than 167 pCi/L in Transects B, C, and F (Table 2.1). A more illustrative depiction of the data is provided in Figure 2.5, where we plot the soil depth normalized  $^{222}\text{Rn}$  concentrations vs. distance for transect B.

## 2.3 Results and Discussion

### 2.3.1 Ayer Granodiorite vs. Chelmsford Granite U Concentration

Although all rocks contain some uranium, rock types such as granites, some sedimentary, and metamorphic rocks derived from these rocks have uranium concentrations of up to 100 ppm (Larsen and Gottfried 1961), which is significantly higher than the  $2.7\pm 0.6$  ppm average for continental crust. Whole rock data from the Chelmsford Granite and Ayer Granodiorite sampled just north of the study site report uranium concentrations of 9.65 ppm and 3.11 ppm, respectively (Walsh et al. 2013). Because these rocks are sufficiently old, uranium is in secular equilibrium with its daughter products, including  $^{222}\text{Rn}$ . Therefore, the higher the uranium concentration in the parent rocks, the higher the radon concentration. All other things being equal, we would expect that Transect A, being located in the Chelmsford, would have radon values of  $\sim 3\times (9.65/3.11)$  that of transects located in the Ayer. A plausible explanation for the high values found in the southeast portion of the NSFZ is a result of change in rock (and U) type rather than an increase in conductivity of the fracture zone.

### 2.3.2 Data Summary

Reported CR-39 detector concentration data (Table 2.1) used in this study have a linear relationship. That is, the number of alpha tracks counted for a detector that has a reported value of 100 pCi/L has two times more fission tracks than does a detector that has a reported concentration of 50 pCi/L. In this study, we present the raw data, mean values, and normalized data. Normalization is done to condition the data presented to a common datum, making the measured values directly comparable to each other. In our study we normalized the raw  $^{222}\text{Rn}$  data to the lowest-measured value (6.6 pCi/L) to better establish relationships between  $^{222}\text{Rn}$  concentrations measured across the study area and to the depth of the soil layer at the measurement point (Table 2.1).

Both normalized  $\text{pCi/L}_{(N)}$  and raw  $\text{pCi/L } ^{222}\text{Rn}$  data measured by the 92 CR-39 detectors deployed in this study from all six transects are presented in Table 2.1. The data presented in Figure 2.2 show the position of the six transects, the location of each measurement point, and the associated  $^{222}\text{Rn}$  concentration overlaid upon a map of known major fractures at the study site. Transect A has a narrow range of concentrations with a mean  $^{222}\text{Rn}$  concentration of 144.9  $\text{pCi/L}$  (21.95  $\text{pCi/L}_{(N)}$ ), a high value of 163  $\text{pCi/L}$  (24.7  $\text{pCi/L}_{(N)}$ ), and a low value of 117  $\text{pCi/L}$  (17.17  $\text{pCi/L}_{(N)}$ ). The  $^{222}\text{Rn}$  data from the CR-39 detectors from Transects B, C, and D have mean-normalized  $^{222}\text{Rn}$  concentrations of 91.9  $\text{pCi/L}$  (13.66  $\text{pCi/L}_{(N)}$ ), 100.5  $\text{pCi/L}$  (15.2  $\text{pCi/L}_{(N)}$ ), and 107  $\text{pCi/L}$  (16.2  $\text{pCi/L}_{(N)}$ ), respectively (Table 2.1). The  $^{222}\text{Rn}$  concentration in Transect B has a broad range in values from a high of  $>167$   $\text{pCi/L}$  to the lowest-measured value of 6.6  $\text{pCi/L}$ . The highest  $^{222}\text{Rn}$  values are associated with the distal areas where this transect crosses both the NSFZ on the northeast and DGFZ on the southwest (Figure 2.2). The  $^{222}\text{Rn}$  concentration in Transect C ranges widely from  $>167$   $\text{pCi/L}$  (25.3  $\text{pCi/L}_{(N)}$ ) to a low of 30  $\text{pCi/L}$  (4.5  $\text{pCi/L}_{(N)}$ ) in a random fashion across a relatively small area. Transect E also has a wide range of measured  $^{222}\text{Rn}$  concentrations, ranging from 43  $\text{pCi/L}$  (6.62  $\text{pCi/L}_{(N)}$ ) to 153  $\text{pCi/L}$  (23.14  $\text{pCi/L}_{(N)}$ ), with a mean value of 105  $\text{pCi/L}$  (15.98  $\text{pCi/L}_{(N)}$ ). Transect F, which is located entirely within the mapped extent of the DGFZ, has a mean concentration of 115.3  $\text{pCi/L}$  (23.5  $\text{pCi/L}_{(N)}$ ), with three of the six detectors exceeding the maximum detection limit of 167  $\text{pCi/L}$ .

### 2.3.3 Statistical Analysis

#### 2.3.3.1 $^{222}\text{Rn}$ Data

Normalized  $^{222}\text{Rn}$  data from the 92 detectors from Transects A through F and the position of these transects relative to the DGFZ and NSFZ are shown in Figure 2.52. The data show that there are zones of both high- and low- $^{222}\text{Rn}$  activity.  $^{222}\text{Rn}$  data from Transect B are plotted in Figure 2.2 as a function of distance from the DGFZ and show that  $^{222}\text{Rn}$  concentration is higher relative to the non-fractured areas and the NSFZ. The  $^{222}\text{Rn}$  data show some interesting characteristics with respect to the mapped fracture zones. Two transects (A and F) are located almost entirely within NSFZ and DGFZ, respectively, and have the highest average values. The data in Figure 2.2 show that Transects A and F are located within zones of high  $^{222}\text{Rn}$ . In the case of Transect F, the high-radon flux zone corresponds to the high-flux zone within the DGFZ. The high-flux zone defined by Transect F and parts of Transects B and C is centered along the eastern margin of the DGFZ, which likely indicates that this is an area of high vertical connectivity that may be capable of rapidly transmitting water through the vadose zone (Glass et al. 2002a, 2002b; Hendrickx and Flury 2001).

### 2.3.4 Transect A Influence of Rock Type

Transect A is located in a zone of anomalously high,  $^{222}\text{Rn}$ -measured flux, contained entirely within the mapped extent of the Chelmsford Granite (Figure 2.2). In this transect, all measured  $^{222}\text{Rn}$  concentrations exceed 117 pCi/L (7.7 pCi/L<sub>(n)</sub>) and the high flux from this rock type does not extend to Transects B and E, located less than 100 m to the northwest.

The fact that there is not an extension of the high- $^{222}\text{Rn}$  zone to the northwest along the trend of the NSFZ means that it is highly unlikely that the NSFZ structure is a uniformly permeable feature.

The most likely explanation for the high  $^{222}\text{Rn}$  measured in Transect A is due to its placement within a narrow zone of the Chelmsford granite (Figure 2.2), which has a higher uranium concentration by a factor of three. Therefore, if all other conditions were equal at the Shepley's Hill study site, the measured concentration of  $^{222}\text{Rn}$  would be expected to be higher at sample points located within the Chelmsford granite.

### 2.3.5 Transect B Influence of Fracture Zones

Transect B is a long transect that crosses both the NSFZ and DGFZ (Figures 2.2 and 2.5) and the area between the fracture zones. Transect B data are quite illustrative, as the sample locations from the portions of the transect that cross the DGFZ are represented by high radon concentrations, while the data from the rest of the transect, including the samples from the NSFZ, have low radon concentrations. The implications of this spatial variability indicate that the major fracture zones (DGFZ and NSFZ) are not uniformly communicative to fluid transport. This suggests that focused recharge to the aquifer cannot simply be attributed uniformly to the major fracture networks at all locations, but that other factors such as sedimentation, fracture dilatation, and mineralization are influencing gas transport at Shepley's Hill and, by inference, infiltration at discrete locations.

#### 2.3.5.1 *Rock and Fracture Variability Analysis*

A geostatistical analysis was conducted on the data using SYSTAT 13 (Systat Software, Inc.) to test two hypotheses: first, active fracture zones (i.e., those capable of rapidly transporting water) have higher radon-emission rates than non-fracture zones, and second, active fractures have higher radon-emission rates than do inactive or low-permeability fracture zones. This was accomplished by first grouping all samples into three populations (Table 2.2) based on their location: 1) outside of the major fracture zones (as background), 2) within the NSFZ, and 3) within the DGFZ. Because of the higher uranium and radon concentrations in the Chelmsford

Granite, data from Transect A were excluded from the analysis. The design of the RDMP allows measurement of  $^{222}\text{Rn}$  at the soil bedrock interface by eliminating soil-generated  $^{222}\text{Rn}$  from the CR-39 detector. In order to account for the influence of soil thickness on radon diffusion out of the bedrock, and hence concentration at the soil bedrock interface (Richon et al. 2010), the non-fractured radon results as a function of soil depth at the sampling location were plotted and the change in radon with depth was determined by a least-squares linear regression ( $R = 0.78$ ; not shown). All of the radon data were then corrected for soil depth using:

$$\text{Rn}_{\text{corrected}} = \text{Rn}_{\text{measured}} - m \times D_{\text{soil}} + b \quad \text{Equation (2.1)}$$

where

$\text{Rn}_{\text{measured}}$  = measured radon concentration ( $\text{pCi L}^{-1}$ )

$D_{\text{soil}}$  = depth of soil cover

$M$  = slope of linear regression of soil depth and radon concentration. (This is derived using data outside of the two fracture zones [i.e., background]. The value for this study is  $4.44 \text{ pCi L}^{-1} \text{ cm}^{-1}$ ,  $R=0.78$  not shown.)

$b$  = constant to ensure all  $\text{Rn}_{\text{corrected}}$  values are positive. (Value for this study is  $104.83 \text{ pCi L}^{-1}$ , resulting in the lowest value of  $\text{Rn}_{\text{corrected}}$  being 0.)

Table 2.2: Values for data grouping used for statistical analysis.

Variable	Fracture Zones	Number	Mean $\text{pCi L}^{-1}$	Variance $\text{pCi L}^{-1}$	Median $\text{pCi L}^{-1}$
$\text{Rn}_{\text{(corrected)}}$ ( $\text{pCi L}^{-1}$ )	Disc Golf Fracture Zone (DGFZ)	19	135	951	132
	Nona-Shep Fracture Zone (NSFZ)	26	91	1286	100
	Non-fractured areas	37	105	758	103

The data were then corrected for soil depth as described above. Using the  $\text{Rn}_{\text{corrected}}$  values, the homogeneity of variances for the three groups of data was evaluated using Bartlett's test ( $p\text{-value} = 0.36$ ) and indicated that subsequent Student's t-tests should be conducted using a pooled variance. Because of the factor of  $\sim 3$  difference in uranium concentration between Chelmsford Granite and Ayer Granodiorite, Student's t-tests were conducted within a single rock type (i.e., the Ayer Granodiorite; Transect A associated with the Chelmsford Granite was excluded).

We conducted separate Student's t-tests to assess whether the NSFZ and DGFZ have radon concentrations greater than the non-fractured areas. The t-test results indicated that mean  $\text{Rn}_{\text{corrected}}$  was significantly higher ( $p\text{-value} = 0.0003$ ) than background for the DGFZ, but not for the NSFZ



( $p$ -value = 0.957). We also assessed the role of rock type on  $Rn_{corrected}$ . A Student's  $t$ -test was conducted comparing Ayer Granodiorite to the Chelmsford granite (Transect A). Both within the NSFZ showed that  $Rn_{corrected}$  associated with the Chelmsford Granite are significantly higher ( $p$ -value < 0.0001) than those associated with the Ayer Granodiorite.

The implication of the statistical analysis is that the NSFZ has uniformly low conductivity across its length and may be only locally important to the infiltration of meteoric water into the Shepley's Hill Landfill, an observation that is largely consistent with the conclusion of Gannett Fleming and U.S. EPA's 2012 bedrock model (Gannett Fleming, Inc. 2012). In contrast, the higher radon concentrations across the length of the DGFZ indicate that it is much more vertically conductive and is likely a source of focused recharge to the landfill area. The conclusion is consistent with the piezometric surfaces associated with precipitation events contained in Gannett Fleming, Inc. (2012). However, the authors of the report conclude that based on the location, the DGFZ does not appear to be important to the hydrology of the landfill, but that it may be important as a hydrologic divide. This apparent discrepancy between our research and the Gannett Fleming, Inc. (2012) report is worthy of further investigation.

### 2.3.6 CR-39 Deployment

We demonstrated that CR-39 detectors can measure  $^{222}Rn$  flux in geologic environments at a resolution sufficient for characterizing fracture networks. Furthermore, the study showed through the use of multiple measurements in the same RDMP and control CR-39 detectors that came back as non-detects, if the detector is emplaced correctly the measured  $^{222}Rn$  concentration is representative of the location and is not impacted by  $^{222}Rn$ -contaminated dust and dirt—especially  $^{222}Rn$  that originated from elsewhere in the study area. This is illustrated in Figures 2.2 and 2.5, where CR-39 detectors that measured high radon flux are located next to detectors that measured low flux. To minimize temporal fluctuations in  $^{222}Rn$  concentration, it is necessary that the detectors be deployed for a sufficient period of time, such that diurnal variation in  $^{222}Rn$  flux (i.e., barometric pumping) would be insignificant. To meet these objectives, the study team developed a new RDMP that could house the CR-39 detector, protecting it from contamination while it was deployed in the shallow vadose zone.

Deployment of the technology was relatively straightforward and rapid. Total time in the field for mobilization, installation, and retrieval of the 92 detectors was on the order of five days for a three-person crew. The only other equipment needed, in addition to the detectors and the RDMP, was a small quantity of coarse bentonite chips and a power soil auger. In addition to the ease of deployment, the technology is particularly promising due to the relatively low cost. The cost for the commercially available CR-39 detectors, including analysis, at the time of the study was less than \$20

per detector. Similarly, the RDMP developed for the project was constructed from inexpensive, easily obtained, commercially available materials. This approach suggests an option that is significantly less expensive than other available alternatives for subsurface bedrock fracture detection. Additionally, because this approach does not require any large or expensive specialized equipment, it has application across a wide range of geologic environments.

## 2.4 Summary

Past studies have shown that  $^{222}\text{Rn}$  is useful for detecting and characterizing larger faults and geothermal systems (Swakoń et al. 2004; İnceöz et al. 2006; Moloney et al. 2010; Richon et al. 2010). This study sought to test whether using  $^{222}\text{Rn}$  could be used as a characterization tool to passively detect pathways in fractured rock that are responsible for transmitting meteoric water from the surface into an underlying aquifer. Understanding the location of preferential pathways for water infiltration is a critical issue for managers of contaminated fractured rock aquifers. Typically, procedures that map the locations of open fractures in buried bedrock formations are marginally successful and come with great cost. The ability to map these fracture pathways at greater resolution and lower cost represents a value proposition that can be deployed across a wide range of fractured-rock-hosted contaminated sites.

We utilized standard CR-39-particle track  $^{222}\text{Rn}$  detector technology, adapted to meet specific criteria, which included a simple, field-rugged, passive sampling design (Figure 2.4). This methodology is characterized by low cost and is minimally invasive and easy to deploy. Without question, our study would have benefited from an evaluation of  $^{222}\text{Rn}$  flux prior to conducting the study to set the exposure time. Additionally, two to three additional long transects like Transect B would have allowed for a more substantial evaluation of the site.

Our study has demonstrated that it is useful in detecting fracture networks at facility scale. The results of this promising initial evaluation suggest that further research is warranted. Additional testing in a variety of geologic environments would add to the knowledge base and help improve methods and practices for implementing the technology. The realm of potential applications of this technology to the field-of-site assessment and remediation begs further exploration. Additionally, our study shows that information related to preferred infiltration pathways elucidated by radon effusion at fractured-rock-hosted sites is of high interest to those charged with managing cleanup at contaminated sites.

Using statistical analysis, the  $^{222}\text{Rn}$  data from the study site reveal some important characteristics regarding the ability of the fractured rock at Shepley's Hill to transmit fluids through the subsurface. The first conclusion is that the fractured granite that makes up Shepley's Hill is not uniformly

communicative. Statistical analysis of the data reveals that even in the NSFZ and DGFZ, where fractures are highly concentrated, the ability of the fractures to transmit radon and, by inference, water is highly variable. The analysis indicates that the fractures contained within the NSFZ are not any more communicative than background rock (Figure 2.2). The fractures contained within the DGFZ are significantly more open and therefore potentially more capable of transmitting water into the subsurface. From a site management point of view, this means that the ability of the NSFZ to transmit water into the subsurface is not significantly different from infiltration through regions outside of the fault zones (Schmelling and Ross 1990). In contrast, these results suggest that there is preferential (above-background) infiltration potential across the DGFZ.

### Acknowledgements

The authors would like to acknowledge several persons for assistance in completing this technology evaluation. Gordon Hamilton of the U.S. EPA Region 1 GIS Center deserves special mention for his substantial help, both in the field and in the GIS center. Michael Daly of U.S. EPA Region 1 and Ed Gilbert of U.S. EPA OSRTI also provided significant assistance in the field. Bryan Olson, Federal Facilities Superfund Section Chief, U.S. EPA Region 1, and Ginny Lombardo, RPM, U.S. EPA Region 1, provided logistical and other project support. Lastly, the authors would also like to thank Felicia Barnett, U.S. EPA Office of Research and Development, for supporting the effort.

### References

- ABB-ES, 1995, *Railroad Roundhouse Supplemental Site Investigation*, U.S. Army Environmental Center, Data Item A009, September 1995.
- Abbas, T. R., 2011, "Effect of Water Table Fluctuation on Barometric Pumping in Soil Unsaturated Zone," *Jordan Journal of Civil Engineering*, Vol. 5, No. 4, October 2011, pp. 504–509.
- Abumurad, K. M., M. Atallah, M. K. Kullab, and A. Ismail, 1997, "Determination of Radon Soil Concentration Levels in the Governorate of Irbid, Jordan," *Radiation Measurements*, Vol. 28, Nos. 1–6, pp. 585–588, DOI: 10.1016/S1350-4487(97)00144-3.
- Akawwi, E., 2014, "Radon-222 Concentrations in the Groundwater along Eastern Jordan Rift," *Journal of Applied Sciences*, Vol. 14, No. 4, DOI: 10.3923/jas.2014.309.316.
- Altshuler, B. and B. Pasternack, 1963, "Statistical Measures of the Lower Limit of Detection of a Radioactivity Counter," *Health Physics*, Vol. 9, No. 3, March 1963, pp. 293–298.
- AMEC, 2009, *Draft Final Supplemental Groundwater and Landfill Cap Assessment for Long-Term Monitoring and Maintenance, Shepley's Hill Landfill, Devens, MA*, USACE-NAE.
- Auer, L. H., N. D. Rosenberg, K. H. Birdsell, and E. M. Whitney, 1996, "The Effects of Barometric Pumping on Contaminant Transport," *Journal of Contaminant Hydrology*, Vol. 24, No. 2, November 1996, pp. 145–166, DOI: 10.1016/S0169-7722(96)00010-1.

- Baixeras, C., B. Erlandsson, L. Font, and G. Jönsson, 2001, "Radon Emanation from Soil Samples," *Radiation Measurements*, Vol. 34, Nos. 1–6, June 2001, pp. 441–443, DOI: 10.1016/S1350-4487(01)00203-7.
- Bear, J., 1988, *Dynamics of Fluids in Porous Materials*, New York: Dover Publications.
- Burton, M., M. Neri, and D. Condarelli, 2004, "High Spatial Resolution Radon Measurements Reveal Hidden Active Faults on Mt. Etna," *Geophysical Research Letters*, Vol. 31, No. 7, April 2004, DOI: 10.1029/2003GL019181.
- Cecil, L. D. and J. R. Green, 2000, "Radon-222," *Environmental Tracers in Subsurface Hydrology*, edited by P. G. Cook and A. L. Herczeg, pp. 175–194, New York: Springer US.
- Davidson, G. R., 1998, "Geochemical Evidence of Preferential Flow of Water Through Fractures in Unsaturated Tuff, Apache Leap, Arizona," *Applied Geochemistry*, Vol. 13, No. 2, March 1998, pp. 185–195, DOI: 10.1016/S0883-2927(97)000063-2.
- Dershowitz, W., K. Klise, A. Fox, S. Takeuchi, and M. Uchida, 2002, "Channel Network and Discrete Fracture Network Modeling of Hydraulic Interference and Tracer Experiments and the Prediction of Phase C Experiments," SKB, Report IPR-02-29, December 2002.
- Duguid, J. O. and P. C. Y. Lee, 1977, "Flow in Fractured Porous Media," *Water Resources Research*, Vol. 13, No. 3, June 1977, pp. 558–566, DOI: 10.1029/WR013i003p00558.
- Fabryka-Martin, J. T., P. R. Dixon, S. Levy, B. Lui, H. J. Turin, and A. V. Wolfsberg, 1996, *Summary Report of Chlorine-36 Studies: Systematic Sampling for Chlorine-36 in the Exploratory Studies Facility*, LA-CST-TIP-96-002, Los Alamos National Laboratory, March 29, 1996.
- Faybishenko, B., C. Doughty, M. Steiger, J. C. S. Long, T. R. Wood, J. S. Jacobsen, J. Lore, and P. T. Zawislanski, 2000, "Conceptual Model of the Geometry and Physics of Water Flow in a Fractured Basalt Vadose Zone," *Water Resources Research*, Vol. 36, No. 12, December 2000, pp. 3499–3520, DOI: 10.1029/2000WR900144.
- Faybishenko, B., P. A. Witherspoon, C. Doughty, J. T. Geller, T. R. Wood, and R. K. Podgorney, 2001, "Multi-Scale Investigations of Liquid Flow in a Fractured Basalt Vadose Zone," *Flow and Transport through Unsaturated Fractured Rock*, edited by D. D. Evans, T. J. Nicholson, and T. C. Rasmussen, pp. 161–182, Washington, D.C.: American Geophysical Union.
- Fukui, M., 1987, "Soil Water Effects on Concentration Profiles and Variations of  $^{222}\text{Rn}$  in a Vadose Zone," *Health Physics*, Vol. 53, No. 2, August 1987, pp. 181–186.
- Gannett Fleming, Inc., 2012, *Shepley's Hill Bedrock Investigation*, EP-W-05-020, U.S. Environmental Protection Agency, July 2012.
- Glass, R. J., M. J. Nicholl, A. L. Ramirez, and W. D. Daily, 2002, "Liquid Phase Structure within an Unsaturated Fracture Network beneath a Surface Infiltration Event: Field Experiment," *Water Resources Research*, Vol. 38, No. 10, October 2002, pp. 17-1–17-16, DOI: 10.1029/2000WR000167.
- Glass, R. J., M. J. Nicholl, S. E. Pringle, and T. R. Wood, 2002, "Unsaturated Flow through a Fracture-Matrix Network: Dynamic Preferential Pathways in Mesoscale Laboratory Experiments," *Water Resources Research*, Vol. 38, No. 12, December 2002, pp. 17.1–17.7, DOI: 10.1029/2001WR001002.
- Gerke, H. H. and M. T. van Genuchten, 1993, "A Dual-Porosity Model for Simulating the Preferential Movement of Water and Solutes in Structured Porous Media," *Water Resources Research*, Vol. 29, No. 2, February 1993, pp. 305–319, DOI: 10.1029/92WR02339.

- Hao, Y., T. -C. Yeh, J. Xiang, W. A. Illman, K. Ando, K. C. Hsu, and C. H. Lee, 2008, "Hydraulic Tomography for Detecting Fracture Zone Connectivity," *Groundwater*, Vol. 46, No. 2, March/April 2008, pp. 183–192, DOI: 10.1111/j.1745-6584.2007.00388.x.
- Harding ESE, 2003, *Revised Draft Shepley's Hill Landfill Supplemental Groundwater Investigation, Devens Reserve Forces Training Area, Devens, Massachusetts*, U.S. Army Corps of Engineers, New England District, Concord, Massachusetts, May 2003.
- Hendrickx, J. M. H. and M. Flury, 2001, "Uniform and Preferential Flow Mechanisms in the Vadose Zone," *Conceptual Models of Flow and Transport in the Fractured Vadose Zone*, edited by Paul A. Hsieh et al., National Research Council, pp. 149–188, DOI: 10.17226/10102.
- İnceöz, M., O. Baykara, E. Aksoy, and M. Dođru, 2006, "Measurements of Soil Gas Radon in Active Fault Systems: A Case Study Along the North and East Anatolian Fault Systems in Turkey," *Radiation Measurements*, Vol. 41, No. 3, March 2006, pp. 349–353, DOI: 10.1016/j.radmeas.2005.07.024.
- Kigoshi, K., 1971, "Alpha-Recoil Thorium-234: Dissolution into Water and the Uranium-234/Uranium-238 Disequilibrium in Nature," *Science*, Vol. 173, No. 3991, July 1971, pp. 47–48, DOI: 10.1126/science.173.3991.47.
- King, C. -Y., B. -S. King, W. C. Evans, and W. Zhang, 1996, "Spatial Radon Anomalies on Active Faults in California," *Applied Geochemistry*, Vol. 11, No. 4, July 1996, pp. 497–510, 10.1016/0883-2927(96)00003-0.
- King, G. E., 2010, "Thirty Years of Gas Shale Fracturing: What Have We Learned?" *SPE Annual Technical Conference and Exhibition, Florence, Italy, September 19–22, 2010*, SPE-133456-MS.
- Kopera, J. P., 2008, "Preliminary Bedrock Geologic Map of the Area Surrounding Shepley's Hill, Towns of Ayer and Devens, Massachusetts," OMSG Open-File Report OFR08-05.
- Koteas, C. G., A. J. Keskula, C. L. Stein, D. F. McTigue, J. P. Kopera, and W. C. Brandon, 2010, "Evidence for Arsenic-Mineralization in Granitic Basement Rocks, Ayer Granodiorite, Northeastern Massachusetts," *Conference Proceedings of the Geological Society of America Northeastern Section (45<sup>th</sup> Annual) and Southeastern Section (59<sup>th</sup> Annual) Joint Meeting, Baltimore, Maryland, March 13–16, 2010*.
- Larsen, E. S., Jr. and D. Gottfried, 1961, *Distribution of Uranium in Rocks and Minerals of Mesozoic Batholiths in Western United States*, U.S. Geological Survey, Bulletin 1070-C, pp. 63–103.
- Manavhela, R. F., 2007, *In-situ Measurements of Radon Concentrations in Soil Gas at a Site on the Cape Flats*, M. S. Thesis: University of the Western Cape, Cape Town, South Africa.
- Mazur, D., M. Janik, J. Łoskiewicz, P. Olko, and J. Swakoń, 1999, "Measurements of Radon Concentration in Soil Gas by CR-39 Detectors," *Radiation Measurements*, Vol. 31, Nos. 1–6, June 1999, pp. 295–300, DOI: 10.1016/S1350-4487(99)00135-3.
- McClure, M. and R. N. Horne, 2013, *Discrete Fracture Network Modeling of Hydraulic Stimulation: Coupling Flow and Geomechanics*, SpringerBriefs in Earth Sciences, New York: Springer US.
- Mishra, R., C. Orlando, L. Tommasino, S. Tonnarini, and R. Trevisi, 2005, "A Better Understanding of the Background of CR-39 Detectors," *Radiation Measurements*, Vol. 40, Nos. 2–6, November 2005, pp. 325–328, DOI: 10.1016/j.radmeas.2004.11.010.
- Moloney, T. P., K. W. Sims, and J. P. Kaszuba, 2010, "Uranium and Thorium Decay Series Isotopic Constraints on the Source and Residence Time of Solutes in the Yellowstone Hydrothermal System," in *University of Wyoming National Park Service Research Center Annual Report Volume 33, 33rd Annual Report*.

- NRC, 2000, *Natural Attenuation for Groundwater Remediation*, Washington, D.C.: National Academy Press.
- Nees, M., 1993, *Quality Assurance Handbook for Air Pollution Measurement Systems: Volume I – A Field Guide to Environmental Quality Assurance*, EPA-600/9-76-005, U.S. Environmental Protection Agency.
- Otton, J. K., *The Geology of Radon*, <https://pubs.usgs.gov/gip/7000018/report.pdf>, published 1992, website visited March 2017.
- Porstendörfer, J., and T. T. Mercer, 1978, “Influence of Nuclei Concentration and Humidity upon the Attachment Rate of Atoms in the Atmosphere,” *Atmospheric Environment*, Vol. 12, No. 11, May 1978, pp. 2223–2228, DOI: 10.1016/0004-6981(78)90178-6.
- Richon, P., Y. Klinger, P. Tapponnier, C. -X. Li, J. Van Der Woerd, and F. Perrier, 2010, “Measuring Radon Flux across Active Faults: Relevance of Excavating and Possibility of Satellite Discharges,” *Radiation Measurements*, Vol. 45, No. 2, February 2010, pp. 211–218, DOI: 10.1016/j.radmeas.2010.01.019.
- Robinson, G. R., Jr., 1981, *Bedrock Geology of the Nashua River Area, Massachusetts – New Hampshire*, USGS Open-File Report 81-593.
- Schmelling, S. G. and R. R. Ross, 1989, *Contaminant Transport in Fractured Media: Models for Decision Makers*, EPA/540/4-89/004, U.S. Environmental Protection Agency.
- Sun, H. and D. J. Furbish, 1995, “Moisture Content Effect on Radon Emanation in Porous Media,” *Journal of Contaminant Hydrology*, Vol. 18, No. 3, May 1995, pp. 239–255, DOI: 10.1016/0169-7722(95)00002-D.
- Swakoń, J., K. Kozak, M. Paszkowski, R. Gradziński, J. Łoskiewicz, J. Mazur, M. Janik, J. Bogacz, T. Horwacik, and P. Olko, 2004, “Radon Concentration in Soil Gas around Local Disjunctive Tectonic Zones in the Krakow Area,” *Journal of Environmental Radioactivity*, Vol. 78, No. 2, October 2004, pp. 137–149, DOI: 10.1016/j.jenvrad.2004.04.004.
- U.S. EPA, 1992, *Indoor Radon and Radon Decay Product Measurement Device Protocols*, EPA 402-R-92-004, July 1992.
- Walsh, G. J., R. H. Jahns, and J. N. Aleinikoff, 2013, *Bedrock Geologic Map of the Nashua South Quadrangle, Hillsborough County, New Hampshire, and Middlesex County, Massachusetts*, U.S. Geological Survey, Scientific Investigations Map 3200.
- Wood, T. R., R. J. Glass, T. R. McJunkin, R. K. Podgorney, R. A. Laviolette, K. S. Noah, D. L. Stoner, R. C. Starr, and K. Baker, 2004, “Unsaturated Flow through a Small Fracture-Matrix Network: Part 1, Experimental Observations,” *Vadose Zone Journal*, Vol. 3, No. 1, pp. 90–100, DOI: 10.2136/vzj2004.9000.
- Wood, T. R., M. J. Nicholl, and R. J. Glass, 2002, “Fracture Intersections as Integrators for Unsaturated Flow,” *Geophysical Research Letters*, Vol. 29, No. 24, December 2002, pp. 44-1–44-4, DOI: 10.1029/2002GL015551.
- Wood, T. R. and G. T. Norrell, 1996, *Integrated Large-Scale Aquifer Pumping and Infiltration Tests, Groundwater Pathways*, INEL-96/0256, Idaho National Engineering Laboratory.
- Yang, I. C., G. W. Rattray, and P. Yu, 1996. Interpretations of chemical and isotopic data from boreholes in the unsaturated-zone at Yucca Mountain, Nevada, U.S. Geol. Surv. Water Resour. Invest. Rep. 96-4058, 1996.

- Yamanishi, H., T. Iida, Y. Ikebe, S. Abe, and T. Hata, 1991, "Measurements of Regional Distribution of Radon-222 Concentration," *Journal of Nuclear Science and Technology*, Vol. 28, No. 4, April 1991, pp. 331–338, DOI: 10.3327/jnst.28.331.
- Zhang, W. and C. -Y. King, 1994, "Measurement of Radon Gas on Major Faults in California, USA," *Acta Seismologica Sinica*, Vol. 7, No. 1, pp. 159–165, DOI: 10.1007/BF02651919.

### CHAPTER 3: Utilizing Rare Earth Elements as Tracers in High TDS Reservoir Brines in CCS Applications

“Utilizing Rare Earth Elements as Tracers in High TDS Reservoir Brines in CCS Applications.”  
*Energy Procedia*, Vol. 63, 2014, pp. 3963–3974.

Travis McLing,<sup>a,b,\*</sup> William Smith,<sup>b,c</sup> Robert Smith<sup>b,c</sup>

<sup>a</sup> Idaho National Laboratory, P.O. Box 1625, Idaho Falls, ID 83415-2107, USA

<sup>b</sup> Center for Advanced Energy Studies, 995 University Blvd., Idaho Falls, ID 83401, USA

<sup>c</sup> University of Idaho, Moscow, ID 83844, USA

\* Corresponding author: Travis L. McLing; E-mail: [travis.mcling@inl.gov](mailto:travis.mcling@inl.gov);  
Telephone: 012085267269; Fax: 012085260875

#### Abstract

In this paper, we report the result of research associated with the testing of a procedure necessary for utilizing natural-occurring trace elements, specifically the rare earth elements (REEs), as geochemical tracers in carbon capture and storage (CCS) applications. Trace elements, particularly REEs, may be well suited to serve as in situ tracers for monitoring geochemical conditions and the migration of CO<sub>2</sub>-charged waters within CCS storage systems. We have been conducting studies to determine the efficacy of using REEs as a tracer and characterization tool in the laboratory, at a CCS analogue site in Soda Springs, Idaho, and at a proposed CCS reservoir at the Rock Springs Uplift, Wyoming. Results from field and laboratory studies have been encouraging, showing that REEs may be effective tracers in CCS systems and overlying aquifers. In recent years, a series of studies using REEs as natural groundwater tracers have been conducted successfully at various locations around the globe. Additionally, rare earth and other trace elements have been successfully used as in situ tracers to describe the evolution of deep sedimentary basins. Our goal has been to establish naturally occurring REEs as a useful monitoring, measuring, and verification (MMV) tool in CCS research because formation brine chemistry will be particularly sensitive to changes in local equilibrium, caused by the addition of large volumes of CO<sub>2</sub>. Because brine within CCS target formations will have been in chemical equilibrium with the host rocks for millions of years, the addition of large volumes of CO<sub>2</sub> will cause reactions in the formation that will drive changes to the brine chemistry, due to the pH change caused by the formation of carbonic acid. This CO<sub>2</sub>-driven change in formation fluid chemistry will have a major impact on water-rock reaction equilibrium in the formation, which will impart a



change in the REE fingerprint of the brine that can be measured and used to monitor in situ reservoir conditions. Our research has shown that the REE signature, imparted to the formation fluid by the introduction of CO<sub>2</sub> to the formation, can be measured and tracked as part of an MMV program. Additionally, this REE fingerprint may serve as an ideal tracer for fluid migration, both within the CCS target formation and should formation fluids migrate into overlying aquifers. However, application of rare earth and other trace elements to CCS systems is complicated by the high salt content of the brines contained within the target formations. In the United States by regulation, in order for a geologic reservoir to be considered suitable for carbon storage, it must contain formation brine with total dissolved solids (TDS) >10,000 ppm. In most cases, formation brines have TDS well in excess of that threshold. The high salinity of these brines creates analytical problems for elemental analysis, including element interference with trace metals in inductively coupled plasma mass spectroscopy (ICP-MS) (i.e., element mass overlap due to oxide or plasma phenomenon). Additionally, instruments that are sensitive enough to measure trace elements down to the parts per trillion level, like the ICP-MS, are quickly oversaturated when water TDS exceeds much more than 1,000 ppm. Normally, this problem is dealt with through dilution of the sample, bringing the water chemistry into the instrument's working range. However, dilution is not an option when analyzing these formation brines for trace metals—specifically REEs, which occur in aqueous solutions at the parts per trillion levels. Any dilution of the sample would make REE detection impossible. Therefore, the ability to use trace metals as in-situ natural tracers in high-TDS brine environments requires the development of methods for preconcentrating trace elements while reducing the salinity and associated elemental interference such that the brines can be routinely analyzed by standard ICP-MS methods. As part of the Big Sky Carbon Sequestration Project, the INL-CAES has developed a rapid, easy-to-use process that preconcentrates trace metals, including REEs, up to 100× while eliminating interfering ions (e.g., Ba, Cl). The process is straightforward and inexpensive and requires little infrastructure, using only a single chromatography column with inexpensive, reusable, commercially available resins and wash chemicals. The procedure has been tested with synthetic brines (215,000 ppm or less TDS) and field water samples (up to 5,000 ppm TDS). Testing has produced data of high quality with REE capture efficiency exceeding 95%, while reducing interfering elements by >99%.

**Keywords:** Rare Earth Elements, CCS, Geochemistry

### 3.1 Introduction

The REEs are a group of 15 elements including lanthanides, atomic number 57-71, some classifications that include scandium, and yttrium as well. Despite their name, REEs are not rare, and except for promethium are relatively plentiful in the earth's crust, with bulk concentrations ranging to near 70 ppm. However, except for a few notable examples such as Bayan Obo, China, they are not found in significant ore-grade concentrations; the name "rare earth" is derived from this scarcity of economic deposits. The utility of REEs as geochemical tracers is related to their remarkably uniform chemical properties, with subtle but important systemic variations. The REEs are lithophile elements (elements enriched in the earth's crust) that almost always occur naturally together because all are trivalent with Eu and Ce, having additional oxidation states of [II] and [IV], respectively. The chemical uniformity of the REE is the result of the electrons in the 6s subshell being complexly filled, and the 4f electrons being very-well shielded. The most significant difference in properties across the REE are decreasing ionic radii with increasing atomic number, referred to as lanthanide contraction. Because of their similar chemical properties, REEs readily substitute for one another.

The REE are commonly grouped into two packages: the light REE (LREE, La to Sm) and the heavy REE (HREE, Gd to Lu). Less commonly, a third group, middle REE (MREE, Pm to Ho), is included. Because REEs are among the least-soluble trace elements, they are quite immobile during low-temperature rock alteration, resulting in aqueous concentrations of parts per trillion for most systems. Although the low concentration makes measuring aqueous concentrations of REEs challenging, this attribute makes the aqueous REE system extremely sensitive to perturbations, such as changes in diagenesis caused by the addition of large volumes of CO<sub>2</sub> to a storage reservoir. Factors that affect the transport of REEs include: the distribution of REEs in the host rock; the types, abundance, and stability of REEs bearing minerals in the rock; the composition ligands, particularly carbonate in the formation brine; and Cl in high-temperature magmatic brines.

#### 3.1.1 REEs as Tracers

Although REEs can provide a powerful tool for evaluating trends in water chemistry and transport (e.g., CO<sub>2</sub> impacts, mixing, and source zones) and are increasingly being used to evaluate aqueous systems (Noack et al. 2014; Wood 2006; Nelson et al. 2004; Ojiambo et al 2003; Johannesson and Hendry 2000; Johannesson et al. 1996, 1997), there are practical difficulties associated with accurately measuring REEs in aqueous systems. The complexation of the REE, except under very acidic conditions, does not occur as hydrated trivalent ions; therefore, transport of REEs in natural systems is dependent on soluble ligand complexes or, to a small degree, adsorption desorption reactions. REEs are considered hard as defined by Pearson (1963), resulting in strong complexes with hard ligands (F,

PO<sub>4</sub>, and at high temperatures, Cl). More than 98% of REEs in aqueous solutions are the result of complexation with SO<sub>4</sub> and CO<sub>3</sub> (Nelson et al. 2004; Sampson and Wood 2005). Therefore, it would be expected that waters with high concentrations of these ligands would have proportionally higher concentrations of REEs.

In addition to the challenges mentioned previously, quantifying REEs in brines present additional challenges because of high concentrations of interfering major elements ions. A goal of our ongoing research is to develop methods and protocols to quantify REEs in high-TDS water characteristic of CCS in saline aquifers, allowing the use of REEs as natural tracers of fluid-rock interactions and migrations.

## 3.2 Methods

The parts-per-trillion concentration of REEs in natural waters are at or below the detection limit for direct quantification by inductively coupled plasma mass spectroscopy (ICP-MS). However, preconcentrating samples overcomes this limitation. Our approach for quantifying REEs uses two separate but related methods based on Strachan et al. (1989) and Stetzenbach et al. (1994)—one for low-TDS (less than 10,000 ppm) waters and one for higher-TDS (10,000 to 200,000 ppm) brines. Both methods rely on a chromatographic separation of REEs from other cations, followed by REE elution and concentration by up to 100 times for quantification using ICP-MS. For lower-TDS waters, a HDPE, gravity-driven, chromatographic column with ion-exchange resin (Bio-Rad's AG 50W-X8) is used. For brines, a borosilicate glass column with chelating resin (Bio-Rad's Chelex 100) is used. The more expensive chelating resin is used for brines because the high salinity caused the AG 50W-X8 to "clump," resulting in poor column performance. The two methods are described below.

### 3.2.1 Separation and Preconcentration

Effective quantification of REEs requires techniques that address their low concentrations in natural waters and analytical interferences from other cation in the waters. We addressed both of these issues using chromatographic approaches described below.

#### 3.2.1.1 *Low-TDS Waters*

Our low-TDS procedure used AG-50W-X8 hydrogen form resin in the 200–400 mesh size. We have found that this size fraction results in a lower flow rate through the column and increases cation and REE capture efficiency. REEs in each sample were concentrated by 50 or 100:1 by gravity feeding 1 to 2 liters of sample through a Bio-Rad Poly Prep AG 50W-X8 with 200- to 400-mesh, resin, gravity-flow chromatography column with a 250-mL sample reservoir. (The reservoir was not allowed to run dry and was capped through the process.) After the sample was drained through the

chromatography column, 40 mL of 1.7 N, ultra-pure nitric acid was applied to the column to elute the divalent cations from the resin, leaving behind only the trivalent cation adsorbed to the AG 50W-X8 resin. The REEs and other trivalent cations are then eluted from the resin using 10 mL of 8.0 N nitric acid and collected in an acid-washed Teflon container. The resulting eluent was evaporated to dryness at 60°C on a hot plate enclosed in a filter box to minimize contamination. The residual bead was dissolved in a 10-mL, 1% nitric acid solution to obtain the final 50:1 or 100:1 concentration ratio. The sample was then placed in a triple acid-washed, sealed, 15-mL centrifuge tube for ICP-MS analysis.

The resin can be recycled several times using the regeneration procedure of Crock et al. (1984). Regeneration was accomplished by flushing the column with five pore volumes of 8.0 N nitric acid. This process converts the resin back to hydrogen form by removing all residual, non-hydrogen cations. Finally, five pore volumes of 18 MΩ H<sub>2</sub>O were applied to the column, removing nitric acid from the reservoir before the column was sealed for storage. Rigorous testing of the regenerated columns with known solutions showed no degradation of the AG-50W-X8 resin after more than twenty cycles.

### 3.2.1.2 *High-TDS Brines*

The high-TDS procedure uses Chelex 100 Na form resin in the 200–400 mesh size modified after a procedure developed by Strachan et al. (1989). The pre-chromatography resin preparation in our procedure is similar to that presented in Strachan et al. (1989), though aliquot volumes are increased to maintain the aliquot/resin volume ratio. First, 16.25 g of resin is added and allowed to settle into an acid-washed, glass drip column, and the resin is flushed with 50 mL of 2.5 N, ultra-pure nitric acid to convert the resin to hydrogen form and remove any non-hydrogen cations. The initial wash is followed by a wash with 50 mL of 18.2 MΩ H<sub>2</sub>O to remove excess nitric acid from the column. The resin was then converted to ammonium form, using 50 mL of 2.0 N ammonium hydroxide, followed by 50 mL 18.2 MΩ H<sub>2</sub>O wash to remove excess ammonium hydroxide and to achieve a neutral pH. The resin pH is adjusted to 5.2–5.4 concentrated, ultra-pure nitric acid. Because the resin characteristics are strongly dependent on pH, it is important to maintain the resin pH close to the optimal pH of 5.3 for best cation capture.

Once the resin is prepared, the REEs in each sample are concentrated by 50 or 100:1 by gravity feeding 1 to 2 liters of sample through the column by first adding two 50-mL aliquots of sample to allow the resin volume to shrink before applying the remaining volume of sample. This is an important step as it allows the resin to shrink to its final volume without the formation of preferential flowpaths. Once the entire sample has passed through the column, 250 mL of 18.2 MΩ H<sub>2</sub>O was applied. The column is eluted with a 25mL- then two 50-mL aliquots of 1.0 M ammonium acetate (pH adjusted to 5.3 with nitric acid) to remove the mono- and divalent cations. 250 mL 18.2 MΩ H<sub>2</sub>O is applied to the

column to remove excess ammonium acetate. Next, two 100-mL aliquots of 2.5 N nitric acid are applied to the column to elute REEs and other trivalent cations into an acid-washed, 50-mL Teflon beaker. This is followed by a wash of 10 mL 18.2 MΩ H<sub>2</sub>O. The collected eluent is evaporated to dryness at 60°C on a hot plate enclosed in a filter box to minimize contamination. The resultant precipitate is dissolved (for 12 hours) using 10 mL, 1% nitric acid to achieve 50 or 100 times REE enrichments relative to the original sample. The REE concentrate is placed in a triple acid-washed, sealed, 15-mL centrifuge tube for ICP-MS analysis.

To recharge the columns for storage and reuse, three pore volumes of 2.5 M nitric is added to remove residual cations and convert resin to the hydrogen form. This is followed by an 18.2 MΩ H<sub>2</sub>O wash to remove the acid from the resin. Finally, at least three pore volumes of 2.0 M ammonium hydroxide is applied until the eluent pH is 10, converting the resin to ammonium form, which is ideal for storage. The column containing the regenerated resin is then sealed for storage. The regeneration procedure will allow the resin to be stored for several months. Prior to use, the column must be prepared as described above. The regenerated resin has been tested with no degradation of the Chelex 100 Na form resin after twenty cycles.

### **3.2.2 Sample Collection**

Prior to each sample collection or laboratory preparation, two 500-mL, high-density, polyethylene bottles were acid-washed using 5% trace metal-grade nitric acid for a minimum of two days. After the acid wash, the bottles were triple-rinsed with 18.2 MΩ H<sub>2</sub>O and then refilled with 18.2 MΩ H<sub>2</sub>O, sealed, and placed into acid-washed plastic Ziploc bags. Prior to filling the bottles, the deionized water was discarded and replaced with sample water or synthetic brine. Personnel wearing new nitrile gloves did all sample collection; gloves were changed between each step of the process (bottle filling, preservation, labeling). Each sample was collected from the fastest-flowing portion of the stream or spring or as far from the edge as possible. Prior to collecting the sample, the pH, temperature, and alkalinity of the water were measured and recorded. For field samples, each were collected using a Geotech peristaltic pump, pushing water through pre-cleaned, acid-washed, Teflon tubing. Water was purged through the sampling apparatus until the temperature, pH, and conductivity stabilized. The samples were filtered using a 0.45-um Gelman Sciences high-capacity, in-line filter capsule with polyether sulfone membrane, dispensing water directly into acid-washed polyethylene bottles. The samples were then acidified to pH <2, using ultra-pure nitric acid and sealed with Parafilm. To minimize the potential for environmental contamination, the exterior of the sample containers were rinsed thoroughly with 18.2 MΩ deionized water, placed into acid-washed plastic bags, and the bagged sample containers were placed in a cooler with dry ice for transport back to the laboratory. The

only deviations from this procedure were at aquifer wells that had fixed piping. In these cases, the Teflon tubing and filter were connected to the existing piping; otherwise, the samples were filtered and preserved as detailed above.

### 3.2.3 Analytical

REEs were analyzed after preconcentration in triplicate, using an Agilent 7500a ICP-MS with a Babington nebulizer and electron multiplier detector. By preconcentrating the samples, we were able to remove 99% of the divalent cations, which increases the REE detection by decreasing the formation of interfering oxides (specifically  $\text{BaO}^+$ ) in the plasma and lowering the overall background interference.

Analyses were to be considered reliable if plasma oxide formation (as measured by  $^{156}\text{CeO}/^{140}\text{Ce}$ ) was less than 0.5%. The largest contributor to the oxide interference is the formation of  $\text{BaO}^+$ , which interferes with  $^{139}\text{La}$ ,  $^{146}\text{Nd}$ ,  $^{147}\text{Sm}$ ,  $^{175}\text{Lu}$ , and, specifically,  $^{152}\text{Sm}$  and  $^{151}\text{Lu}$ . Because the separation and preconcentration methods used in our study are extremely effective in removing interfering ions, especially Ba, analysis has not required correction for oxides.

Instrumental drift is accounted for by periodically analyzing a fixed-concentration Rh internal standard, instrument blanks, and REE standards. All analyses were corrected by comparison to these known samples. Instrument drift was encountered, especially when larger numbers of samples were analyzed. Over time, the ICP-MS procedure was altered to minimize instrumental drift, including running fewer samples during a single series, increasing wash time, adding a small amount HF to facilitate rinse efficiency, and including more blanks (deionized water) between samples. The standards used to make up the calibration solutions for the ICP-MS were obtained from Inorganic Ventures, Inc. The standards were also used to spike known samples to test for instrumental drift. Blanks were run every 10 samples and were made up of DIW and 5% ultra-pure nitric acid.

## 3.3 Results

The above-described procedures were tested using 14 synthetic laboratory brines made from reagent grade salts ( $\text{NaCl} \gg \text{CaCl}_2 > \text{MgCl}_2 > \text{KCl}$ ) with TDS from 7,500 to 215,000 ppm and NASS-6-certified seawater reference sample obtained from the National Research Council Canada (NRCC). These samples were either spiked with known amounts of REE or, in the case of the NASS-6 reference seawater, were established reference material with REE concentration measured and documented.

Once the procedures were tested and verified using the synthetic brines and reference seawater, they were applied to waters from two CCS-relevant locations: the low-TDS Soda Springs, Idaho, natural CCS analogue site and the high-TDS, University of Wyoming Carbon Management Institute CCS test site on the Rock Springs Uplift in West Central Wyoming.

### **3.3.1 Methods Verification**

Our analytical methods described above were thoroughly tested and verified to assess their efficacy for application to CCS-relevant brines. The results of this testing are reported below.

#### **3.3.1.1 Synthetic Brines**

Early on during the development and testing of the REE separation procedures on synthetic brines, we experienced a great deal of difficulty with contamination. The analytical results exhibited a significant amount of LREE contamination, especially La (Figure 3.1, black trend line). The saw-tooth effect observed for the HREE in Figure 3.1 is common and reflects the Oddo-Harkins effect (Oddo 1914; Harkins 1917), where atoms with even atomic numbers have a higher natural abundance than do their neighbors with odd atomic numbers. Initially, LREE enrichment was attributed to particulate mobilized by a major HVAC cleaning and reconstruction in the laboratory facility, as research using La had previously been conducted in a neighboring laboratory. Consequently, the experiments were moved to another laboratory at the University of Idaho campus. The ICP-MS was thoroughly cleaned, and all tubing, rinse containers, and anything else that could have been contaminated was replaced. However, the LREE contamination continued to persist. We then suspected that the reagent-grade salts being used to make up the synthetic brine were the source of the observed REE contamination. This suspicion was supported by the pronounced Oddo-Harkins effect observed for all processed brines, indicating a natural component for the source of REE contamination. To test the salt contamination hypothesis, the chromatographic separations were conducted in a box constructed from HEPA filters to minimize any potential atmospheric contamination. Great care was used, and the filter box was only opened to place and remove samples. Additionally, a large, pressurized, Sentry Air Systems forced-air HEPA filtration system was moved into the lab proximal to the filter box. Once the potential for external contamination was reduced, we proceeded to test the possibility that the reagent-grade salts were responsible for the anomalous LREE contamination. The synthetic brines were made up as before using the same suite of salts. However, this time, before the brines were spiked with REEs, half were passed through the chromatography column to remove any REEs that may have been present from the salts used to make the brines. Both sets of brines were then spiked with 5 ppb REEs and passed through the chromatography column, as described in Section 3.2.1.2, to preconcentrate the REEs. The resulting data (Figure 3.2, red trend line) show that the samples passed through the column

prior to being spiked had REE concentrations of 5 ppb as expected. However, the brine samples that were not passed through the chromatography column prior to being spiked with REEs had the same LREE contamination as previously observed (Figure 3.1, black trend line), indicating that the salts used to make up the synthetic brines were the source of LREE contamination of approximately 2 ppb at 75 g/L. These results also confirmed that our procedure for quantitatively separating REEs is effective for simple brines with TDS up to 200 g/L. Twenty-four additional synthetic brines across a range of TDS from 20,000 ppm to more than 200,000 ppm were then tested. The resulting data showed an REE capture efficiency exceeded 95% across the entire TDS and REE concentration range, giving us confidence that the procedure could successfully be applied to CCS-relevant natural systems.

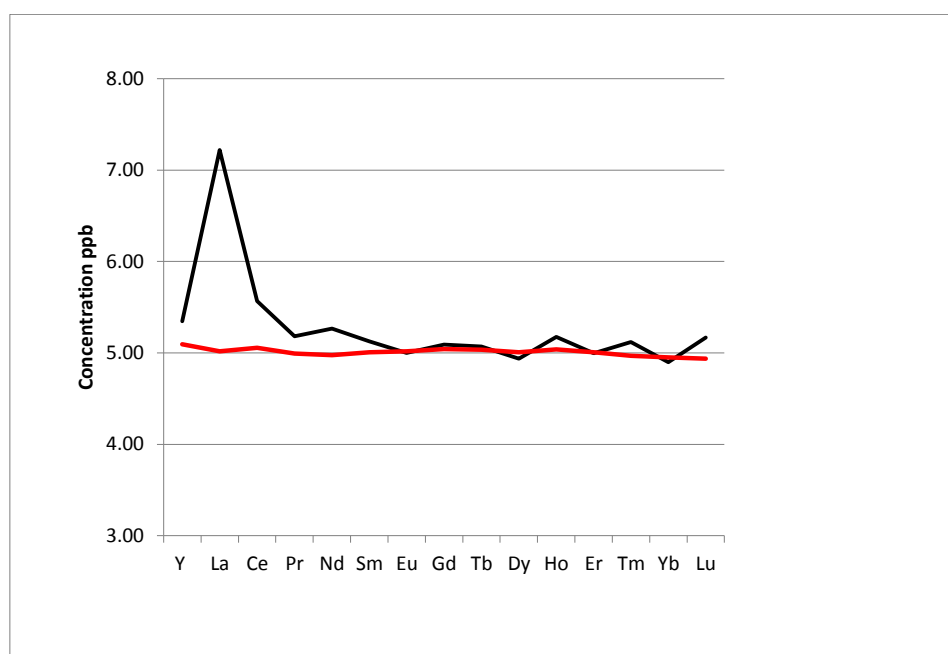


Figure 3.1: Results from test of the high-TDS Chelex resin extraction of REEs. The black trend shows the results of the chromatography of a 5-ppb REE solution using reagent grade salts. A clear contamination of the sample in LREE, especially La, is obvious. The red trend line shows the results of the same experiment after running the synthetic brine solution, through the extraction column, prior to spiking with REE.

### 3.3.1.2 NASS Standard

Reference seawater standard (NASS-6) was analyzed using the high-TDS method to evaluate the suitability of the method for waters with more complex compositions. The NRCC has rigorously characterized and documented (Lawrence 2007) NASS-6 for use as a chemical standard for ocean water. Two 500-mL, NASS-6 reference standards were processed as described in Section 3.2.1.2. They were also spiked with 1 ppb yttrium to quantify the REE recovery efficiency of the method.



The results showed that background corrected-measure REE concentrations were within 0.2% (Ln) to 1.9% (La) of the concentrations reported by NRCC; this is less than the 3% uncertainty we associate with our general ICP-MS analysis.

### 3.3.2 CCS Systems

In order to assess the suitability of REEs as potential tracers for CCS settings, our methods were tested with samples that exhibit a range of water chemistry and rock types. Waters from the CO<sub>2</sub>-charged Soda Springs CCS analogue site were analyzed to evaluate the suitability of REEs to quantify the CO<sub>2</sub>-driven, water-rock interaction at this unusual site. There are two types of water at the Soda Springs site: a deep, carbonate-sourced, CO<sub>2</sub>-charged water that is believed to be the result of the interaction between acidic magmatic fluids and Paleozoic carbonates deep in the basin. There is also a shallow freshwater system, which overlies the CO<sub>2</sub>-rich water and is recharged by seasonal precipitation and leakage from a reservoir located at the head of the basin. The deeper, CO<sub>2</sub>-charged system is naturally pressurized, and wells that penetrate the basalt cap rock into the CO<sub>2</sub> aquifer often result in geysering wells that can shoot water more than 30 meters into the air. The second set of CCS-relevant water was collected from the Rock Springs Uplift, a large structure located in West Central Wyoming that has been studied for its large, theoretical capacity to store CO<sub>2</sub>. A single sample of formation brine from the Weber (~90,000 ppm TDS) and Madison (~75,000 ppm TDS) formations were collected. The Madison Formation is comprised of a thick sequence of marine carbonates, while the Weber Formation is primarily a diagenetically altered siliciclastic. Because of the differences in rock type, the very-long residence time of the brine, and the presence of sealing formations between them, these brines provided an ideal test for both the high-TDS procedures' ability to delineate differences in REE chemistry between formations in stable sedimentary basins.

#### 3.3.2.1 Soda Springs, Idaho

Samples collected from Soda Springs were analyzed for REEs using the low-TDS procedure (Section 3.2.1.1). The resulting chondrite normalized data are presented in Figure 3.2 and do not show the characteristic positive-Eu anomaly as would be expected if plagioclase were strongly implicated in the calcite mineralization reaction. The absence of a positive-Eu anomaly in the Soda Springs system indicates that calcite precipitation initiated by the neutralization of H<sub>2</sub>CO<sub>3</sub> plagioclase dissolution alone cannot be responsible for the significant calcite precipitation that occurs in the system. This requires another method to explain the sealing of conductive structure in the capping basalts by calcite precipitation. Therefore, the most likely driving force behind the precipitation of calcite in the basalt is due to CO<sub>2</sub> degassing of the deep Ca-CO<sub>2</sub>-charged waters as they move into the shallow subsurface (Equation [3.1]). The total REE concentration varies over an order of magnitude across the samples,

with Pavilion Well having the highest concentration. More investigation is needed to explain the high REE concentration and the lack of Eu anomaly observed in the Soda Springs water. However, it is likely that the variability in REE concentration is due to a combination of selective adsorption and mixing of waters from multiple sources.



Drill cuttings from monitoring wells drilled into the basalt provided by the Monsanto Corporation Soda Springs operations show significant secondary mineralization in the basalts at-depth, with the pore space and fractures being completely filled with primarily carbonate precipitate. Additionally, the observation that the CO<sub>2</sub> system at Soda Springs is over-pressured below the basalt contact suggests that the normally permeable basalt has been sealed by mineralization resulting from CO<sub>2</sub> basalt interactions. Our results from the Soda Springs study site suggest that REEs may potentially be used to assess processes within a CCS target formation and track CO<sub>2</sub>-impacted water sites.

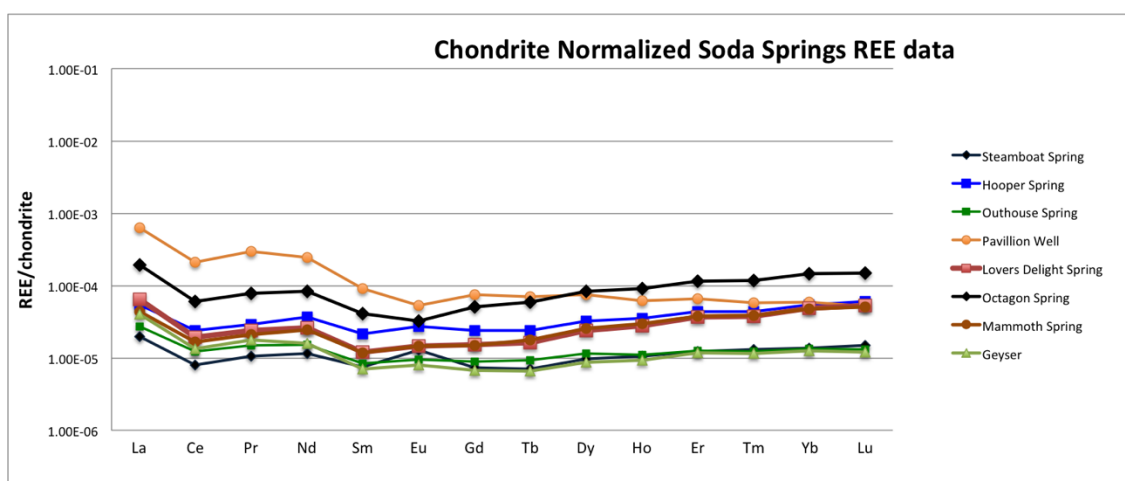


Figure 3.2: Graphs of ICP-MS-measured REE concentrations from water samples taken from Soda Springs, Idaho, normalized to chondrite composite (Wakita et al. 1971). The data show characteristic high-LREE, chondrite-normalized concentration and generally a slightly positive slope from Eu to Lu.

### 3.3.2.2 *Rock Springs Uplift, Wyoming*

Brine samples from Weber and Madison formations collected from the Rock Springs Uplift were analyzed for REEs using the high-TDS procedure (Section 3.2.1.2). Extreme care was exercised with the Rock Springs Uplift samples (collected at the end of the water production cycle), as they were irreplaceable and the only true formation brines available for this study (Surdam 2013). The resulting chondrite-normalized REE concentration for the Weber and Madison brines are presented in Figure 3.3. Both brines show LREE enrichment, and like seawater, both brines have a slightly negative Ce anomaly although the anomaly is much less pronounced in the brines than in seawater. Both samples have

positive Gd anomalies. The largest differences between the two formation brines are the very-positive HREE enrichment observed in the Weber brine, the HREE depletion in the Madison Brine, and the higher REE concentration of REE in the Madison Formation. The relatively high REE concentration in the Madison Formation is expected, as the Madison Formation is a carbonate-dominated system. The data suggest that although the two formations have some similarities in their REE distributions, the HREE enrichment and the significantly higher REE concentrations in the Madison Formation indicate that these two formations are hydrologically isolated from each other as expected. Although we were only able to analyze two brine samples, our results indicate that our analytical methods are robust—that REEs may have applicability in understanding the fate of CO<sub>2</sub> in CCS systems sited in saline formations.

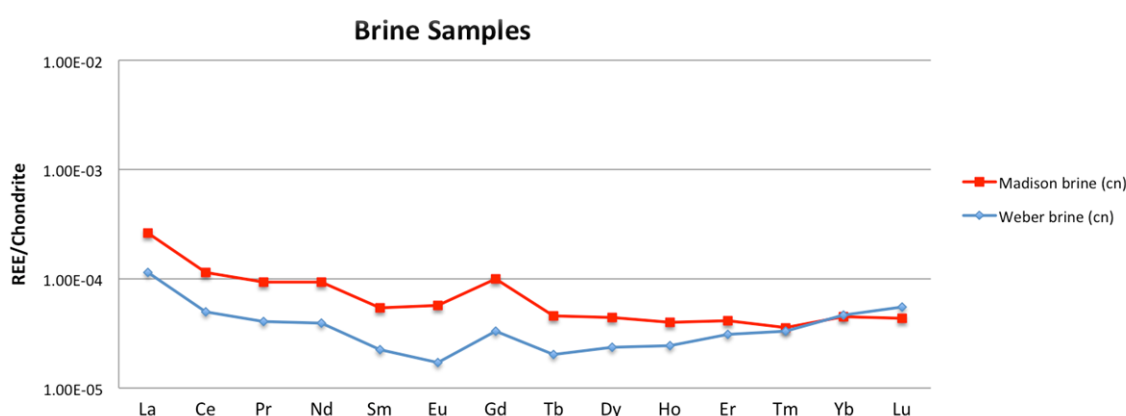


Figure 3.3: Graphs of ICP-MS measured chondrite-normalized REE concentrations from water samples taken from Madison and Weber formations at the Rock Springs Uplift (Wakita et al. 1971). Both these brines exhibit prominent Gd spikes and enrichments in LREE and HREE.

### 3.3.2.3 CO<sub>2</sub> Impacted vs. Unimpacted Waters

Although only two systems have been evaluated to date, there are some important inferences that can be drawn from the Soda Springs and the Rock Springs Uplift results. First, the chondrite-normalized concentration of REEs in deep formation brines higher than for lower-TDS water. Second, if the Soda Springs system is representative of CO<sub>2</sub> waters that have migrated from their place of origin into an adjacent formation, then the REE chemical signature may be useful for early detection of displaced formation brines impinging into overlying potable aquifers. The ability for early detection of migration would be highly desirable to CCS operators, regulators, and other vested parties. Another important characteristic of the data is the enrichment of LREE relative to chondrite in the unimpacted waters, indicating that these waters are close to equilibrium and are not undergoing rapid diagenesis. In contrast, the Soda Springs water has a flatter trend with a slight HREE enrichment—more indicative of a system that is undergoing relatively rapid change.

### 3.4 Summary

The objectives of this work are a small part of the overall goal of demonstrating the efficacy of using REEs as tracers in CCS or other relevant environments. The first objective was to develop a methodology to measure REEs across a range of CCS environments, from freshwater to high-TDS, saline-formation fluid. Our efforts resulted in two procedures: one for high-TDS brine and one for low-TDS water. Both of the procedures are equally effective in concentrating REEs and removing interfering ions so they can be analyzed by ICP-MS. The high-TDS procedure is slightly more involved but both procedures are inexpensive and can easily be conducted in most laboratories that do trace metal work. The sampling procedures needed to support these REE preconcentration procedures are more involved than a standard water analysis, but it would not be overly burdensome to apply to a CCS Pilot or industrial application.

The second objective was to demonstrate that REEs can be applied as natural tracers across a wide range of geologic environments and CCS applications. REEs have a long history of use as tracers in magmatic, ore deposits, and, more recently, groundwater studies. The ability to use existing water chemistry to track flow in the subsurface is appealing for a variety of reasons; most importantly, it does not rely on introduction of a thoroughly mixed tracer into the system. In our study, we evaluated REEs from three formations or systems: the Madison and Weber Formations in the Rock Springs Uplift, Wyoming, and a naturally leaking CO<sub>2</sub> system at Soda Springs, Idaho. In each of these systems, we were able to use REEs to elucidate the effectiveness of the seals capping the formations at the Wyoming location and the specific water-CO<sub>2</sub>-mineral reactions that are occurring in the Soda Springs system.

The procedures and methodologies described in this paper will be field tested at the Big Sky Carbon Sequestration Partnerships Saline CO<sub>2</sub> storage Pilot at Kevin Dome, Montana. Additional samples will be collected from collaborators throughout the CCS community, with the goal of sufficiently testing REEs such that they will routinely be applied as tracers as the CO<sub>2</sub>-storage technology matures.

### Acknowledgements

This material is based upon work supported by the U.S. Department of Energy and the National Energy Technology Laboratory under Award Number DE-FC26-05NT42587.

Disclaimer: “This report was prepared as an account of work sponsored by an agency of the United States Government. Neither the United States Government nor any agency thereof, nor any of their employees, makes any warranty, express or implied, or assumes any legal liability or

responsibility for the accuracy, completeness, or usefulness of any information, apparatus, product, or process disclosed, or represents that its use would not infringe privately owned rights. Reference herein to any specific commercial product, process, or service by trade name, trademark, manufacturer, or otherwise does not necessarily constitute or imply its endorsement, recommendation, or favoring by the United States Government or any agency thereof. The views and opinions of authors expressed herein do not necessarily state or reflect those of the United States Government or any agency thereof.”

We would like to acknowledge the staff at the University of Wyoming’s Carbon Management Office for collecting samples from the Rock Springs Uplift in the early hours of the morning and under difficult circumstances, and for reviewing the REE data with respect to the sedimentary stratigraphy of the Rock Springs Uplift.

### References

- Gosselin, D. C., M. R. Smith, E. A. Lepel, and J. C. Lau, 1992, “Rare Earth Elements in Chloride-Rich Groundwater, Palo Duro Basin, Texas, USA,” *Geochimica et Cosmochimica Acta*, Vol. 56, No. 4, April 1992, pp. 1495–1505, DOI: 10.1016/0016-7037(92)90219-9.
- Harkins, William D., 1917, “The Evolution of the Elements and the Stability of Complex Atoms,” *Journal of the American Chemical Society*, Vol. 39, No. 5, May 1917, pp. 856–879, DOI: 10.1021/ja02250a002.
- Johannesson, K. H. and M. J. Hendry, 2000, “Rare Earth Element Geochemistry of Groundwaters from a Thick Till and Clay-Rich Aquitard Sequence, Saskatchewan, Canada,” *Geochimica et Cosmochimica Acta*, Vol. 64, No. 9, May 2000, pp. 1493–1509, DOI: 10.1016/S0016-7037(99)00402-0.
- Johannesson, K. H., K. J. Stetzenbach, V. F. Hodge, D. K. Kreamer, and X. Zhou, 1997, “Delineation of Ground-Water Flow Systems in the Southern Great Basin using Aqueous Rare Earth Element Distributions,” *Groundwater*, Vol. 35, No. 5, September 1997, pp. 807–819, DOI: 10.1111/j.1745-6584.1997.tb00149.x.
- Lawrence, M. G. and B. S. Kamber, 2007, “Rare Earth Element Concentrations in the Natural Water Reference Materials (NRCC) NASS-5, CASS-4 and SLEW-3,” *Geostandards and Geoanalytical Research*, Vol. 31, No. 2, June 2007, pp. 95–103, DOI: 10.1111/j.1751-908X.2007.00850.x.
- Nelson, B. J., S. A. Wood, and J. L. Osiensky, 2004, “Rare Earth Element Geochemistry of Groundwater in the Palouse Basin, Northern Idaho–Eastern Washington,” *Geochemistry: Exploration, Environment, Analysis*, Vol. 4, No. 3, August 2004, pp. 227–241, DOI: 10.1144/1467-7873/04-203.
- Nelson, D. T., 2005, *Rare Earth Elements as a Natural Tracer of Ground Water Flow in the Eastern Snake River Plain Aquifer, Idaho*, M. S. Thesis: University of Idaho, Moscow, Idaho.
- Oddo, Giuseppe, 1914, “Die Molekularstruktur der radioaktiven Atome,” *Zeitschrift für anorganische Chemie*, Vol. 87, No. 1, June 1914, pp. 253–268, DOI: 10.1002/zaac.19140870118.

- Ohly, S. R., 2013, *A Comparative Study of Geochemistry, Microfacies, and Depositional Processes of Travertine Deposits in the Blackfoot Volcanic Field: Implications for Potential Blind Geothermal Systems in Southeastern Idaho*, M. S. Thesis: Idaho State University, Pocatello, Idaho.
- Ojiambo, S. B., W. B. Lyons, K. A. Welch, R. J. Poreda, and K. H. Johannesson, 2003, "Strontium Isotopes and Rare Earth Elements as Tracers of Groundwater-Lake Water Interactions, Lake Naivasha, Kenya," *Applied Geochemistry*, Vol. 18, No. 11, November 2003, pp. 1789–1805, DOI: 10.1016/S0883-2927(03)00104-5.
- Pearson, Ralph G., 1963, "Hard and Soft Acids and Bases," *Journal of the American Chemical Society*, Vol. 85, No. 22, November 1963, pp. 3533–3539, DOI: 10.1021/ja00905a001.
- Stetzenbach, K. J., M. Amano, D. K. Kreamer, and V. F. Hodge, 1994, "Testing the Limits of ICP-MS: Determination of Trace Elements in Ground Water at the Part-per-trillion Level," *Groundwater*, Vol. 32, November 1994, pp. 976–985, DOI: 10.1111/j.1745-6584.1994.tb00937.x.
- Strachan, D. M., 1989, "Preconcentration of Trace Transition Metal and Rare Earth Elements from Highly Saline Solutions," *Analytica Chimica Acta*, Vol. 220, pp. 243–249, DOI: 10.1016/S0003-2670(00)80267-6.
- Surdam, R. C., S. A. Quillinan, and Z. Jiao, 2013, "Displaced Fluid Management—The Key to Commercial-Scale Geologic CO<sub>2</sub> Storage," in *Geological CO<sub>2</sub> Storage Characterization: The Key to Deploying Clean Fossil Energy Technology*, edited by R. C. Surdam, pp. 233–244, New York: Springer Science+Business Media, DOI: 10.1007/978-1-4614-5788-6\_11.
- Wakita, H., P. Rey, and R. A. Schmitt, 1971, "Abundances of the 14 Rare-Earth Elements and 12 Other Trace Elements in Apollo 12 Samples: Five Igneous and One Breccia Rocks and Four Soils," *Proceedings of the Second Lunar Science Conference, Houston, Texas, January 11–14, 1971*, Vol. 2, pp. 1319–1329.
- Wood, S. A., 2006, "Rare Earth Element Systematics of Acidic Geothermal Waters from the Taupo Volcanic Zone, New Zealand," *Journal of Geochemical Exploration*, Vol. 89, Nos. 1–3, April-June 2006, pp. 424–427, DOI: 10.1016/j.gexplo.2005.11.023.

## CHAPTER 4: The Use of Rare Earth Elements as Natural Tracers to Characterize a Leaky CO<sub>2</sub> CCS Natural Analogue Site, Soda Springs, Idaho

“The Use of Rare Earth Elements as Natural Tracers to Characterize a Leaky CO<sub>2</sub> CCS Natural Analogue Site, Soda Springs, Idaho.” Submitted to the Journal of Volcanology and Geothermal Research.

Travis L. McLing,<sup>a,d,\*</sup> Ghanashyam Neupane,<sup>a</sup> Robert W. Smith,<sup>b</sup> and William Smith<sup>c</sup>

<sup>a</sup> Idaho National Laboratory, P.O. Box 1625, Idaho Falls, ID 83415-2107, USA

<sup>b</sup> University of Idaho, Moscow, ID 83844, USA

<sup>c</sup> Terra Tek, Oklahoma City, 8100 N. Classen, Unit 114, Oklahoma City, OK 73114, USA

<sup>d</sup> The Center for Advanced Energy Studies, 995 University Blvd., Idaho Falls, ID 83401, USA

\* Corresponding author: Travis L. McLing: E-mail [travis.mcling@inl.gov](mailto:travis.mcling@inl.gov);  
Telephone: 012085267269; Fax: 012085260875

### Abstract

This study was conducted to determine whether or not a suite of in-situ natural chemical tracers, specifically rare earth elements (REEs), can be used as tracers to track CO<sub>2</sub> and CO<sub>2</sub>-charged waters in carbon capture and sequestration (CCS) applications. Here we utilize a naturally leaking CO<sub>2</sub> system located at Soda Springs, Idaho, as an analogue for industrial-scale CCS deployment. Analogue sites are particularly relevant and useful for studying consequences of CCS because they offer the chance to examine a geologic system on a temporal and spatial scale that laboratory and field experimentation cannot. One such example of a mafic rock, CO<sub>2</sub> analogue is the Soda Springs site located in Caribou County of Southeast Idaho, USA. At the Soda Springs site, CO<sub>2</sub> and formation fluids generated by the dissolution of Paleozoic carbonates and shale at-depth are migrating into the shallow subsurface, where they migrate into a shallow aquifer. The vertically rising waters also degas significant amounts of CO<sub>2</sub>, which causes a significant amount of calcite to precipitate in the once-porous basalt, sealing much of the permeability. The CO<sub>2</sub> and small amounts of deep water are expressed as either carbonated springs or as CO<sub>2</sub>-pressurized geysers created by wells that penetrate the upper aquifer into the deep, CO<sub>2</sub>-charged system. Analysis of wells, springs, and creek water at the study site reveal that the waters can be classified into four water types based on the presence of travertine, bubbling CO<sub>2</sub>, physical characteristics, and temperature—with the exception of Sulphur Springs, which is a high-flux, dry, CO<sub>2</sub> and H<sub>2</sub>S system—their REE signature.

The results of the study show that water chemistry, especially REE, can be useful tools in delineating the movement of CO<sub>2</sub>-influenced waters migrating from deep reservoir. Additionally, at Soda Springs the calcite mineralization caused by the degassing of CO<sub>2</sub> from vertically rising waters has sealed much of the permeability in series of basalts that cap the system, forming an effective aquitard. Except where penetrated by wellbores or along major faults, the mineralized basalt prevents deep CO<sub>2</sub>-charged brine from reaching the shallow aquifer. However, the seal is less effective with regard to CO<sub>2</sub>, as there are a number of locations along fault zones where CO<sub>2</sub> gas escapes to the surface in large volumes, forming effervescing carbonated springs.

**Keywords:** Soda Springs, CO<sub>2</sub> water chemistry, rare earth elements, groundwater

## 4.1 Introduction

Since the beginning of the Industrial Revolution, atmospheric concentration of CO<sub>2</sub> has increased from its pre-industrial level of 280 ppmv to its present value of approximately 385 ppmv (Prentice et al. 2001; Solomon et al. 2013), due primarily to the burning of fossil fuels. Several modeling scenarios investigated by the Intergovernmental Panel on Climate Change (IPCC) predict that CO<sub>2</sub> concentrations in the atmosphere may increase to 1,100 ppmv by 2100 (White et al. 2004; IPCC 2007). Accompanying this rise in atmospheric CO<sub>2</sub> is a predicted increase in global temperature between 2 and 6°C (IPCC 2007). The recognized correlation between increasing CO<sub>2</sub> levels and climate change, with its associated deleterious impacts (Solomon et al. 2009; Whitehead et al. 2009), is motivating investigation and development of science and engineering solutions to minimize anthropogenic CO<sub>2</sub> emissions. One approach to mitigate CO<sub>2</sub> emissions is through the long-term storage of anthropogenic CO<sub>2</sub> in geologic formations by carbon capture and storage (CCS). Demonstrating that CO<sub>2</sub> can be permanently stored at reasonable cost is important to ensure global adoption (Lokey-Aldrich et al. 2012; Benson and Cook 2005).

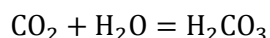
Global adoption of CCS will require the development of significant new science and engineering-based solutions to ensure that CO<sub>2</sub> remains safely stored in the geologic formations and does not migrate into shallow, potable aquifers. In the United States, the Environmental Protection Agency (EPA) has established a regulatory standard that stipulates that CCS cannot be conducted in formations containing less than 10,000-ppm total dissolved solids (TDS) (EPA 2014). As a result, early deployments of CCS will likely focus on deep saline aquifers and depleted oil and gas reservoirs. These types of formations are good CCS targets because many are known to have trapped naturally occurring CO<sub>2</sub>, hydrocarbons, and other geofluids over geologic time. However, CCS activities in such formations have the potential to displace formation fluids into potable aquifers due to over pressurization of the target reservoir. This may require the production and



reinjection of brines from the target formations to manage reservoir pressure and control the CO<sub>2</sub> plume. In addition to the sheer volume of brine that could be displaced, several studies have determined that several metals of concern (e.g., Pb, Cu, Co, Ni, Zn, Mn, and Fe) could be mobilized due to decreased pH and associated dissolution of metal-scavenging phases, such as Fe-hydroxides (Zheng et al. 2012; Kharaka et al. 2010; Siirila et al. 2012; Assayag et al. 2009; Zheng et al. 2009; Alfredsson et al. 2008; Apps et al. 2008; Wang and Jaffe 2004; Spycher et al. 2003; and Xu et al. 2003). Therefore, the ability to track the movement of formation fluids in geologic formations will be critical to effective MMV efforts and ensuring environmental and regulatory compliance.

An alternative to saline formations that is being considered for CCS is storage in deep basalt formations because of their high reactive potential, which may result in the precipitation of CO<sub>2</sub> as stable carbonate minerals through water-rock-CO<sub>2</sub> reactions, thus permanently securing it from release to the atmosphere (Gislason et al. 2009; Goldberg et al. 2009; Schaef and McGrail 2006; Schaef et al. 2009, 2010). This CO<sub>2</sub>-driven reactivity will impart chemical signatures of the formation to the brines and the groundwater if leakage occurs. In this situation, the use of groundwater chemical signatures as tracers to support MMV activities at CCS sites represents a viable method for tracing the movement of CO<sub>2</sub> and/or displaced brines. Some examples of commonly used environmental tracers that may have application to CCS are isotopes (e.g., δ<sup>18</sup>O, <sup>3</sup>He/<sup>4</sup>He, δ<sup>34</sup>S, <sup>234/238</sup>U, <sup>222</sup>Rn, <sup>36</sup>Cl, and <sup>87/86</sup>Sr), noble gases (e.g., He, Ar, and Kr), and major element chemistry (e.g., Ca<sup>2+</sup>, Na<sup>+</sup>, HCO<sub>3</sub><sup>-</sup>, and Cl<sup>-</sup>) and REEs.

Here we focus on application of major elements and REEs as geochemical tracers for a natural analogue for CCS. Because REE concentrations in rock are measured in the parts per million, and their concentrations in the groundwater are generally in parts per trillion, REE trends are very sensitive to water-rock interactions, making them well suited for tracing water flow and geochemical processes in groundwater systems (Smedley 1991). REEs have also been successfully used as in-situ tracers to describe the evolution of sedimentary systems (Banner et al. 1989; Bertram and Elderfield 1993; Gosselin et al. 1992). These previous works have direct application to tracing CO<sub>2</sub> transport in CCS systems, as brine chemistry may be particularly sensitive to changes in local equilibrium caused by the addition of CO<sub>2</sub>. The addition of large volumes of CO<sub>2</sub> in CCS operations will change the brine chemistry due to a decrease in pH caused by the dissolution of CO<sub>2</sub> in the brine (Equation [4.1]). The geochemical signature imparted to the formation fluids by this change could be a useful tracer for fluid migration, both within the formation and, should it migrate, into overlying formations.



Equation (4.1)

Of particular relevance to this study is a growing body of work focused on the use of REEs to ascertain groundwater flow paths and chemical evolution along flow paths (Johannesson et al. 2017; Chevis et al. 2015; Wood et al. 2006; Nelson et al. 2004; Johannesson et al. 2000; Ojiambo et al. 2003; Stetzenbach et al. 2001; Zhou et al. 2005; Johannesson et al. 1997a, 1997b; Gosselin et al. 1992; Nelson et al. 2005). These earlier studies have demonstrated the success of tracking groundwater migrating through a variety of host rocks using REEs as natural elemental tracers.

#### **4.1.1 Natural CCS Analogues**

The study of naturally occurring CO<sub>2</sub> deposits, and especially the leaky systems, as analogues for long-term CO<sub>2</sub> behavior in CCS systems (Kampman et al. 2016; Bertier et al. 2015; Burnside et al. 2013; Bickle and Kampman 2013; Kampman et al. 2010; Jeandel et al. 2010) may provide relevant insight about the environmental risks associated with the global adoption of this technology. These natural analogues are widely distributed throughout the world and provide useful field laboratories for assessing the long-term interactions of migrating CO<sub>2</sub> within geologic formations similar to those expected in CCS reservoirs (Keating et al. 2010; Allis et al. 2001; Baines and Worden 2004; Haszeldine et al. 2005; Moore et al. 2005).

An example of a natural analogue site that captures features relevant to CCS in brine reservoirs and basalt-hosted systems is located near the city of Soda Springs in Southeast Idaho (Figure 4.1). This site has been recognized as an analogue for a leaking CCS reservoir (Jeandel et al. 2010; Lewicki et al. 2013; McLing et al. 2012; Maskell et al. 2015). The Soda Springs study site is unique in that the deep pressurized-CO<sub>2</sub> system has its origin in sedimentary rocks at depth that are capped near the surface by mineralized Quaternary basalt flows.

At the Soda Springs site, a large number of CO<sub>2</sub> springs, leaking wells, and associated travertine deposits are distributed throughout an approximately 65-km<sup>2</sup> surface expression of the leaking CO<sub>2</sub> system. The source of the CO<sub>2</sub> at the site has been suggested to be the dissolution of Paleozoic marine carbonates and marine shale by deeply derived acidic geothermal fluids (Mayo et al. 1985; Maskell et al. 2015; Lewicki et al. 2013; Reilly et al. 1994; McLing et al. 2012).

#### **4.1.2 Geologic Setting**

The study area is located in the Blackfoot Valley (Figure 4.1) in Southeast Idaho, within the Sevier thrust tectonic belt and along the northeastern margin of the Basin and Range Province. Here, a thick succession of Paleozoic and Mesozoic sedimentary rocks have been thrust more than 150 km eastward toward the midcontinent over a period of 60 million years (Fiesinger et al. 1982; Allmendinger 1981; Hutsinpillar and Parry 1985). Locally, the area is underlain at-depth by

Archean crust, capped with up to 10 km of over-thrust sedimentary rock (Oriol and Platt 1980; Sparlin et al. 1982; Link and Phoenix 1996; Peng and Humphreys 1998) capped by Quaternary tholeiitic basalt flows of the Blackfoot Volcanic Field (BVF). Regionally, mountains and valleys associated with east-west Basin and Range Province extensions dominate the topography of the area.

The geology of the highlands surrounding the BVF consists primarily of early-to-middle Paleozoic marine quartzite, limestone, and dolomite. However, the area also subordinately contains the Precambrian Brigham Group and Late Paleozoic units, including the Mississippian Mission Canyon Limestone, Lodgepole Limestone, and the Permian Phosphoria Formation (Figure 4.2). Quaternary basalts and intercalated sediments that constitute BVF extend farther to the north from the study area (Welhan 2002; Mansfield and Girty 1927; Armstrong 1969; Armstrong and Oriol 1965). Based on the geologic relationship, a thick section of Paleozoic sediments underlie the basalts of the BVF. The basalt flows in the BVF range from a few meters to more than 300 m thick in the central portion of the valley and thin to the south (Pickett 2004; Armstrong and Oriol 1965; Armstrong 1969; Mabey and Oriol 1970; Ford 2005). The basalts in the BVF range in age from 100 to 1,000 ka (Luedke and Smith 1983) and generally become younger in the southern part of the valley.

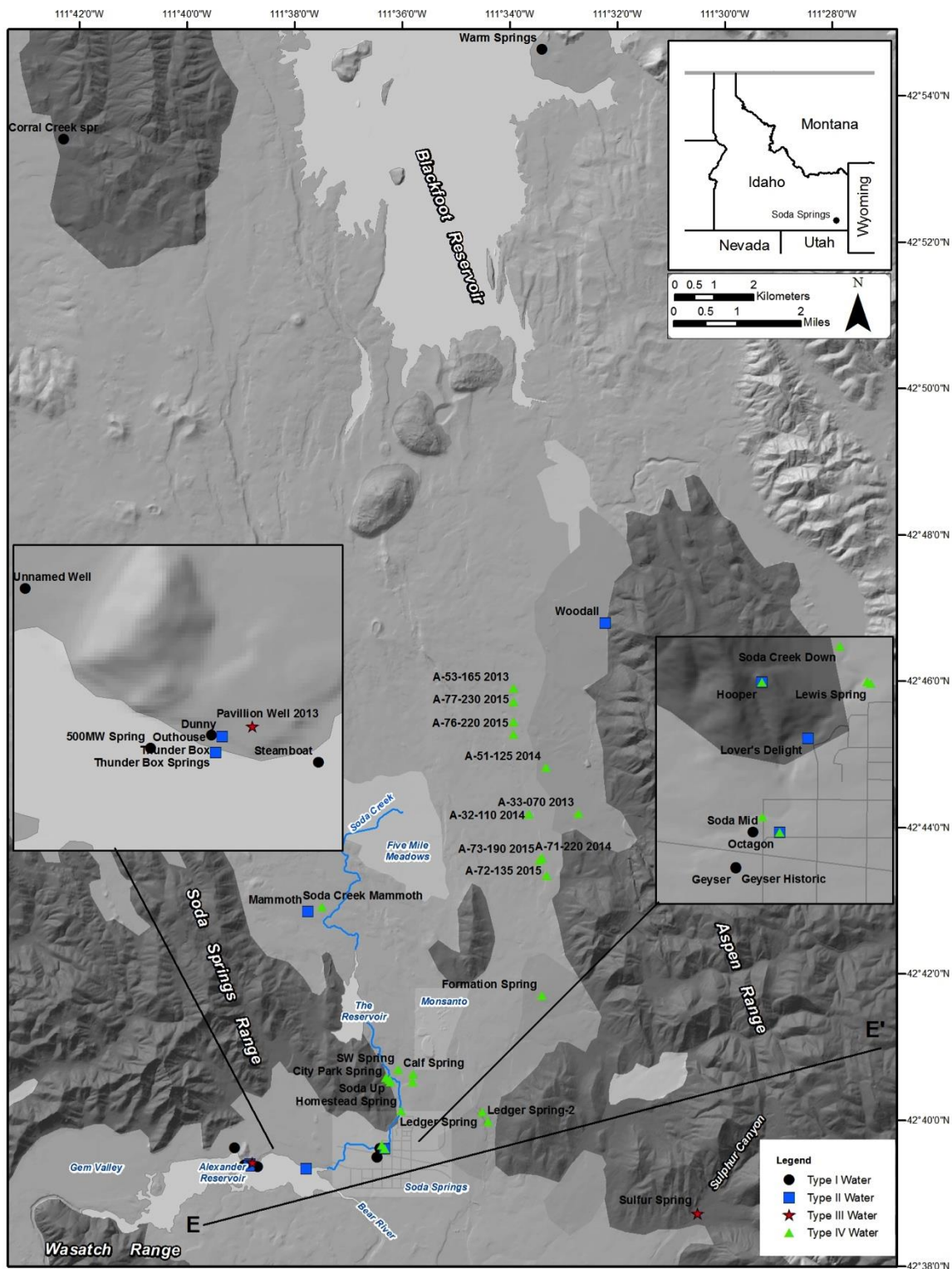


Figure 4.1: Map of major geologic and hydrologic features of the Blackfoot Valley and Sulphur Canyon. Also shown are the sample locations for this study. Most of the CO<sub>2</sub>-charged springs and wells are located on the southeast side of Blackfoot Valley and along the shores of Alexander Reservoir, which impounds water from the Bear River.

The BVF is a typical graben and horst-type Basin and Range valley, aligned in a north-south direction. The associated extension has controlled the development of the north-south trending valley with major range-bounding faults along its east and west margin. Faulting and fracturing within the valley is also aligned north to south and has been associated with extension caused by late-stage basalt-dike injection (Polun 2011). The east-west-extending Bear River Valley, which truncates the Valley to the south (Figure 4.1) is not normal-fault controlled; instead, it is a valley along a tear fault that separates the Ninety-Percent Range to the north and the Wasatch Range to the south (Allmendinger 1981; Carney and Janecke 2005; Christiansen and Lipman 1972; Armstrong 1969).

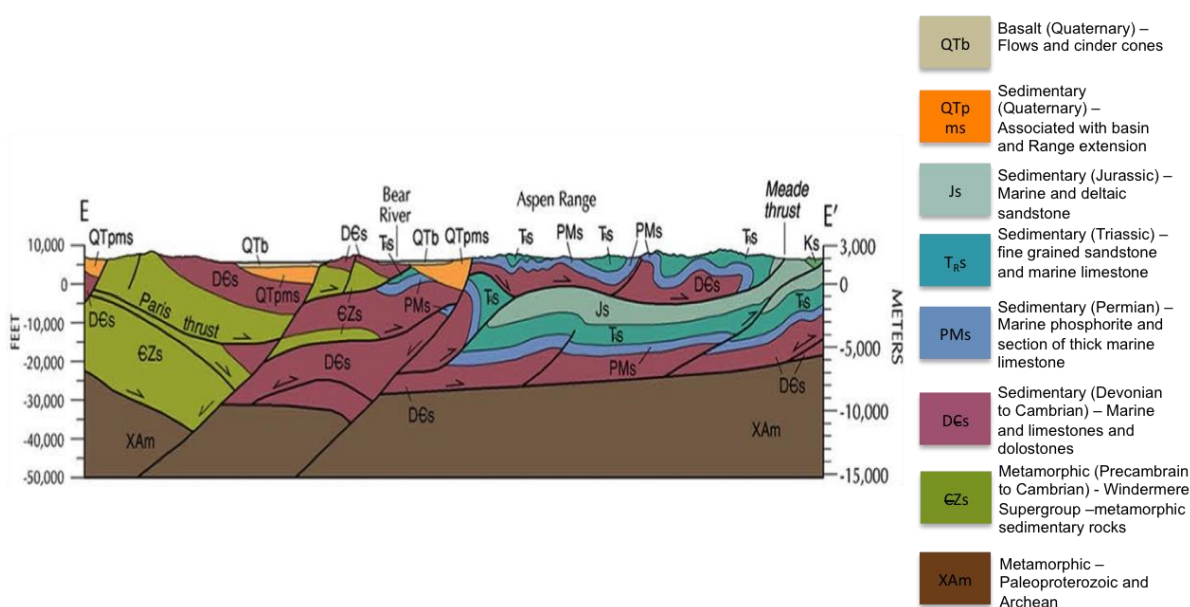


Figure 4.2: Regional cross-section of the southern Blackfoot Valley E-E.' (Figure 4.1) (Link 1996; Lewis et al. 2012). Used with permission from the Idaho Geologic Survey.

#### 4.1.3 Regional Hydrology

The Soda Springs area is located in an arid environment with a mean annual precipitation of 40.4 cm, with May having the highest and December the lowest mean monthly precipitation (www.wrcc.dri.edu, Soda Springs Airport [108535]). Groundwater in the Blackfoot Valley aquifer flows from the north to south, with the Bear River marking the southern boundary of the system (Figure 4.1). The dominant sources of recharge to the regional Blackfoot Valley aquifer are leakage from the Blackfoot Reservoir (Mansfield and Girty 1927; Dion 1974), located 20 km north of Soda Springs, and snowmelt from the mountain ranges that surround the Blackfoot Valley (Hutsinpillier and Parry 1985; Mayo et al. 1985). Value of  $\delta D$  and  $\delta^{18}O$  reported by Maskell et al. (2015) show that water from all of the various sources are meteoric in origins.

The Blackfoot Valley aquifer is a highly productive, shallow aquifer system with productivity decreasing from north to south as a result of porosity-filling mineralization in the southern portion of the valley (Dion 1974). Surface water in the BVF is dominated by Soda Creek, which flows from its source at Fivemile Meadows to where it is captured by a canal near the Bear River on the east side of the city of Soda Springs. Along its flow path, Soda Creek is impounded by a small reservoir 2 km north of the city of Soda Springs (Figure 4.1). Stream discharge for Soda Creek averages  $1.5 \text{ m}^3/\text{s}$  and is entirely effluent, with discharge not varying significantly throughout the year.

Prior to 2012, the most consequential hydrochemical study conducted in the Southern Blackfoot Valley was associated with shallow groundwater contamination from Monsanto's Soda Springs elemental phosphate plant (Figure 4.1). Well logs from this ongoing Comprehensive Environmental Response, Compensation and Liability Act (CERCLA) study show that the basalt in the subsurface is highly mineralized (Figure 4.3), especially below 80–90 m below land surface (BLS). Wells that penetrate this horizon are warm ( $\sim 30^\circ\text{C}$ ), highly pressurized with  $\text{CO}_2$ , and are capable of erupting more than 30 m above land surface. The impermeability of this horizon creates a seal that largely prevents migrating  $\text{CO}_2$ -charged thermal water from reaching the surface, except along the range-bounding faults.

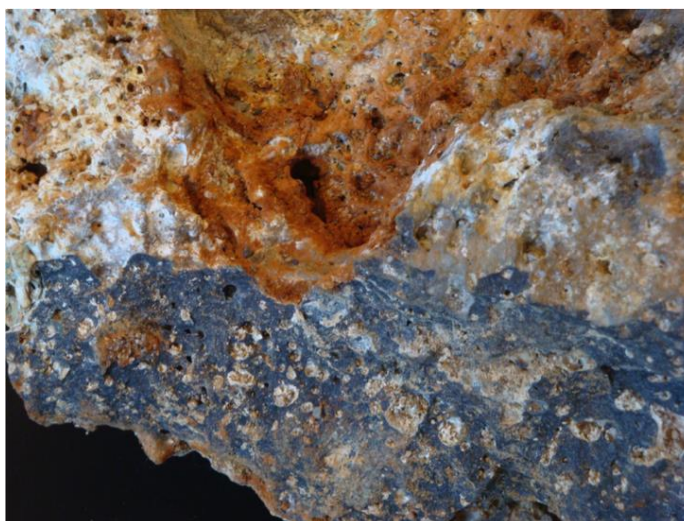


Figure 4.3: Photo of highly mineralized basalt collected from the subsurface near Hooper Springs. The heavily mineralized basalt is characteristic of basalt chips from wells drilled into the subsurface in the Southern Blackfoot Valley. The orange mineralization is hydrous ferric oxide (HFO), which commonly co-precipitates with calcite at springs and wells.

#### **4.1.4 Carbon-Dioxide-Charged Aquifer**

##### **4.1.4.1 Carbon Dioxide System**

During this study and other recent studies (Lewicki et al. 2013; Maskell 2015; McLing 2012), numerous carbonated springs, both thermal and non-thermal, were mapped. The carbonated springs (except for the springs in Sulphur Canyon) are located along the western boundary of the Blackfoot Valley and along a line stretching from the city of Soda Springs westward along the Bear River toward Gem Valley (Figure 4.1). The highest density of CO<sub>2</sub>-charged springs and associated travertine deposits is located along the Bear River west to Gem Valley (Figure 4.1). Along this east-west transect, dry CO<sub>2</sub> leaks (gas only) and carbonated springs are extremely abundant. Isotope data (e.g., <sup>3</sup>He/<sup>4</sup>He, δ<sup>34</sup>S, and δ<sup>13</sup>C<sub>CO2</sub>) from gas emission indicate that the CO<sub>2</sub> in the carbonated waters are sourced from the carbonate and shale rocks that occur at-depth (Figure 4.2) (Lewicki et al. 2013; Armstrong 1969; Armstrong and Oriel 1965). The carbonated waters have been estimated to circulate to depths of 1,000 to 2,000 m (Mayo et al. 1985), where the water likely interacts with the Paleozoic marine limestone and dolomite (DCs in Figure 4.2).

##### **4.1.4.2 Structural Control for Carbon Dioxide Release**

Prior studies (Wood and Norrell 1996; Young and Mitchell 1973; Mitchell 1976; Muller and Mayo 1983; Hutsinpillar and Parry 1985; Mayo et al. 1985; Dion 1974) have concluded that faults provide permeability pathways for water and CO<sub>2</sub> to move from depth to the surface and control the surface expression of the springs in the Blackfoot Valley. Geologic structures appear to control the pattern and surface expression of the CO<sub>2</sub> system (Maskell 2015; Lewicki et al. 2013; Polun 2011) in the area such that the carbonated springs and travertine deposits associated with active and extinct springs mostly aligned with topography-defining faults.

## **4.2 Methods**

### **4.2.1 Sampling Methods**

Our sampling methods are modified after the methods of Stetzenbach et al. (1994), Samson and Wood (2005), Wood (2006), and Nelson (2005) to maintain the integrity of the samples by minimizing sources of contamination. At each sample location, samples were collected for anions, cations and REEs. For cations and REE samples, high-density polyethylene bottles (250 mL for cations and 500 mL or 1 L for REEs) were acid washed using 5–7% trace-metal-grade nitric acid. After a minimum of two days in the acid wash, the bottles were triple-rinsed and filled with 18 MΩ deionized water (DIW), sealed, and placed into acid-washed plastic bags for transportation to the field. For anion samples, DIW water-washed/filled bottles were used. Once in the field, the DIW water in the sample bottles was discarded, and the bottles were rinsed three times with sample water before being filled and transported to the lab.



Each sample was collected from the main vent (maximum outflow) of the spring when accessible, from the fastest-flowing portion of the stream, or spring runoff channel when the main vent was not accessible. The pH, temperature, conductivity, and alkalinity were measured and recorded for each sample. A Geotech peristaltic pump was used to pump water from the source to the sample bottles through pre-cleaned, acid-washed, Teflon tubing fitted with a 0.45-um Gelman Sciences high-capacity capsule filter containing polyether sulfone membrane. The cation and REE samples were acidified to pH <2, using Optima-grade nitric acid, and sealed with Parafilm. To minimize the potential for environmental contamination, the exteriors of the sample containers were rinsed thoroughly with DIW water and placed into acid-washed plastic bags, and the bagged sample containers were placed in a cooler with dry ice for transport back to the laboratory. The only deviations from this procedure were at aquifer wells that had fixed piping. In these cases, the Teflon tubing and filter apparatus was connected to the existing piping; samples were filtered and preserved as described above. For monitoring potential contamination, a field blank consisting of DIW water brought from the laboratory was processed through the same procedure in the field. Once the samples arrived at the laboratory, they were inventoried and refrigerated until processing and analysis.

#### **4.2.2 Aqueous Mineral Speciation**

The Geochemist's Workbench (GWB, Aqueous Solutions LLC) (v 9.0), and its associated database ([thermo.com.V8.R6+.tdat](http://thermo.com.V8.R6+.tdat)), a commercially available, mixed equilibrium-kinetics geochemical computer code (Bethke 2014) was used to calculate speciation (aqueous species, gaseous phases) and mineral saturation indexes ( $\log(Q/K)$ ), where Q is the ion activity product and K is the temperature-dependent equilibrium constant for the mineral dissolution). In addition, GWB was used to calculate the partial pressure of CO<sub>2</sub> at different pressures for the deep aquifer at Soda Springs based on results from analytical and field measurements.

#### **4.2.3 REE Sample Preconcentration**

Because REEs in natural waters occur at the pictogram/liter (pg/l) level, special procedures must be used to preconcentrate the REE from the samples at least 50-fold and remove interfering cations prior to analysis. By preconcentrating the samples, we were able to remove >99% of the divalent cations, which decreases the REE detection limit and lowers the overall background interference. Additionally, by removing BaO, which interferes with <sup>139</sup>La, <sup>146</sup>Nd, <sup>147</sup>Sm, <sup>175</sup>Lu, and, specifically, <sup>152</sup>Sm and <sup>151</sup>Lu, we were able to improve the accuracy of our measurement.



Prior REE studies (Wood et al. 2006; Nelson et al. 2004; Johannesson et al. 1997a, 1997b; Johannesson et al. 2000; Johannesson and Hendry 2000; Ojiambo et al. 2003; Stetzenbach et al. 2001; Zhou et al. 2000; Gosselin et al. 1992) have focused on a small family of samples with similar chemistry, and the methods developed for these studies were not entirely appropriate for the wide range of water compositions present in samples from the Soda Springs area. REE preconcentration was accomplished using methods described in McLing et al. (2014) and described below. Samples collected for this study range over three orders of magnitude in TDS. A low-TDS method after (e.g., Elderfield and Greaves 1982; Klinkhammer et al. 1994; Nelson 2005; Johannesson et al. 2011; McLing et al. 2014) was used for samples containing TDS less than 1,500 mg/L and a high-TDS method after (Strachan et al. 1989) was used for samples with TDS higher than 1,500 mg/L.

Preconcentration of low-TDS sample for REE analysis was performed using AG-50W-X8 hydrogen form resin in the 200–400-mesh size. Previous studies (e.g., Elderfield and Greaves 1982; Klinkhammer et al. 1994; Johannesson et al. 2011; McLing et al. 2014) reported that this size fraction results in a lower flow rate through the column and increases the REE capture efficiency. The samples were processed to concentrate the REE by continuous gravity feeding of sample through a resin containing chromatography column (20 mL Bio-Rad column) with a 250-mL sample reservoir. After the sample chromatography was completed, the eluent was discarded. Forty mL of 1.7 N Optima nitric acid was then added to the reservoir to elute divalent cations from the resin, leaving behind only the trivalent cations retained in the resin. The REE and other trivalent cations are then eluted from the resin using 10 mL of 8-N Optima nitric acid and collected in an acid-washed Teflon container. For this method, the amount of resin used varies based on the cation makeup and total TDS of the water as follows:

$$\text{AG-50W-X8 (mL)} = 0.0038 \times \text{TDS (mg/L) for Ca-Mg rich waters} \quad \text{Equation (4.2)}$$

$$\text{AG-50W-X8 (mL)} = 0.0046 \times \text{TDS (mg/L) for Na rich waters} \quad \text{Equation (4.3)}$$

For some very-low TDS water, the calculated volume of AG-50W-X8 can be as little as 1 or 2 mL. This allows very rapid flow of water through the column; in such cases, we used 5 mL of AG-50W-X8 to increase sample residence time in the column. For a given volume of water, TDS, and major cations, the volume of AG-50W-X8 ranges from 5 to 20 mL (20 mL is the maximum volume our columns can hold). If the calculated amount of AG-50W-X8 needed is more than 20 mL, we used the chelex-100 procedure described below.

For high-TDS samples, a modified method based on Strachan et al. (1989) was used to concentrate the REE from solution. This procedure uses 200–400-mesh Chelex 100 resin in the Na form. In summary, each column containing 16.25 g of resin was flushed with 50 mL of 2.5 N Optima nitric

acid to convert the resin to hydrogen form and remove any non-hydrogen cations. The initial acid wash was followed by a 50-mL DIW water wash to remove excess nitric acid from the resin. Then the resin was converted to  $\text{NH}_4^+$  form by passing 50 mL of 2.0 N of high-purity ammonium hydroxide solution, which was followed by DIW water washes to a neutral pH. The resin pH was then adjusted to  $5.3 \pm 0.1$  using Optima nitric acid to attain the optimal pH of 5.3 for the best cation capture.

Once the resin was prepared, the REEs in each sample were nominally concentrated by 50:1 or 100:1 by gravity-feeding nominally 500 mL or 1,000 mL of sample through the column, first adding two 50-mL aliquots of sample to allow the resin volume to shrink without forming preferential flowpaths. Once the entire sample was passed through the column, 250 mL of DIW water was applied. The column was then eluted with a 25-mL then two 50-mL aliquots of pH-adjusted ( $\text{pH} = 5.3 \pm 0.1$ ) 1.0 M, high-purity ammonium acetate to remove the mono- and divalent cations. Then, 250 mL of DIW water was applied to the column to remove excess ammonium acetate. Next, two 100-mL aliquots of 2.5 N Optima nitric acid were applied to the column to elute REEs and other trivalent cations into an acid-washed Teflon beaker.

The final REE extract obtained with both low- and high-TDS procedures was evaporated to dryness at  $60^\circ\text{C}$  on a hot plate enclosed in a filter box to eliminate contamination by dust. The resulting bead was then dissolved in a 10-mL 1% Optima nitric acid to obtain the final concentration ratio of approximately 50:1 or 100:1. The sample was then sealed in a triple acid-washed, 15-mL centrifuge tube for ICP-MS analysis. A detailed description of the REE preconcentration methods can be found in McLing (2014). Based on repeat analysis, the relative standard deviation of both extraction methodologies is less than 15%.

#### **4.2.4 REE Data**

Like all other elements, REE elements are subject to the Oddo-Harkins effect, which is that the cosmic abundance of all elements with an even atomic number is greater than the neighboring elements with odd atomic numbers. The effect of this phenomenon is that when raw REE concentrations in geologic materials and fluids are plotted versus atomic number, the resulting plot will have a characteristic saw-tooth pattern (Shannon and Wood 2005). This saw-tooth pattern can make it much more difficult to elucidate fractionation trends due to chemical and physical processes in natural systems. To make REE data more useful, the saw-tooth pattern is removed by normalization to a known reference material (Samson and Wood 2005; Rollinson 1993; Hollings and Wyman 2005). Typically, the reference materials of choice for normalization are carbonaceous chondrite (Shinotsuka et al. 1995; Boynton 1984; Wakita et al. 1971), shale composites such as North American Shale Composite (NASC) (Gromet et al. 1984), or average Post-Archean Average Australian Shale (PAAS)

(Nance and Taylor 1976), European Shale composite (ESC) (Taylor and McLennan 1995), and unfractionated mantle (Sun 1982). Here, chondrite normalization was used.

The raw, REE-concentration results were normalized using the average of 12 carbonaceous chondrites (Wakita et al. 1968). Eu and Ce may exhibit anomalously higher or lower normalized concentrations when compared with their neighboring elements because of their ability to exist in multiple oxidation states ( $\text{Ce}^{4+}$ ,  $\text{Ce}^{3+}$  and  $\text{Eu}^{2+}$ ,  $\text{Eu}^{3+}$ ). The anomalous, normalized concentration was quantified by comparing the observed concentration to an interpolated concentration ( $\text{REE}^*$ ) using

$$\left(\frac{z\text{REE}}{z\text{REE}^*}\right)_{cn} = \log\left(\frac{2 z\text{REE}}{z_{-1}\text{REE} + z_{+1}\text{REE}}\right) \quad \text{Equation (4.4)}$$

where  $z\text{REE}$  is the chondrite-normalized concentration of the REE with atomic number  $Z$  (58 for Ce and 63 for Eu) and  $z_{-1}\text{REE}$  and  $z_{+1}\text{REE}$  are the chondrite-normalized concentration of the REE with atomic numbers  $Z-1$  and  $Z+1$ , respectively.

REEs are typically subdivided into two groups: the light rare earth elements (LREE), comprised of elements La to Gd, and the heavy rare earth elements (HREE), comprised of elements Tb to Lu (Henderson 1984). Another less-common but useful classification is middle rare earth elements (MREE), which include elements Sm to Dy. The slight difference in affinity for co-precipitation and sorption between the HREE and LREE is primarily due to the effect of lanthanide contraction: the LREEs have lower atomic masses but larger ionic radii; the HREEs have higher atomic masses but smaller ionic radii.

#### 4.2.5 Analysis

All analytical measurements were made at the Center for Advanced Energy Studies (CAES) in Idaho Falls, Idaho. Each trace metal, major cation, and REE sample was analyzed in triplicate using an Agilent 7500c Inductively Couple Plasma Mass Spectrometer (ICP-MS), equipped with a Babington nebulizer and an electron multiplier detector. Calibration standards were prepared from concentrated standard purchased from Inorganic Ventures Inc. For analyses of REEs, the plasma oxide formation was maintained at  $<0.5\%$  for  $^{156}\text{CeO}/^{140}\text{Ce}$ . Instrumental drift was accounted for by periodically analyzing a fixed concentration Rh internal standard, instrument blanks, and quality-control standards. All analytical results have less than 5% of deviations as calculated from the known samples.

Anions were analyzed in triplicates using a Thermo Scientific Dionex Model ICS-2100 ion chromatograph, using a potassium hydroxide eluent (Dionex EluGen Cartridge EGC-KOH). Replicate analyses of each sample were measured to meet the system-specified range of a standard deviation of  $\leq 3\%$ .

Alkalinity was determined by titration using a Hach Company alkalinity kit, and the results were expressed as mg/L of  $\text{CaCO}_3$  and bicarbonate (Kehew 2001). The temperature, conductivity, and pH were measured using an Orion field-combination pH meter with temperature and conductivity.

### 4.3 Results

For this study, samples were collected from 44 locations in the BVF near Soda Springs, Idaho, and Sulphur Canyon, 6.5 km to the east (Figure 4.1). Of these samples, 12 were analyzed for REEs. To verify consistency of water chemistry with time, samples were collected and analyzed for major elements and field parameters multiple times across the three-year study. The results presented here are associated with the sampling campaign where REE samples were collected. The TDS was estimated from the field-measured conductivity. Following laboratory analysis, the TDS was calculated from elemental concentrations and ranged from 841 ppm at Ledger Spring (the water supply for the city of Soda Springs) to more than 6,300 ppm in some of the warm, high,  $\text{CO}_2$ -charged water. Based on the concentrations of major elements, waters sampled range from the dominant, circum-neutral Ca-Mg- $\text{HCO}_3$  water to acidic Ca- $\text{SO}_4$  water. The latter occurs only at the Sulphur Springs complex (Figure 4.1).

For comparison, waters were grouped based on the presence of  $\text{H}_2\text{S}$  odor, sulfur precipitation or travertine precipitation, effervescing  $\text{CO}_2$ , and temperature (Table 4.1). Results of other studies as well as our own sampling over three years shows that with the exception of Sulphur Springs, all of the sample locations have been chemically consistent over time (Mayo et al. 1985; Maskell et al. 2015; Lewicki et al. 2013; Reilly et al. 1994; McLing et al. 2012). Several springs (Steamboat Spring, 500 M, Bathtub) (Figure 4.4) are rarely available for study, as they are normally covered by several meters of water from Alexander Reservoir. However, we were able to sample Steamboat Spring, 500 M Spring, and Bathtub Spring during the summer of 2012, when Alexander Reservoir was drained for dam maintenance.

A summary of major and REE-chemical characteristics of the water samples collected from the Soda Springs study site is given in Tables 4.2 and 4.3.

Table 4.1: Heuristics used for water classification in this study. Three of the water types (Types I, II, and III) are waters that effuse CO<sub>2</sub>. Only Type I water is warm and is actively precipitating travertine.

Water Type	Characteristic	H <sub>2</sub> S Odor	Mineral Precipitation	Temperature	Presence of Effervescing CO <sub>2</sub>
Type I Water	Iron stained artesian flow Slight H <sub>2</sub> S odor	Yes	Copious travertine precipitation	Warm >25°C	Yes; capable of geysering when encountered by wells
Type II Water	Iron stained along margin	No	No	Cold <15°C	Yes; quiescent bubbling
Type III Water	High gas flux Strong H <sub>2</sub> S odor	Yes	Sulfur precipitation on land surface and in water	Cold <10°C	Yes, CO <sub>2</sub> is released under pressure, which causes roaring sound
Type IV Water	Flowing clear creek and spring water	No	No	Cold <15°C	No

#### 4.3.1 Type I Water – Warm CO<sub>2</sub>-Charged Water

A total of 11 Type 1 water samples were collected and analyzed (Table 4.2). Type I water is characterized by highly CO<sub>2</sub>-charged warm water (~27°C), with a TDS >5,000 ppm and is actively precipitating travertine at surface expression. The chemistry of the Type I water [shown as filled black circles in the Piper diagram (Figure 4.5)] is dominated by Ca-Mg-HCO<sub>3</sub>, and is highly CO<sub>2</sub>-charged with effervescing bubbles and outflow from the spring or wellbore activity. These waters are also characterized by anoxic conditions and high, dissolved, Fe concentrations (presumed Fe<sup>2+</sup>), resulting in prominent hydrous ferric oxide (HFO) precipitation where the water contacts atmospheric oxygen (Maskell 2015). Pavilion Well and Outhouse Springs are located approximately 30 m from each other and 130 m from Steamboat Spring along the Bear River; 500 M Spring and Bathtub Spring are located to the west, along the bank of the reservoir. The Geyser is located in the center of the city of Soda Springs (Figure 4.1). Corral Creek water is different on the Piper diagram in Figure 4.5 because it has a lower concentration of calcium than the other Type I waters.

In places where this water type is encountered by well drilling, the wellbore is over-pressurized by CO<sub>2</sub>, causing the well to spontaneously erupt (e.g., Pavilion Well, Unnamed well, and Soda Springs Geyser Well). There are numerous locations where Type I water is expressed at the surface as warm travertine-precipitating springs (e.g., Outhouse Spring, Steamboat Spring, Bathtub Spring, Hippie Spring, 500 M Spring, and numerous unnamed springs along the Bear River).

Table 4.2: Presented here are data from the 45 samples collected and analyzed for this study, including location, temperature, major element data, TDS, and calcite saturation index.

WaterType	SampleID	Lat	long	TempC	pH	HCO3-	Ca++	K+	Na+	Mg++	SiO2(aq)	Fe++	SO4--	Cl-	F-	TDS	Calcite <sup>Q</sup> /K <sup>sp</sup>
TypeWater	500mWspring	42.644755	-111.645825	29.7	6.2	4902	953.8	27.3	12.1	195.6	37.65	10.7	885	ND	0.9	6243	0.783
TypeWater	Bathub	42.655372	-111.642429	15.3	6.3	4749	883.4	43.5	26.4	258.6	26.39	4.4	1001	ND	0.8	6310	0.866
TypeWater	Outhouse	42.655685	-111.644595	25.6	6.27	4906	990.7	26.5	12	199.2	31.25	11.3	876.8	ND	0.9	6326	0.895
TypeWater	Steamboat	42.655024	-111.641984	30.7	6.5	3421	972.4	26.6	12.1	196.9	32.78	9.8	913.9	ND	0.8	5190	1.063
TypeWater	Geyser	42.657258	-111.605213	30.1	6.44	4640	856	25.3	13.2	173.6	16.54	3.6	787	4.8	1.4	5933	1.049
TypeWater	WarmSprings	42.910092	-111.556494	22.0	6.33	951	217	11	18.8	65.54	9.25	1.5	75.35	24.0	25.8	1259	-0.110
TypeWater	HippleSprings	42.659307	-111.604218	25.2	6.23	2144	597.6	17.7	5.799	131.6	24.36	3.5	383.3	9.4	1.5	2976	0.394
TypeWater	CorralCreekSpr	42.888745	-111.704573	17.0	6.5	4598	620	24.2	97	246	30.43	0.7	755	4.0	1.9	6068	0.986
TypeWater	ThunderBox	42.655264	-111.644489	28.0	6.35	4458	863.5	24.1	9.725	165.9	27.61	8.5	809.9	4.3	6.3	5757	0.918
TypeWater	PhallertonWell	42.645066	-111.506048	28.0	6.31	4649	899.8	25	9.656	171.1	28.06	8.9	852.1	4.2	0.8	5984	0.896
TypeWater	Dummy	42.655661	-111.644334	29.6	6.34	2570	912.3	24.8	9.077	168.7	2.458	8.5	836.7	4.3	0.0	4174	0.732
TypeWater	Octagon	42.659307	-111.602717	15.0	6.11	5585	565.5	19.9	23.2	164.4	23.4	10.9	434.1	13.4	0.0	5862	0.530
TypeWater	LowerSdelight	42.664713	-111.601088	9.2	5.8	6620	180	15.8	41	170.1	78.96	9.6	62.6	26.9	0.2	5743	-0.302
TypeWater	Hooper	42.667898	-111.603722	9.8	5.6	7520	135	12.8	33.4	132.3	76.6	7.2	54.1	12.0	0.2	6148	-0.721
TypeWater	Mammoth	42.713183	-111.627056	12.3	5.8	5660	137	17.3	42.4	149	104	11.0	53.5	12.0	0.2	4930	-0.461
TypeWater	Woodall	42.779439	-111.535816	9.1	8.7	610	132.6	1.42	4.115	46.16	11.72	0.4	18.15	3.5	0.3	1181	2.033
TypeWater	IronSpring	42.654616	-111.626958	9.3	7.4	960	200	27.3	12.4	87.5	10.25	9.5	410	13.0	0.9	1791	0.866
TypeWater	Sulfur99	42.645066	-111.506048	5.9	2.99	4445	599.5	7.8	12.8	53.4	97.9	101.2	145.6	4.0	0.3	5464	-5.530
TypeWell	SulfurSpring97	42.645066	-111.506048	5.5	5.97	2443	415.6	3.91	11.62	78.6	30.34	3.1	880.3	9.7	0.1	3364	-0.151
TypeWater	SodaCreekMamm	42.713183	-111.627056	17.3	6.4	1082	84.6	6.3	17.7	67	45.89	0.2	35.6	9.9	0.0	1200	-0.321
TypeWater	SodaCreekHooper	42.667898	-111.603722	16.8	7.2	752	94.7	7.9	26.6	94.8	52.91	0.2	146	54.9	1.0	1194	0.513
TypeWater	SodaMiddle	42.660190	-111.603689	16.6	7.5	890	111	12.3	37	126	45.09	0.3	58	14.7	0.6	1265	0.967
TypeWater	SodaCreekDown	42.669973	-111.599246	20.5	7.33	842	126	14.7	60.7	129	46.92	0.5	146	54.9	1.0	1385	0.796
TypeWater	SodaCreekOctagon	42.659307	-111.602717	19.1	6.5	1293	106.3	8.5	37.8	96.5	41.54	0.3	78	14.9	1.0	1521	-0.053
TypeWater	SodaDownWeir	42.674561	-111.601169	17.6	7.22	577	86.2	9.1	37.4	78.2	42.55	0.3	48.5	30.8	0.4	882.5	0.429
TypeWater	SodaUpstream	42.675059	-111.601565	17.0	7.46	572	82.7	9.2	23.4	82	45.59	0.0	42.8	11.5	0.4	848.8	0.668
TypeWater	Ledgespring-2	42.665687	-111.570989	9.6	7.22	1600	121	1.69	5.736	40.78	13.39	0.1	30.84	4.6	0.2	849.4	0.649
TypeWater	FormationSpring	42.694529	-111.554585	9.3	7.4	560	163.8	1.6	3.9	43.5	5.268	0.5	31	ND	0.0	787.3	0.894
TypeWater	Ledgespring	42.667915	-111.572811	9.7	6.75	1600	397	31.5	26.5	17.3	0.1014	0.3	490	11.1	0.0	2431	0.811
TypeWater	CitySpring	42.676410	-111.594216	8.6	7.97	710	170	25.1	87.7	128	55.75	ND	461	110.0	4.2	1728	1.142
TypeWater	CityParkSpring	42.675491	-111.602576	9.2	7.4	907	133	7.9	38.8	67.2	48.64	ND	90.5	39.7	0.7	1299	0.956
TypeWater	HomesteadSpring	42.667940	-111.597692	8.8	7.5	1085	121	6.7	37.1	108	52.7	ND	103	29.8	0.4	1506	1.068
TypeWater	LewisSpring	42.667861	-111.597511	8.9	6.8	660	116	6.8	37.7	69.3	45.6	ND	151	45.1	0.6	1077	0.098
TypeWater	MormonSpring	42.674573	-111.594386	13.8	7.36	710	128	23.3	87.2	131	42.57	ND	466	119.0	4.0	1673	0.699
TypeWater	SWSpring	42.677419	-111.598743	12.0	7.4	834	122	13	41	140	38.51	ND	61.3	13.7	0.9	1233	0.872
TypeWater	A-32-1102014	42.735870	-111.558864	* 8.02	7.4	233.1	57.2	4.43	26.5	24.4	*	0.4	79	5.9	3.8	428.6	0.758
TypeWater	A-33-0702013	42.736049	-111.543609	* 6.46	392	392	441	27.7	177	242	*	0.8	1620	210.0	28.8	3768	-0.268
TypeWater	A-51-1252014	42.746482	-111.553784	* 6.18	1081	1081	308	8.17	86.4	120	*	0.0	449	17.5	11.5	1892	-0.221
TypeWater	A-52-2852014	42.768669	-111.563909	* 7.14	499	499	111	3.41	5.7	52.9	*	0.5	48	4.3	6.0	705.2	0.406
TypeWater	A-53-1652013	42.764459	-111.563879	* 7.5	435	435	93.1	2.47	5.97	38.9	*	0.2	37.8	7.7	4.2	611.3	0.682
TypeWater	A-71-2202014	42.725830	-111.554780	* 7.3	539	539	145	9.02	78.3	46	*	0.3	176	26.7	5.8	1002	0.672
TypeWater	A-72-1352015	42.721784	-111.553386	* 6.9	754	754	169	4.23	17.4	61.2	*	0.0	36.8	7.4	4.6	1001	0.455
TypeWater	A-73-1902015	42.725361	-111.555656	* 7.24	581	581	169	7.31	37	61.4	*	0.0	224	21.0	3.8	1086	0.712
TypeWater	A-76-2202015	42.754047	-111.5639438	* 7.26	493	493	105	5.5	10.7	51.4	*	0.0	42.6	4.2	4.2	694.4	0.514
TypeWater	A-77-2302015	42.761367	-111.563902	* 7.32	445	445	94.3	3.77	6.88	49.2	*	0.0	29.7	3.4	5.4	619.1	0.503

Table 4.3: Chondrite normalized REE concentrations for springs wells, surface water and travertine from the Soda Springs area. Also included are concentrations for a brine from the Madison formations McLing et al 2014 and a Paleozoic limestone (Madhavaraju and Gonzalex-Leon 2012). Aqueous samples are presented as mg/l rock samples are presented as mg/kg.

Sample	REE Data Blackfoot Valley														Eu/Eu*	Ce/Ce*
	La	Ce	Pr	Nd	Sm	Eu	Gd	Tb	Dy	Ho	Er	Tm	Yb	Lu		
Mammoth	4.42E-05	1.66E-05	2.09E-05	2.46E-05	1.18E-05	1.45E-05	1.50E-05	1.77E-05	2.58E-05	2.94E-05	3.78E-05	3.86E-05	4.77E-05	5.05E-05	3.44E-02	-2.92E-01
Lover's Delight	6.40E-05	1.93E-05	2.42E-05	2.62E-05	1.20E-05	1.46E-05	1.53E-05	1.64E-05	2.40E-05	2.78E-05	3.65E-05	3.74E-05	4.89E-05	5.33E-05	3.07E-02	-3.58E-01
Octagon	1.94E-04	6.10E-05	7.81E-05	8.36E-05	4.09E-05	3.24E-05	5.06E-05	5.88E-05	8.36E-05	9.08E-05	1.16E-04	1.17E-04	1.45E-04	1.50E-04	-1.50E-01	-3.49E-01
500 M Spring	9.94E-06	5.62E-06	4.81E-06	3.21E-06	1.95E-06	4.45E-06	1.92E-06	3.66E-06	3.62E-06	4.56E-06	4.38E-06	5.82E-06	5.08E-06	8.88E-06	3.61E-01	-1.18E-01
Hooper	5.44E-05	2.40E-05	2.92E-05	3.70E-05	2.13E-05	2.72E-05	2.42E-05	2.42E-05	3.24E-05	3.51E-05	4.35E-05	4.34E-05	5.48E-05	6.08E-05	7.83E-02	-2.41E-01
Outhouse	2.74E-05	1.22E-05	1.48E-05	1.53E-05	8.40E-06	9.60E-06	8.87E-06	9.28E-06	1.16E-05	1.11E-05	1.27E-05	1.23E-05	1.34E-05	1.32E-05	4.59E-02	-2.38E-01
Steamboat	1.98E-05	7.95E-06	1.05E-05	1.16E-05	7.52E-06	1.29E-05	7.41E-06	7.04E-06	9.67E-06	1.06E-05	1.24E-05	1.32E-05	1.36E-05	1.48E-05	2.36E-01	-2.80E-01
Geyser	4.04E-05	1.35E-05	1.77E-05	1.58E-05	6.99E-06	7.99E-06	6.72E-06	6.56E-06	8.78E-06	9.39E-06	1.18E-05	1.15E-05	1.25E-05	1.20E-05	6.69E-02	-3.33E-01
Sulphur Spring 5.97	4.99E-03	1.36E-03	2.00E-03	1.69E-03	6.30E-04	3.71E-04	5.31E-04	4.49E-04	4.49E-04	3.86E-04	4.07E-04	3.26E-04	3.32E-04	2.96E-04	-1.94E-01	-4.09E-01
Pavillion Well(cn)	6.31E-04	2.09E-04	2.96E-04	2.43E-04	9.19E-05	5.31E-05	7.56E-05	7.09E-05	7.43E-05	6.15E-05	6.61E-05	5.73E-05	5.95E-05	5.15E-05	-1.98E-01	-3.46E-01
Soda Creek Mammoth	1.81E-05	2.89E-06	6.82E-06	6.98E-06	3.19E-06	6.96E-06	3.77E-06	3.91E-06	6.27E-06	7.30E-06	9.90E-06	1.07E-05	1.27E-05	1.47E-05	3.01E-01	-6.35E-01
Soda Creek Octagon	2.38E-05	5.49E-06	8.20E-06	7.55E-06	3.21E-06	1.75E-05	3.31E-06	2.86E-06	4.69E-06	5.06E-06	6.62E-06	7.49E-06	8.59E-06	1.02E-05	7.30E-01	-4.65E-01
Madison brine	2.60E-04	1.15E-04	9.34E-05	9.26E-05	5.42E-05	5.70E-05	9.97E-05	4.58E-05	4.43E-05	3.96E-05	4.10E-05	3.58E-05	4.48E-05	4.38E-05	-1.30E-01	-1.89E-01
Paleozoic Lms	5.28E+00	2.30E+00	2.62E+00	2.74E+00	1.57E+00	9.46E-01	1.13E+00	1.37E+00	1.27E+00	1.22E+00	1.14E+00	1.25E+00	1.17E+00	9.38E-01	-1.55E-01	-2.35E-01
Ohly travertine	1.21E+00	8.93E-01	7.15E-01	6.46E-01	3.48E-01	7.57E-01	2.48E-01	2.35E-01	1.87E-01	1.35E-01	1.52E-01	1.25E-01	1.61E-01	1.25E-01	4.05E-01	-3.00E-01
Chondrite wakita et al 1971	3.20E-01	9.00E-01	1.30E-01	5.70E-01	2.10E-01	7.40E-02	3.10E-01	5.10E-02	3.00E-01	7.40E-02	2.10E-01	3.20E-02	1.80E-01	3.20E-02	-5.46E-01	6.95E-01



Figure 4.4: Photographs of nine of the sample locations. The Geyser Well located in the center photograph is the most prominent feature in the area. This well erupts  $\text{CO}_2$ -charged water more than 30 meters above ground level every hour. Note the greenish hue in the water at Sulphur Springs in the upper left photograph. This color is due to the precipitation of elemental sulfur in the highly  $\text{CO}_2$  and  $\text{H}_2\text{S}$  water. The ubiquitous iron staining is common at all locations where  $\text{CO}_2$  is bubbling to the surface.

More than 90% of Type I springs occur along Bear River southwest of Soda Springs. Prior to this study, the number of Type I springs was thought to be approximately 10 to 12. However, during the study, due to the draining of Alexander Reservoir in 2012, we noticed an exceptionally large number of Type I Springs, as evidenced by their temperature and the presence of travertine. Attempting to count and map the number of springs contained was a futile exercise, due to the extremely high number of mostly small springs along the northern edge of the empty reservoir. Springs range in size from centimeters in diameter, with discharges of milliliters per minute, to very-large springs such as Steamboat Spring (Figure 4.4) that are meters across, with discharges of hundreds of liters per minute.



The most notable occurrence of Type I water is the Soda Springs Geyser Well, which is located in the center of the city of Soda Springs (Figure 4.1). This well was drilled in 1937 by a group of Soda Springs businessmen attempting to find warm water for a public swimming pool (Barnard et al. 1958). The well penetrated to a depth of 96 m BLS, where it encountered a zone of highly pressurized, warm, CO<sub>2</sub>-charged water, which began to spontaneously erupt to a height of more than 30 m. The Geyser Well has been capped and is allowed to erupt every hour for tourists. Occasionally, due to maintenance the well is allowed to erupt unfettered for weeks at a time with no evidence of depletion. This prolonged eruption suggests that the system deeper than 100 m BLS is well-connected, and that there is abundant CO<sub>2</sub>-charged water available at-depth. Other wells, including an Unnamed well and Pavilion Well, are also erupting wells. Pavilion Well began violently erupting in 2009 after lying quiescent for three decades. In 2012, Unnamed well was drilled 30 m BLS by a private party for drinking water, approximately 0.75 km west of the golf course on the north bank of Alexander Reservoir. However, the well had to be abandoned due to the presence of high-pressure, CO<sub>2</sub>-charged warm water, which did not allow it to be sampled. This is a common occurrence for the few groundwater wells that have been drilled in the southern Blackfoot Valley.

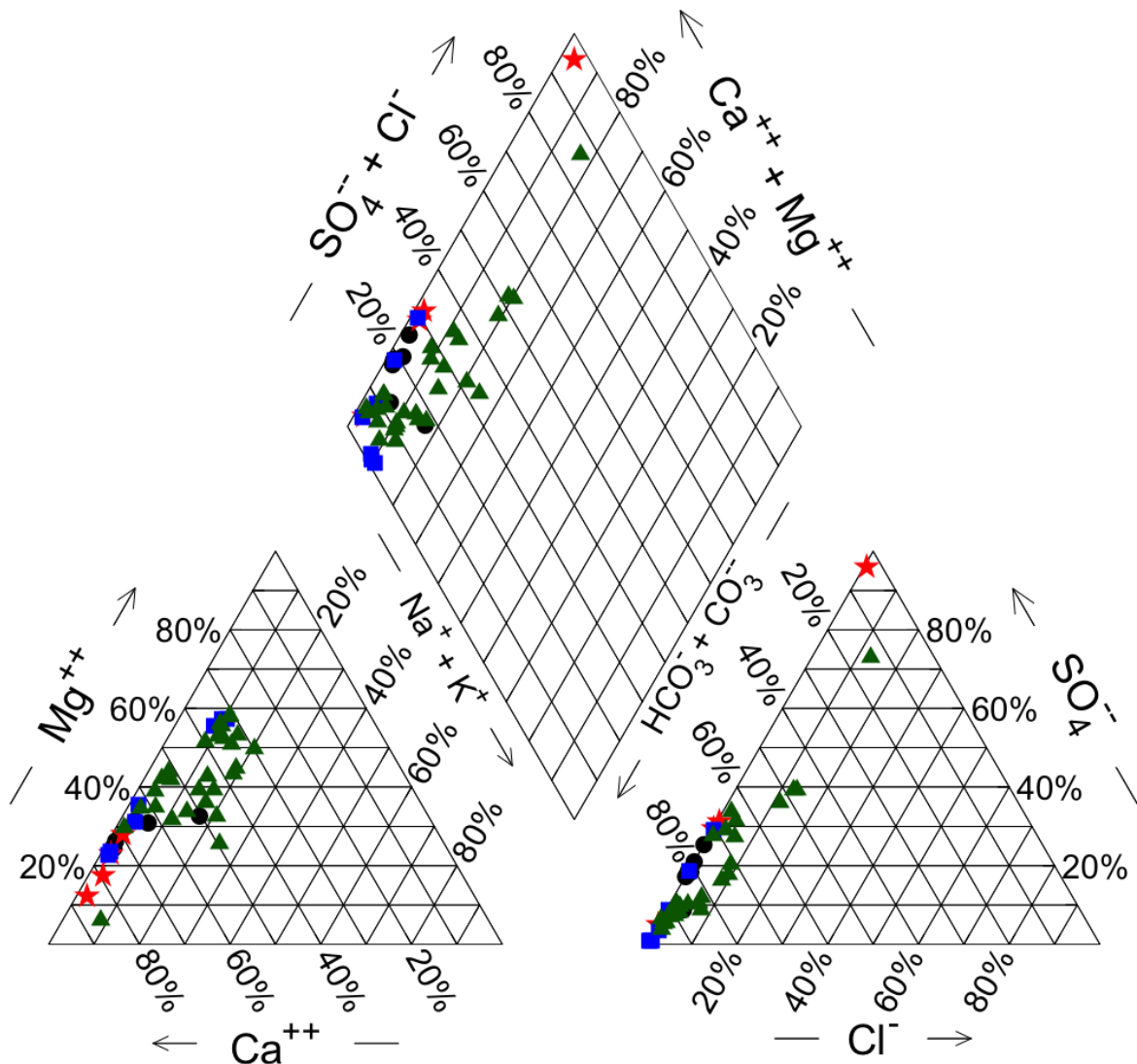


Figure 4.5: Piper diagram (Piper 1944) of Blackfoot Valley region water chemistry. Type I waters are shown as filled black circles, Type II waters are shown as filled blue squares, Type III waters are shown as filled red stars, and Type IV waters are shown as filled green triangles. The three Type III water samples shown are all from Sulphur Springs at different times of the year. Water chemistry ranges from Ca-Mg-HCO<sub>3</sub>-dominated for most locations to Ca-SO<sub>4</sub>-dominated at Sulphur Springs.

#### 4.3.1.1 Rare Earth Elements – Type I Water

REE concentrations were measured in 12 samples (multiples from Soda Geyser) from five features that produce Type I water: Geyser Well, Outhouse Spring, Pavilion Well, 500 M Spring, and Steamboat Spring (Figure 4.1). The Type I REE chemistry is presented in Table 4.3 and is typified by enrichment in La and a general enrichment in HREEs (Figure 4.6, Table 4.1). These waters are also characterized by a negative Ce/Ce\*, ranging from -0.24 Ce/Ce\* for Outhouse Spring to -0.33 Ce/Ce\* for the Geyser Well. Two of these waters—Steamboat Spring and Geyser Well—have positive

Eu/Eu\*<sub>cn</sub>, although it is much more pronounced for Steamboat Spring (0.19) and Bath tub (0.36) and is very small for the Geyser Well (0.02). Also presented in Figure 4.6 and Table 4.3 are REE data from brine collected from Madison limestone (McLing et al. 2014). These brines were collected and analyzed from a deep CCS Study well (Surdam and Bentley 2013) drilled in Wyoming's Rock Springs Uplift.

### 4.3.2 Type II Water – Cold Carbon-Dioxide-Charged Springs

Six Type II springs were sampled, including four for REE's. Type II waters (filled blue squares shown in Figure 4.5) are cold (10–15°C), have moderately high TDS (1,180 mg/L at Woodall Spring to 6,148 mg/L at Hooper Springs), and are chemically classified as Ca-Mg-HCO<sub>3</sub> water. The effervescing bubbling of CO<sub>2</sub> ranges from a few rising bubble trains at Hooper Springs to vigorous effervescing at Octagon Spring. Water discharge ranges from a few L/s at Octagon Spring to 190 L/s at Mammoth (Idan-ha) Spring (Lewicki et al. 2013). These springs have been active at their current locations since before the time they were first described in the late 1800s (Carney 1998). These springs range in size from 0.024 m<sup>2</sup> at Octagon Spring to more than 40 m<sup>2</sup> at Mammoth Spring. The long-term persistence of these springs is matched by their consistent water chemistry. Major element concentrations are in general agreement with the results reported by Mitchell (1976); in the case of Hooper Spring, a bronze plaque affixed to the spring gazebo lists a water chemistry analysis from the 1930s that are within a few percent of our measurements and those of other recent studies (Lewicki et al. 2013; Maskell et al. 2015).

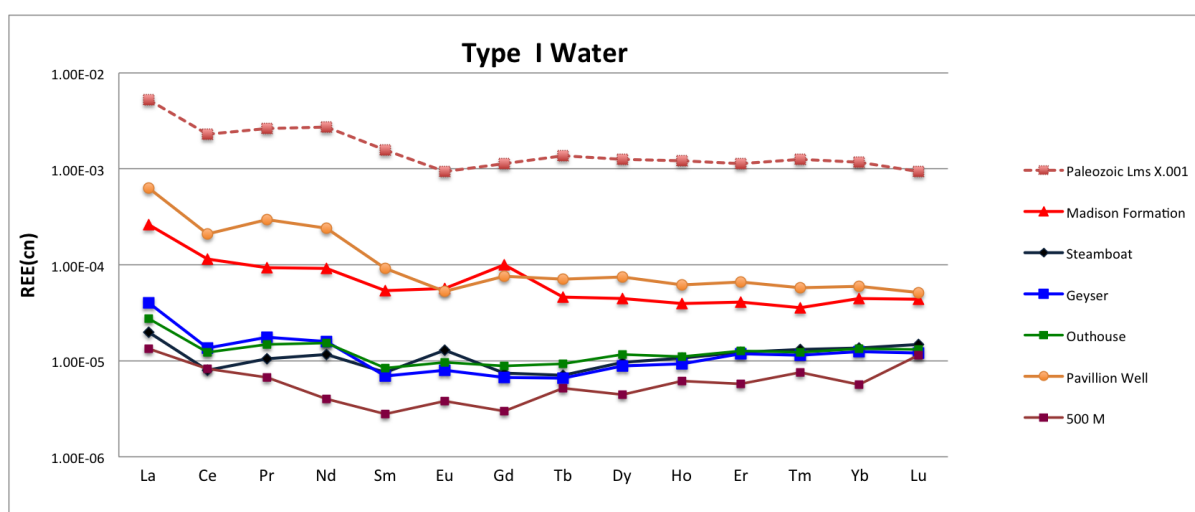


Figure 4.6: REE trends for Type I water, Paleozoic Limestone (concentration divided by 1000) (Madhavaraju and González-León 2012), and brine from Madison Formation at the Rock Springs Uplift. In order to facilitate comparison between limestone and aqueous REE trends, the Chondrite normalized REE values for the Paleozoic limestone were divided by 1,000.

As with Type I water, Type II water has elevated iron concentration (up to 11 mg/L), indicative of anoxic conditions (Table 4.2). In contrast to Type I water, springs with Type II water do not precipitate travertine in any significant volume. However, calculated calcite SI values indicate that Dunny, Thunder Box, and Octagon Spring are oversaturated with calcite. The presence of significant HFO precipitation around the margin of these springs is a universal characteristic. This HFO fizzes when reacted with acid, indicating that calcite is co-precipitating with the HFO where these springs discharge into fresh water or are in direct contact with the atmosphere.

#### **4.3.2.1 Rare Earth Elements – Type II Water**

REE concentrations from four Type II waters (Mammoth, Octagon, Lovers Delight, and Hooper) are presented in Figure 4.7. Except for a slight increase in chondrite-normalized concentration from Ce to Eu for Hooper Spring and Octagon Spring, the REE trends for these four waters are similar, except as noted below. The springs have enriched La, negative  $(Ce/Ce^*)_{cn}$ , and pronounced depletion in Sm relative to Nd and Eu. Additionally, the springs all have positive HREE slopes and, except for Octagon Spring, which has a negative  $(Eu/Eu^*)_{cn}$  (-0.20), these waters do not have a significant  $(Eu/Eu^*)_{cn}$ . Of these three waters, Octagon Spring is different in that the REE curve does have a concave shape from Sm to Tb. The chondrite-normalized REE trends for both Lovers Delight and Mammoth springs are virtually identical from Sm to Lu, having a positive slope through Lu. The REE trend for Hooper Springs is similar to both of these springs but higher in REE concentration from Ce to Er, with a same prominent convex shape from Sm to Tb.

#### **4.3.3 Type III Water – Acid Sulfate Water**

Type III water is only found in a series of gas-rich springs located in Sulphur Canyon (Figure 4.1) on the east side of the study area. Repeat samples showing the range of water chemistry measured at the Sulphur Springs complex during a single field season in 2012 are shown in Figure 4.5. The mapped extent of the gas discharge area is approximately 0.5 km<sup>2</sup> at two locations in the canyon. Although there are no obvious CO<sub>2</sub> vents, it is likely that the system extends to the west toward Soda Springs as evidenced by the presence of calcareous soil.

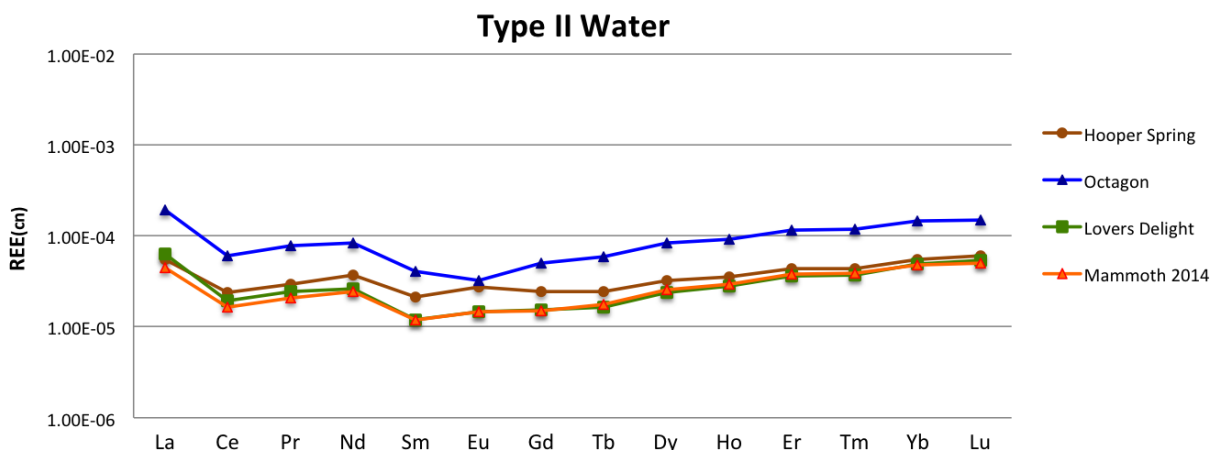


Figure 4.7: REE trends for Type II waters.

Sulphur Springs is characterized by its cold spring water ( $\sim 5^{\circ}\text{C}$ ),  $\text{CO}_2$  and  $\text{H}_2\text{S}$  gas emissions, and its lack of water during the dry season (Table 4.1).  $\text{CO}_2$  emissions have been locally estimated as greater than 51 Mt/day (Lewicki et al. 2013). This spring is also precipitating elemental sulfur and has measured pH below 3.0 during the dry season. As shown in Figure 4.5, the water chemistry for Sulphur Springs varies significantly depending on the time of year. During dry periods, water in the southernmost portion of the spring complex, where a seasonally persistent pond is located, takes on a green hue (Figure 4.4) as a result of suspended native sulfur precipitates. By late summer, the volume of water at the surface expression of the system decreases significantly, replaced by dry,  $\text{CO}_2$  and 50 ppm  $\text{H}_2\text{S}$  by volume fumaroles, resulting in higher concentrations of dissolved constituents and lower pH (Lewicki et al. 2013).

#### 4.3.3.1 Rare Earth Elements – Type III Water

REE concentrations were measured from one location in the Sulphur Springs complex. The REE data in Figure 4.8 is from water collected in the late fall, when water levels were near a seasonal low and had a pH of 5.97. For the purpose of comparison, REE data from a Paleozoic limestone (concentration divided by 1000) (Madhavaraju and González-León 2012) and a deep brine sample collected from the Madison Limestone (McLing et al. 2014) in Wyoming are also shown. REE concentrations at Sulphur Springs are the highest measured in the Blackfoot Valley with  $\Sigma\text{REE}_{\text{cn}} > 0.0142$ , nearly an order of magnitude higher than the next-highest concentration, at Pavilion Well. The Type III water shows a negative  $(\text{Ce}/\text{Ce}^*)_{\text{cn}}$  and  $(\text{Eu}/\text{Eu}^*)_{\text{cn}}$  and is enriched in LREE, especially La. Sulphur Springs has a slightly negative HREE trend.

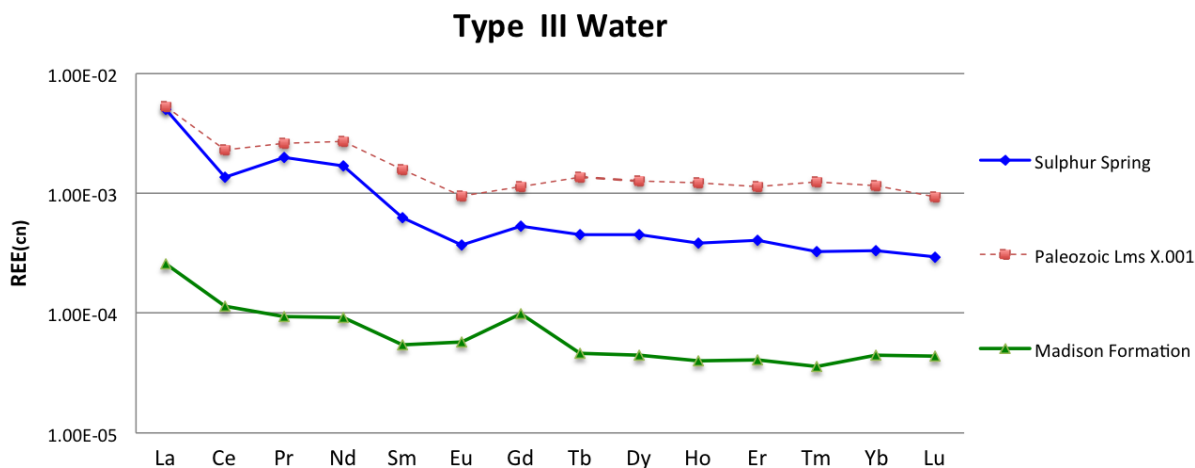


Figure 4.8: REE trends plotted for Type III water (Sulphur Springs) and brine from Madison Formation at the Rock Springs Uplift (McLing et al 2012). In order to facilitate comparison between limestone and aqueous REE trends, the Chondrite normalized REE values for the Paleozoic limestone were divided by 1,000.

#### 4.3.4 Type IV Water – Non-carbonated Groundwater, and Surface Water

Type IV water is made up of 26 sample locations including Soda Creek and cold, non-carbonated springs (Table 4.1) in the Southern BVF (Figure 4.1). Two of the samples were analyzed for REE. Type IV waters are shown as filled green triangles on Figure 4.1 and Figure 4.5. Type IV waters have a circum neutral-pH ranging from 6.4 at the headwaters of Sulphur Creek to 7.4 downstream the city of Soda Springs. These waters are chemically dominated by Ca-Mg-HCO<sub>3</sub> (Figure 4.5), with TDS ranging from 840 mg/L at the headwaters of Soda Creek to 2,431 mg/L at Ledger Spring east of the Soda Springs (Figure 4.1).

##### 4.3.4.1 Rare Earth Elements – Type IV Water

The REE trend for the Type IV waters shows enrichment in La relative to other LREEs and a convex pattern from Ce to Sm (Figure 4.9). Figure 4.9 also shows a pronounced positive (Eu/Eu\*)<sub>cn</sub>, which ranges from 0.30 for Soda Creek at its origin near Mammoth Spring to high of 0.74 downstream near Octagon Spring. For comparison purposes, average REE data trend from groundwater collected from the basalt rock-hosted Eastern Snake River Plain (ESRP) aquifer is also shown on Figure 4.9. The  $\Sigma\text{REE}_{\text{cn}}$  concentrations for Soda Creek near Octagon Spring and for Soda Creek near Mammoth Spring are the lowest measured in the study. Also presented in Figure 4.9 is an REE data trend from a travertine deposit in the southern Blackfoot Valley (Ohly 2016). The travertine has a high, positive Eu/Eu\*<sub>cn</sub>.

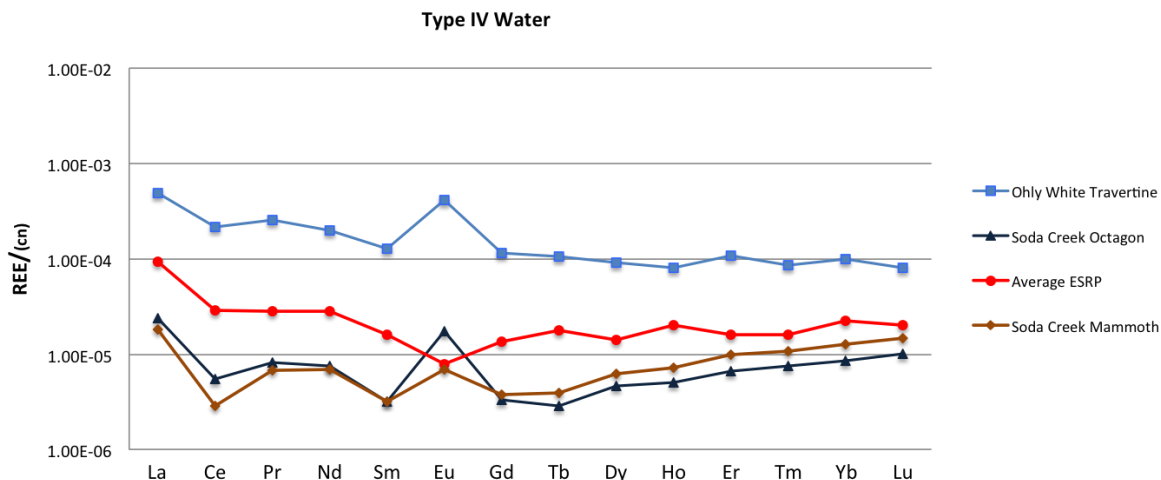


Figure 4.9: REE data trends for Type IV water, REE data from the ESRP aquifer (Nelson 2005), and travertine from the Blackfoot Valley.

#### 4.4 Discussion

Water chemistry coupled with REEs can be a useful tool in tracking groundwater sources and mixing, especially for an aquifer system where multiple sources of water and water-rock interactions are implicated. Based on the commonly accepted geologic conceptual model of the Soda Springs area, the Quaternary volcanism has introduced a large amount of thermal energy into the base of the Paleozoic carbonate- and organic-rich shale at a depth greater than 3 km beneath the BVF (Armstrong and Oriel 1965; Armstrong 1969; Mabey and Oriel 1970) (Figure 4.2). This thermal input generates large fluxes of  $\text{CO}_2$  and  $\text{H}_2\text{S}$  through interaction with carbonates and organic-rich shale. Hutsiniller and Parry (1985) attributed the  $\text{H}_2\text{S}$  in the springs to the presence of numerous black-shale lenses in the thick carbonate sections. Additionally, the presence of the 150 m-thick Phosphoria Formation, which contains up to 2.1% organic matter, provides an additional possible source for  $\text{H}_2\text{S}$ . We propose that this mixture of  $\text{CO}_2$ ,  $\text{H}_2\text{S}$ , and deep basin-sourced brine then moves vertically through fracture pathways to the near surface, where the carbonic acid-rich water encounters the Quaternary basalts of the Blackfoot Lava Field. At the base of the basalts, the precipitation of large volumes of carbonate and other secondary minerals effectively seal much of the conductive structure in the basalts (Figure 4.10), significantly limiting the vertical movement of water and, to a lesser extent,  $\text{CO}_2$  and  $\text{H}_2\text{S}$ .

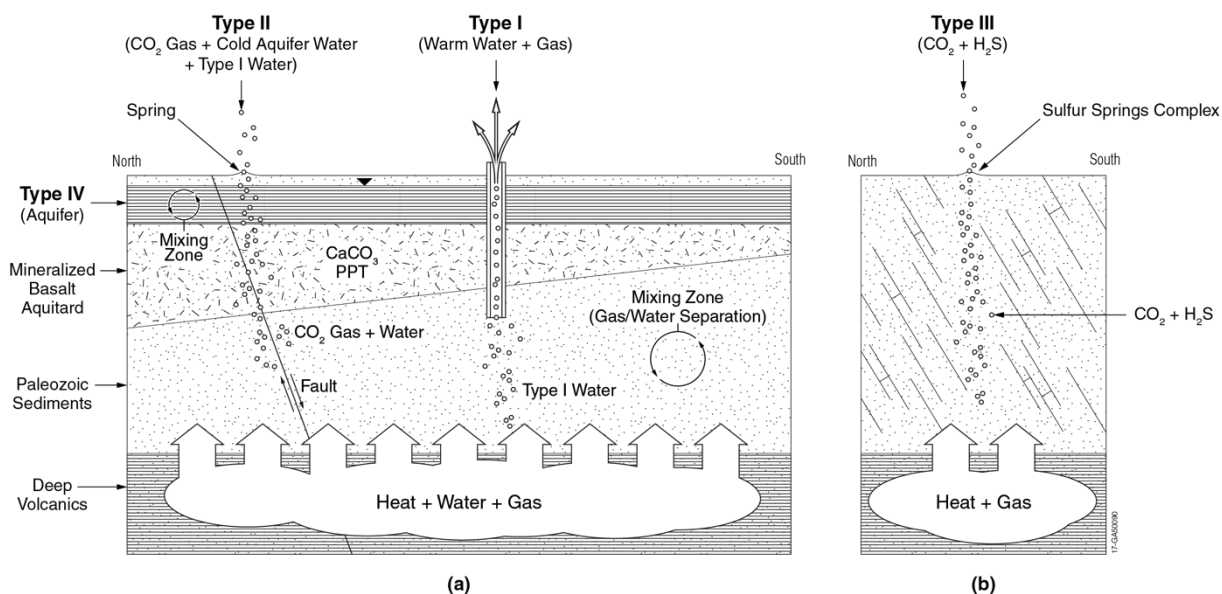


Figure 4.10: Simplified hydrogeological conceptual model for the Southern Blackfoot Valley, showing the stylized relationship between the four water types, host rock, and the deep thermal source that drives the  $\text{CO}_2$  system. Note the basalt aquitard that has been formed over time by the precipitation of calcite that fills conductive structure in the rock.

#### 4.4.1 Type I Water

Type I wells and springs are common throughout the southern portion of the study area, especially along the north bank of Alexander Reservoir west of the city of Soda Springs. The majority of springs in the Southern BVF have associated travertine deposits reflecting the presence of Type I water. Type I waters are warmer ( $>25^\circ\text{C}$ ) compared with the other  $\text{CO}_2$ -effervescing springs (Type II water), which are cold ( $10\text{--}15^\circ\text{C}$ ) and are prevalent in the area from the city of Soda Springs north to Fivemile Meadows (Figure 4.1). Although most of the Type I springs sampled for this study have persisted over recorded time, there is evidence that these features wax and wane over geologic time. This is evidenced by the numerous dry, travertine mounds located throughout the study area. The extinction of flowing springs (as evidenced by the dry, travertine mounds) is likely a result of dissolution/precipitation reactions that have led to the self-sealing of the flow path to the springs at-depth and the resulting creation of new springs, as proposed by Mitchell (1976).

To understand the influence of  $\text{CO}_2$  fugacity at-depth on calcite precipitation, GWB was used to calculate a  $\text{CO}_2$  fugacity and infer a depth at which calcite is in equilibrium with Soda Geysers water. This calculation provides an indication of maximum depth for calcite precipitation, and, therefore, the effective thickness of the mineralized basalt seal. The parameter for this modeling exercise is based on the hydrostatic pressure in the Geysers of 12.6 bars. This pressure comes directly from adding the observed eruption height (30 m) to the well depth of 96 m. The water chemistry of the degassing



Geysir Well water collected at the surface has a GWB-calculated saturation index of 1.04 (oversaturated) with respect to calcite; however, when the CO<sub>2</sub> fugacity is raised to a downhole pressure of 12.6 bars, the saturation index with respect to calcite is -0.0. This implies that the base of the mineralized basalt seal is at a depth of approximately 96 m BLS, the same depth that the driller encountered CO<sub>2</sub>-pressurized water when drilling the Soda Geysir Well in 1937.

The elevated CO<sub>2</sub>, TDS, H<sub>2</sub>S, and temperature indicate that the Type I springs have a relatively direct path to the surface. One possible explanation for the large number of Type I springs is a combination of the presence of the east-west-trending Bear River tear fault, coupled with a significant thinning of the basalt formations in this area. The preferred pathway created by the fault, combined with the thinning of mineralized basalt, would allow for a more direct path to the surface for CO<sub>2</sub> and associated thermal water in this area than farther north where the basalt flows thicken significantly.

To evaluate if the source for the Type I water is due to the interaction between the deep thermal source and the Paleozoic sediments, the REEs for Type I water are compared to the whole rock REE trend from a North American limestone of similar age (Madhavaraju and González-León 2013) (Figure 4.6). Also included in Figure 4.6 is the REE date trend from brine collected from the Madison Limestone Formation at a deep CCS Study well drilled in Wyoming's Rock Springs Uplift (Surdam et al. 2013; McLing et al. 2014). Based on the REE trends shown in Figure 4.6, there is little similarity between the REE trends for the Madison Formation brine and Type I water. The notable differences in the Madison Brine compared to the Type I waters are a Gd<sub>cn</sub> high, lesser-LREE enrichment, and the lack of HREE enrichment, indicating that it is unlikely that the Type I water is the result of the same geochemical process responsible for the REE chemistry of the Madison Formation brine. However, except for the positive (Eu/Eu\*)<sub>cn</sub> in Steamboat Spring, and the expected three-to-four orders of magnitude higher concentration in the rock, the comparison of the Type I REE trend to the whole rock REE chemistry of the Paleozoic Limestone shows a strong relationship between Type I water and the limestone. This provides strong evidence that the dissolution of limestone of similar chemistry in the subsurface through the neutralization of acid fluids is the likely source of the Type I REE signature. Whether this chemical fingerprint is a result of processes that occur deep in the subsurface or much shallower cannot be elucidated from this data and is worthy of further study.

#### 4.4.2 Type II Water

Type II waters are distributed along the range-bounding fault on the west side of the BVF, from Fivemile Meadows south to the city of Soda Springs, and west along the range front for approximately 4.5 km. Similar to the Type I water, Type II water has characteristic anoxic conditions as evidenced by the high dissolved-iron concentrations (presumed to be Fe<sup>2+</sup>) of up to ~11 ppm (Table 4.2). However,

in contrast to the Type I water, Type II water does not actively precipitate travertine in any significant amount. Although, where Type II water contacts atmospheric oxygen or oxygenated Type IV water, HFO (Figure 4.4) precipitates, leaving a characteristic orange stain. At Mammoth Spring (Figure 4.4), the largest of the Type II springs, the water has high Fe content that supports growth of iron-oxidizing bacteria (unpublished data), creating large rust-colored floating mats that over time collect dust sufficient enough that plants are thriving (Figure 4.4). These mats have the effect of forming floating islands where grass and other vegetation grow completely suspended in the 1.5-m deep water.

The range of chondrite-normalized  $REE_{cn}$  concentrations for Type II springs is shown in Figure 4.7. This figure shows that the REE concentration and trends are very similar for Lovers Delight and Mammoth Spring; Octagon and Hooper Springs are noticeably different. Hooper Springs has higher MREE than does Lovers Delight and Mammoth. Octagon is both higher in  $REE_{cn}$  concentration by approximately half an order of magnitude and has a slight  $(Eu/Eu^*)_{cn}$ . The springs all have enriched La, negative  $(Ce/Ce^*)_{cn}$ , and pronounced depletion in Sm relative to Nd and Er. Additionally, all of the springs have positive HREE slopes and, except for Octagon Spring, which has a slightly negative  $(Eu/Eu^*)_{cn}$  (-0.20), these waters do not have a significant  $(Eu/Eu^*)_{cn}$ . One possible explanation for this difference is that Octagon Spring may actually be the surface manifestation of deeper-sourced water. Although the State of Idaho and the City of Soda Springs classify Octagon Spring as a free-flowing spring, there is evidence that it may actually be a shallow well that penetrates some depth into the basalt. The spring discharges through a circular orifice (Figure 4.4). The opening has long-been assumed to be a shallow pipe inserted to concentrate flow at the spring site, much like at Lovers Delight (Figure 4.4). However, during this study we probed the pipe to a depth of greater than 2 m without encountering any obstruction, making it more likely to be some type of well casing. Because the water temperature is only approximately 9°C and is not precipitating copious quantities of travertine, it is unlikely that this suspected well penetrates the heavily mineralized basalt horizon that is the expected source of deeper Type I waters observed at Geysers and Pavilion wells. However, the REE chemistry of Octagon Spring water suggested that it is more influenced by deeper-sourced water than the other Type II springs and that Type II water may be derived from modified Type I water.

#### **4.4.2.1 Geysers Outflow**

Previous studies by Lewicki et al. (2013) and Maskell et al. (2015) established that the majority of the  $CO_2$  in the BVF is sourced deep in the system (Ralston and Mayo 1983). However, based on the REE trend, lack of  $H_2S$ , and temperature, Type II water must have experienced a different history than Type I water. The Soda Geysers Well is allowed to erupt for approximately 15 minutes each hour by the City of Soda Springs; the outflow from this eruption falls on the land surface, creating a large,

travertine platform with water channeled off to the north and then west by the City (Figure 4.11). In addition to the timed major eruptions, the Geyser Well also has continuous leakage flow around the well annulus. Both eruption and leakage water of the Geyser Well is directed down a drainage channel to a dispersion area approximately 350 m to the northwest. As shown in Figure 4.11, as the water flows from the wellbore 350 m downstream, it precipitates a significant mass of calcite and co-precipitated HFO. This precipitation, driven by a loss of CO<sub>2</sub> and oxygenation, may serve as an analogue for water chemistry evolution that occurs in the subsurface as vertically migrating water loses CO<sub>2</sub>, providing insight on the possible geochemical evolution of Type I and the gneiss of Type II waters.

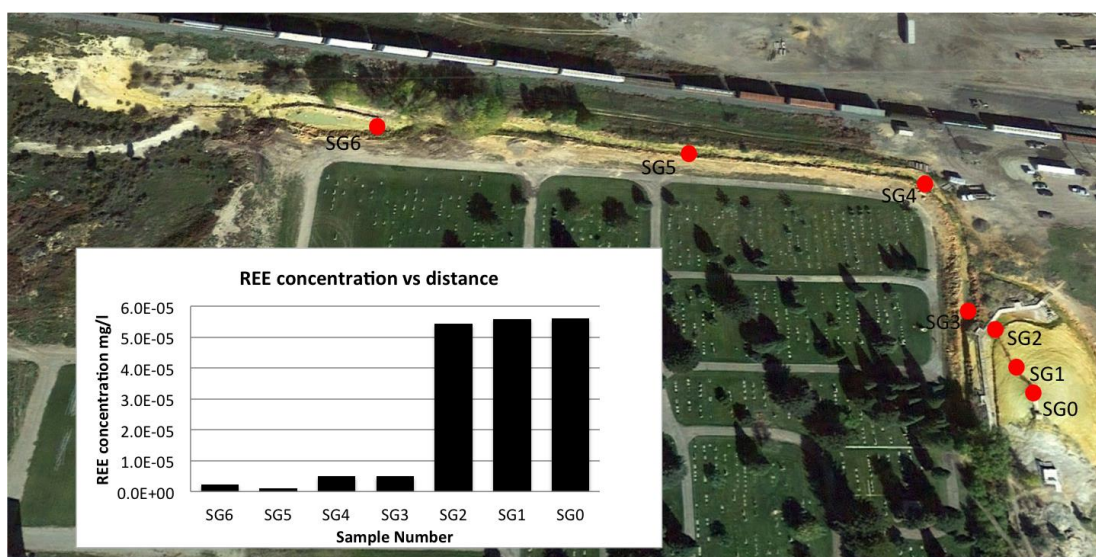


Figure 4.11: Location of samples collected to evaluate water chemistry changes along the flow path from the Geyser Well to the spreading area 350 m downstream. The inset figure shows the concentration drop in dissolved REE from sample location SG0 (at the Geyser Well) downstream to SG6.

To address this question, we collected a series of water samples from the Geyser Well outflow during eruption of the well, stretching from the point of discharge to 350 m downstream, marked by red circles in Figure 4.11. Along this flow channel (Figure 4.11), the water temperature decreased from 30.2°C to 25.1°C and the pH increased from 6.35 to 7.5, resulting in travertine precipitation. The chemistry of the Geyser water changes significantly with distance from the discharge, with specific conductivity decreasing from over 5,450 to 4,000  $\mu\text{S}/\text{cm}$ .

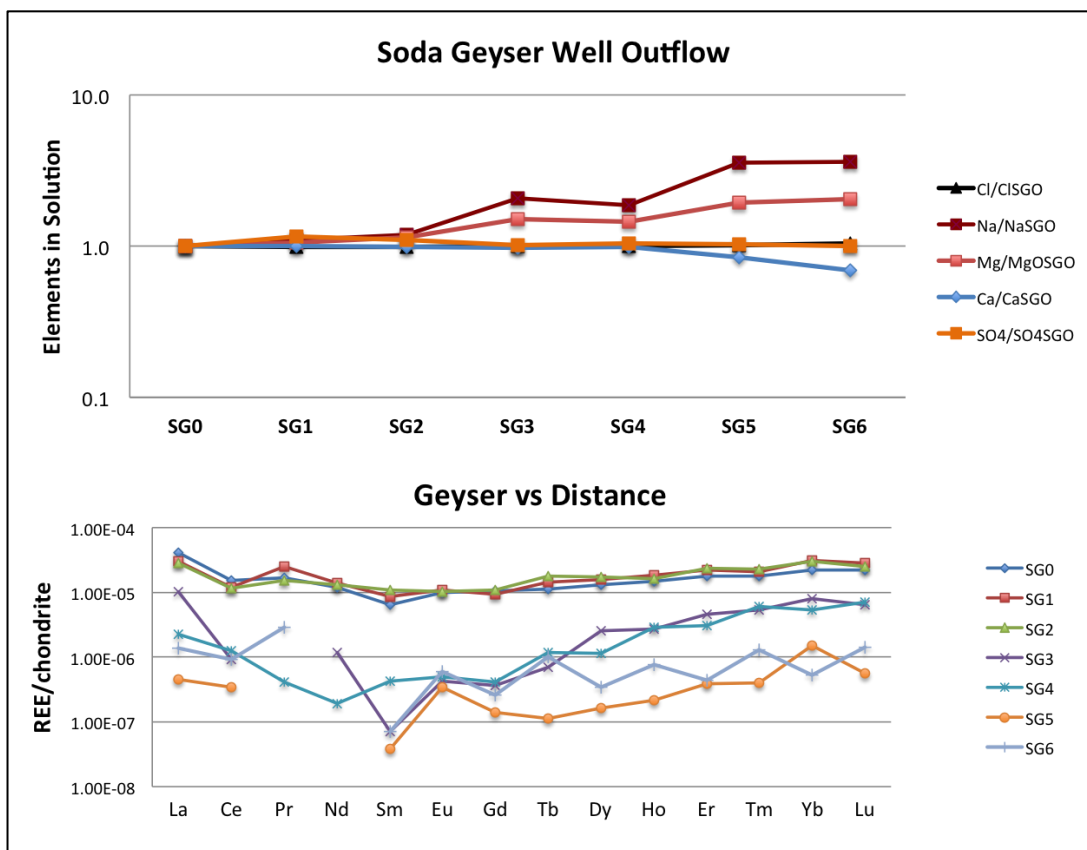


Figure 4.12: The top figure shows the changes in major element concentration for Soda Geyser outflow study. (Note the increase in  $\text{Na}^+$  and decrease in  $\text{Ca}^{2+}$ .) The bottom figure shows the changes in chondrite-normalized REE trends and concentration relative to distance from the Soda Geyser Well.

Because the eruptions only last 15 minutes, we sampled water along the flow path across three eruptive cycles at the locations shown on Figure 4.11, with sample SG0 (Soda Geyser discharge pipe) being collected right at the well discharge pipe and SG6 collected at the most distant part of the flow channel, 300 m downstream. The results from the Soda Geyser outflow sampling are shown in Figure 4.12 and Figure 4.11 inset. The figures show a dramatic change in water chemistry along the flow channel (Table 4.3), including a large drop in concentration of REE,  $\text{Ca}^{2+}$ , and  $\text{HCO}_3^{2-}$ . Other elements, such as  $\text{Na}^+$  and  $\text{Mg}^{2+}$ , increase in concentration, whereas  $\text{SO}_4^{2-}$  and  $\text{Cl}^-$  remain constant along the flow channel (Figure 4.12).

Locations closest to the Geyser discharge point (SG0, SG1, and SG2) show nearly identical REE concentration and trend, while locations further downstream (SG3, SG4, SG5, and SG6) show marked changes in concentrations and trends. The rate of decrease in concentration increases downstream of sample SG2 to near-detection limits by the time the water reaches SG5 (Figure 4.12). REE trends become progressively more enriched in HREE as water moves downstream, which is likely the result of selective removal of LREE by travertine precipitation process. The decrease in total REE concentrations (Figure 4.11) is probably associated with non-selective adsorption of REEs by HFO that co-precipitates with travertine. This process is repeated with each eruption, as new reduced iron is available for the precipitation of fresh HFO, effectively providing a nearly unlimited capacity for REE adsorption over time.

The change in REE trend with distance at the Geyser Well provides some important insight into the relationship between Type II and Type I water. The enrichment of HREE with increased distance from the source shows that based on REE data, it is possible to evolve Type I, which has a flat HREE trend, to Type II water, which has a prominent, positive HREE trend, by the precipitation of calcite. The positive HREE trend observed here is also seen in the Type II waters (Figure 4.8), indicating that the REE trend in Type II waters is likely inherited from calcite precipitation deeper in the system. Support for this can be found in our earlier calculation (Section 4.4.1). Where we found at-depth less than 100 m, the water was supersaturated with respect to calcite. Loss of CO<sub>2</sub> as the water and gas move upward through the mineralized basalt causes the water to become oversaturated with respect to calcite. Over time, the precipitation of calcite in this zone has sealed the basalts sufficiently that the vertical flow of water is restricted while the gas phase is able to move to the surface more easily. The result is that Type II springs have copious amounts of deep-sourced CO<sub>2</sub> present, and because of restricted permeability in the basalt host rock, these springs have much-less deep-sourced water. However, the similarities between the positive HREE trends from the Geyser Well outflow samples and the positive HREE trend from the Type II springs cannot be ignored. These similarities suggest that the REE chemistry in Type II water is inherited from Type I, modified by calcite precipitation. Furthermore, the presence of a pressurized zone at 96 m at the Geyser Well (e.g., calcite-sealed basalt) and lack of travertine precipitation at Type II springs further suggest that the calcite precipitation is occurring at-depth as calculated in Section 4.4.1.

### 4.4.3 Type III Water

Type III water is different from the other water types for several reasons, such as the exceptionally high volume of CO<sub>2</sub> and H<sub>2</sub>S, accompanied by low volume of water released from the numerous fumaroles. Geologically, Sulphur Springs lies outside the surface expression of the Quaternary basalts of the BVF; however, it is clear based on the voluminous effusive CO<sub>2</sub> and H<sub>2</sub>S that the area is within the influence of the deep regional heat source. During dry periods, nearly all of the Sulphur Springs Complex is devoid of water except for a small ponded area in the southernmost portion, which stays wet throughout the year (Figure 4.4). As the flow from Sulphur Creek is reduced along with the enhanced evaporation in late summer, the ponded area takes on a prominent yellow-green color (Figure 4.4), caused by the oxidation of H<sub>2</sub>S and the associated precipitation of native sulfur, by the reaction shown in Equation (4.5). As a consequence of the oxidation of S<sub>(c)</sub> and H<sub>2</sub>S to sulfuric acid (Equations [4.6] and [4.7]) and its subsequent neutralization by the limestone host rock, Sulphur Springs has high concentration of Ca<sup>2+</sup>, SO<sub>4</sub><sup>(2-)</sup>, and HCO<sub>3</sub><sup>-</sup> in the water.



The REE concentration in Sulphur Springs is approximately an order of magnitude higher than it is at Pavilion Well, the next highest value in the study. The high REE concentration measured at Sulphur Springs may in part be the result of lower pH, which significantly increases the solubility of metals in aqueous solutions. The REE data presented in Figure 4.10 are for water collected in the late summer when the water level in the pond was still relatively high (Figure 4.4) and had a pH of 5.97. Although the concentrations are higher at Sulphur Springs (Figure 4.8), the trend of REE at this spring is very similar to that observed at Pavilion Well (Figure 4.6). The similarity in REE trends for Type I waters, such as Pavilion Well (Figure 4.6) and Sulphur Springs (Figure 4.8) to the Paleozoic limestone (Madhavaraju and González-León 2012), suggests that REEs for both the Type I and Type III are sourced in similar host rock, namely the regional abundant limestone and dolomite.

### 4.4.4 Type IV Water

The chemistry for Type IV waters exhibits a large composition range with chemistry varying by location in the Valley, with TDS calcite saturation increasing in the southern portion of the Valley. Plotted on a Piper diagram (Figure 4.5) is water chemistry data from Formation Spring (one of the

drinking water sources for the City of Soda Springs), which has one of the lowest TDS (849 mg/l) and is an almost-entirely Ca-HCO<sub>3</sub> water type. Higher-TDS waters (>1,000 ppm), including Mormon, Ledger, and Calf Spring, have higher-relative Mg<sup>2+</sup> and SO<sub>4</sub><sup>(2-)</sup> concentrations (Figure 4.5).

Two Type IV samples were analyzed for REE (Soda Creek Mammoth and Soda Creek Octagon). Based on the limited data from two samples, the REE in Soda Creek is constant along its flowpath. The relative increase in LREE and the decrease in HREE for the Soda Creek Octagon Sample compared to the upstream sample (Soda Creek Mammoth in Figure 4.9) is unexpected as HREE are thought to be preferentially transported in aqueous systems relative to the LREE by forming stronger bicarbonate complexes, while LREE tend to preferentially sorb on reactive mineral surfaces (Humphris 1984; Fleet 1984; Cantrell and Byrne 1987; Johannesson 1997b; Johannesson et al. 1999). Clearly, some other explanation is needed but the current sample density of two is not sufficient for further evaluation.

Another important characteristic of Type IV water is a positive (Eu/Eu\*)<sub>cn</sub>, which, except for Steamboat Spring and 500 M Spring, is not observed in any other water in the study area. Here, it is useful to compare the REE signatures of Type IV water to the ESRP aquifer (Nelson 2005). The ESRP aquifer, like the shallow aquifer in the Blackfoot Valley, is hosted by Quaternary basalt of the similar chemical composition. The REE trends for both Type IV and the average REE concentration for eleven samples collected from the southern ESRP are shown on Figure 4.9. The REE trends from these two locations are very different; most notably is the negative (Eu/Eu\*)<sub>cn</sub> for the ESRP water and the positive (Eu/Eu\*)<sub>cn</sub> for the Type IV water. Given the similarities in aquifer host rock, climate, and temperature, the REE trends for waters from the ESRP aquifer and BVF Type IV should be similar if basalt water interaction represents the dominant control on REE composition for both systems. Given the difference in chemistry between the two localities (especially with respect to the (Eu/Eu\*)<sub>cn</sub>), this cannot be the case.

One explanation for the (Eu/Eu\*)<sub>cn</sub> is the selective dissolution of plagioclase from the basalt rocks that host the upper aquifer as proposed by Maskell et al. (2015), which would provide an explanation for the positive (Eu/Eu\*)<sub>cn</sub>. Because Eu<sup>2+</sup> is more soluble than Eu<sup>3+</sup> at elevated temperatures, it is possible that hydrothermal waters may have positive (Eu/Eu\*)<sub>cn</sub>, even if the rocks from which they react with does not (Wood 1990). Consistent with plagioclase dissolution, the most downgradient Type IV water sample has the highest (Eu/Eu\*)<sub>cn</sub> (0.68 at Octagon Spring vs. 0.25 at Mammoth Spring). This would seem to support the Maskell et al. (2015) model, at least for Type IV water in the upper aquifer, as there may be other explanations for the lower (Eu/Eu\*)<sub>cn</sub> in the downgradient sample.

Another possible explanation for the positive  $(Eu/Eu^*)_{cn}$  observed for Type IV water is the reaction with other rocks along the aquifer and creek flowpaths. One rock type found in abundance in the area and that possesses a strongly positive  $(Eu/Eu^*)_{cn}$  is the travertine deposits (Figure 4.9) (Ohly 2016) that occur in the valley. Therefore, based on the presence of positive  $(Eu/Eu^*)_{cn}$  in the travertine, and because the Soda Creek water is under-saturated with respect to calcite at Octagon Spring, it is possible that the positive  $(Eu/Eu^*)_{cn}$  in Type IV is the direct result of the dissolution of travertine along Soda Creek.

#### 4.4.5 Soda Spring Hydrogeology

The Southern BVF hydrogeology reflects a complex interaction between deep-sourced, CO<sub>2</sub>-charged thermal waters, a leaky mineralized basalt seal, and cold aquifer water recharged by local precipitation and leakage from Blackfoot Reservoir to the north. For time immemorial, the bubbling springs have been a wonder to humans living in the area. However, in spite of the intense curiosity, there have been relatively few studies conducted to characterize the system. Recently, the interest in CCS in geologic systems has renewed interest in the hydrogeology of the area due to the presence of large volumes of leaking CO<sub>2</sub>. To that end, our study was undertaken to evaluate the use of water chemistry, specifically REEs, to trace CO<sub>2</sub>-influenced water in the study area.

Our hydrogeological conceptual model for the Southern Blackfoot Valley is based on four identified water types (Figure 4.10). These waters have very different characteristics (Table 4.1) and, consequently, different histories. Type I water is highly CO<sub>2</sub>-charged thermal water sourced deep in the valley. The majority of these springs are located along the north side of the Bear River west from the city of Soda Springs (Figure 4.1). The source of the CO<sub>2</sub> is from the thermal decarbonation of Paleozoic carbonates and organic shales at perhaps 2,000 to 3,000 m (Lewicki et al. 2013; Hutsinpiller and Parry 1985). The source of the thermal energy that drives this reaction is from the recent volcanism in the valley (Pickett 2004; Armstrong and Oriel 1965; Armstrong 1969; Mabey and Oriel 1970; Ford 2005). Type I water migrates from a depth to the shallow subsurface (~100 m BLS at the Soda Geyser). The vertical movement of this water and CO<sub>2</sub> is restricted by heavily mineralized basalt flows that form an aquitard. The mineralized basalt aquitard is not a perfect seal, allowing fairly large amounts of CO<sub>2</sub> and lesser amounts of water to move to the surface, especially along the major fault zones. The loss of CO<sub>2</sub> through this leaky aquitard drives calcite precipitation, which further seals permeability in the aquitard over time. In places where the basalt aquitard has been penetrated by wells, along fault zones, or where the basalt formation thins significantly near the Bear River, the water has a more direct path to the surface. In these areas, Type I springs are characterized by CO<sub>2</sub>-effervescing, warm (~30°C) water that precipitates large volumes of HFO-stained travertine.



Type II waters are high-CO<sub>2</sub>-charged cold springs (<11°C) that occur along the main range-bounding fault on the west side of the BVF (Figure 4.10). The association of Type II springs and the major range fault suggests that structure plays a large role in the migration of CO<sub>2</sub> and, to a lesser degree, water to the surface. Unlike Type I water, Type II springs do not precipitate travertine in any significant volume, although these springs are typified by the presence of heavy staining by HFO precipitation. At the start of the study, it was assumed that because Type II springs are located within the shallow aquifer, the springs were comprised of deep CO<sub>2</sub> detached from Type I water and aquifer water (e.g., Type IV water). In fact, the presence of the springs within the aquifer requires that there is a significant component of aquifer water (Type IV) in these features. However, based on REE we propose that the water in Type II springs is a mixture of aquifer water and a component of Type I water, modified by calcite precipitation. This is significant as it implies that the basalt aquitard transmits small volumes of deep-sourced Type I water to the surface along fault traces.

Type III water is a special type of water that occurs in a complex of springs located in Sulphur Canyon. At these locations, high volumes of CO<sub>2</sub> and H<sub>2</sub>S and very little if any water are released to the surface. Based on the hydrogeologic model presented in Figure 4.10, it can be reasonably concluded that the CO<sub>2</sub> and H<sub>2</sub>S emanating from the study area are primarily sourced through the same metamorphic processes (e.g., decarbonation of carbonates and shale) as Type I and II water. This conclusion is supported by the REE trends from Sulphur Springs, which show a similarity with whole rock REE data from Paleozoic limestone as well as Pavilion Well (Figure 4.6; Madhavaraju and González-León 2012). This suggests that the neutralizing of acidic fluids derived from near-surface oxidation of reduced sulfur by limestone and dolomite host rocks gives the water present at Sulphur Canyon its characteristic REE signature.

Type IV water is comprised of shallow aquifer water and surface water from Soda Creek, which flows from the recharge zones north of Blackfoot Reservoir toward the Bear River (Figure 4.10). The presence of the mineralized basalt aquitard largely separates Types I and IV, except where leaking conduits exist, leading to Type II springs as explained above. Type IV waters have a wide range of chemistry with TDS increasing in the southern part of the Blackfoot Valley. In the southern reaches of the valley, the water in the stream and aquifer is not potable or suitable for irrigation. As a result, the City of Soda Springs pipes its water from upgradient sources. The low-quality Type IV water is due to high TDS that can exceed 2,400 ppm. This high TDS of Type IV water results from CO<sub>2</sub>-associated fluids upwelling into the shallow aquifer. REE trends from two samples show the presence of a positive (Eu/Eu\*)<sub>cn</sub> that may result from the dissolution of travertine, plagioclase from the basalt, or both as the water flows through the CO<sub>2</sub>-influenced system.

## 4.5 Implications for CCS

If large-scale CCS is ever globally adopted as a means of controlling CO<sub>2</sub> emissions to the atmosphere, it may very well rival hydrocarbon development and groundwater production as the largest perturbations of the Earth's subsurface undertaken by humans. Therefore, it is of the utmost urgency that scientists and engineers develop the necessary tools to ensure that the solution does not do more harm than the threat of climate change. The numerous, natural, CO<sub>2</sub>-leaking sites around the world may very well represent the best opportunity to study the impacts and monitoring requirements that will be needed for industrial CCS adoptions.

The natural CCS analogue at Soda Springs has proven to be an outstanding field laboratory to test and evaluate scientific techniques needed to understand how CO<sub>2</sub>-charged fluids can be traced in geologic environments. In this study, we were able to measure and evaluate the hydrogeology of the southern BVF at a scale relevant to large-scale CCS application. Some concluding remarks of this study are:

1. Because of the interaction between multiple water types, including a shallow aquifer (Type IV) and a deep water and CO<sub>2</sub> source (Type I), the southern BVF is well suited to conduct studies of the impact of migrating CO<sub>2</sub> into the near surface that may be expected at a leaking CCS site.
2. Although there is much debate regarding the suitability of basalt formations as CCS targets, our study, specifically at the Soda Springs Geyser, demonstrates that through self-sealing by secondary minerals, basalt has the potential to limit vertical flow of CO<sub>2</sub> fluids, either through mineralization reaction between the basalt and acidic CO<sub>2</sub>-charged fluids, or as is the case with the BVF, by direct precipitation of calcite from rising CO<sub>2</sub>-charged water.
3. Faults play a major role in forming pathways for CO<sub>2</sub>-charged fluids to migrate to the surface.
4. Results from our study show that CO<sub>2</sub> leaking from a large source may not leak in catastrophic fashion but could occur as small, distributed leaks such as those observed at Soda Springs.
5. The chemical signature of CO<sub>2</sub>-related processes manifest a geochemical signature that can be used to track where CO<sub>2</sub>-enriched water impacts aquifer waters.

In the southern Blackfoot Valley, a large number of people live and work atop a very significant, leaky, CO<sub>2</sub> system. Evidence from the analogue site indicates that should a large-scale CCS reservoir fail, the leaks would likely be relatively small and diffuse as they are in Soda Springs—not catastrophic, large-scale leaks. Nearly every aspect of the people's lives is impacted by the CO<sub>2</sub> system. They cannot have below-ground basements, bubbling springs appear in their yards,

construction must account for springs that exist throughout the city, and, most importantly, the entire community must pipe in potable water from elsewhere. Yet, in spite these circumstances caused by the leaking CO<sub>2</sub>, Soda Springs, the largest city in Southeast Idaho, has flourished for more than 100 years. In fact, the local population is quite proud of their unique geologic location and count on associated tourism to bring revenue into the community. Although this study was not designed to assess the impacts of subsurface CO<sub>2</sub> emissions on the local population, it was difficult not to notice how little thought the people give to the CO<sub>2</sub> system. The one notable exception is that people who park in downtown Soda Springs always pay attention to the wind direction to keep from getting scale on their cars from the Geysers; the authors quickly learned the same.

### References

- Alfredsson, H. A., B. S. Hardarson, H. Franzson, and S. R. Gislason, 2008, "CO<sub>2</sub> Sequestration in Basaltic Rock at the Hellisheidi Site in SW Iceland: Stratigraphy and Chemical Composition of the Rocks at the Injection Site," *Mineralogical Magazine*, Vol. 72, No. 1, February 2008, pp. 1–5, DOI: 10.1180/minmag.2008.072.1.1.
- Allis, R., T. Chidsey, W. Gwynn, C. Morgan, S. White, M. Adams, and J. Moore, 2001, "Natural CO<sub>2</sub> Reservoirs on the Colorado Plateau and Southern Rocky Mountains: Candidates for CO<sub>2</sub> Sequestration," *Proceedings of the First National Conference on Carbon Sequestration, Washington, D.C., May 14–17, 2001*.
- Allmendinger, R. W., 1981, "Structural Geometry of Meade Thrust Plate in Northern Blackfoot Mountains, Southeastern Idaho," *American Association of Petroleum Geologists Bulletin*, Vol. 65, No. 3, March 1981, pp. 509–525.
- Apps, J. A., Y. Zhang, L. Zheng, T. Xu, and J. T. Birkholzer, 2009, "Identification of Thermodynamic Controls Defining the Concentrations of Hazardous Elements in Potable Ground Waters and the Potential Impact of Increasing Carbon Dioxide Partial Pressure," *Energy Procedia*, Vol. 1, No. 1, February 2009, pp. 1917–1924, DOI: 10.1016/j.egypro.2009.01.250.
- Armstrong, F. C., 1969, *Geologic Map of the Soda Springs Quadrangle, Southeastern Idaho*, U.S. Geological Survey, I-Map 557.
- Armstrong, F. C. and S. S. Oriel, 1965, "Tectonic Development of Idaho-Wyoming Thrust Belt," *American Association of Petroleum Geologists Bulletin*, Vol. 49, No. 11, November 1965, pp. 1847–1866.
- Assayag, N., J. Matter, M. Ader, D. Goldberg, and P. Agrinier, 2009, "Water-Rock Interactions during a CO<sub>2</sub> Injection Field-Test: Implications on Host Rock Dissolution and Alteration Effects," *Chemical Geology*, Vol. 265, Nos. 1–2, July 2009, pp. 227–35, DOI: 10.1016/j.chemgeo.2009.02.007.
- Barnard, L., F. Bybee, and L. Walker, 1958, *Tosoiba ["Sparkling Water"]*, Soda Springs, Idaho: Camp Meads Daughters of Utah Pioneers.
- Baines, S. J. and R. H. Worden, 2004, "The Long-Term Fate of CO<sub>2</sub> in the Subsurface: Natural Analogues for CO<sub>2</sub> Storage," in *Geological Storage of Carbon Dioxide Baines*, edited by S. J. Baines and R. H. Worden, pp. 59–85, London: The Geological Society Publishing House.

- Banner, J. L., G. J. Wasserburg, P. F. Dobson, A. B. Carpenter, and C. H. Moore, 1989, "Isotopic and Trace Element Constraints on the Origin and Evolution of Saline Groundwaters from Central Missouri," *Geochimica et Cosmochimica Acta*, Vol. 53, No. 2, February 1989, pp. 383–398, DOI: 10.1016/0016-7037(89)90390-6.
- Benson, S. M. and P. Cook, 2005, "Underground Geological Storage," *IPCC Special Report on Carbon Dioxide Capture and Storage*, edited by B. Metz, O. Davidson, H. de Coninck, M. Loos, and L. Meyer, New York: Cambridge University Press.
- Bentley, R. D. and R. C. Surdam, 2013, "The Story of the Wyoming Carbon Underground Storage Project (WY-CUSP), and the Regional Inventory and Prioritization of Potential CO<sub>2</sub> Storage Reservoirs in Wyoming," in *Geological CO<sub>2</sub> Storage Characterization: The Key to Deploying Clean Fossil Energy Technology*, edited by R. C. Surdam, pp. 15–20, New York: Springer Science+Business Media, DOI: 10.1007/978-1-4614-5788-6\_2.
- Bertier, P., A. Busch, S. Hangx, N. Kampman, G. Nover, H. Stanjek, and P. Weniger, "The Werkendam Natural CO<sub>2</sub> Accumulation: An Analogue for CO<sub>2</sub> Storage in Depleted Oil Reservoir," poster presented at the European Geosciences Union General Assembly, Vienna, Austria, April 12–17, 2015, EGU2015-7683.
- Bertram, C. J. and H. Elderfield, 1993, "The Geochemical Balance of the Rare Earth Elements and Neodymium Isotopes in the Oceans," *Geochimica et Cosmochimica Acta*, Vol. 57, No. 9, May 1993, pp. 1957–1986, DOI: 10.1016/0016-7037(93)90087-D.
- Bethke, C. M. and S. Yeakel, 2014, *The Geochemist's Workbench User's Guides, Version 9.0. Aqueous Solutions LLC*.
- Bickle, M. and N. Kampman, 2013, "Lessons in Carbon Storage from Geological Analogues," *Geology*, Vol. 41, No. 4, April 2013, pp. 525–526, DOI: 10.1130/focus0420132.1.
- Boynnton, W. V., 1984, "Cosmochemistry of the Rare Earth Elements: Meteorite Studies," in *Developments in Geochemistry, Rare Earth Element Geochemistry 2*, edited by P. Henderson, pp. 63–114, Amsterdam, The Netherlands: Elsevier.
- Burnside, N. M., Z. K. Shipton, B. Dockrill, and R. M. Ellam, 2013, "Man-Made Versus Natural CO<sub>2</sub> Leakage: A 400 K.Y. History of an Analogue for Engineered Geological Storage of CO<sub>2</sub>," *Geology*, Vol. 41, No. 4, February 2013, pp. 471–4, DOI: 10.1130/G33738.1.
- Carney, S. M. and S. U. Janecke, 2005, "Excision and the Original Low Dip of the Miocene-Pliocene Bannock Detachment System, SE Idaho: Northern Cousin of the Sevier Desert Detachment?" *Bulletin of the Geological Society of America*, Vol. 117, Nos. 3–4, March/April 2005, pp. 334–353, DOI: 10.1130/B25428.1.
- Carney, E., 1998, *Historic Soda Springs: Oasis on the Oregon Trail*, Wayan, Idaho: Traildust Pub. Co.
- Cantrell, K. J. and R. H. Byrne, 1987, "Rare Earth Element Complexation by Carbonate and Oxalate Ions," *Geochimica et Cosmochimica Acta*, Vol. 51, No. 3, March 1987, pp. 597–605, DOI: 10.1016/0016-7037(87)90072-X.
- Chevis, D. A., K. H. Johannesson, D. J. Burdige, J. Tang, S. B. Moran, and R. P. Kelly, 2015, "Submarine Groundwater Discharge of Rare Earth Elements to a Tidally-Mixed Estuary in Southern Rhode Island," *Chemical Geology*, Vol. 397, March 2015, pp. 128–142, DOI: 10.1016/j.chemgeo.2015.01.013.
- Christiansen, R. L. and P. W. Lipman, 1972, "Cenozoic Volcanism and Plate-Tectonic Evolution of the Western United States. II. Late Cenozoic," *Philosophical Transactions of the Royal Society A*, Vol. 271, No. 1213, January 1972, pp. 249–284, DOI: 10.1098/rsta.1972.0009.

- Dion, N. P., 1974, *An Estimate of Leakage from the Blackfoot Reservoir to Bear River Basin, Southeastern Idaho*, Water Information Bulletin No. 34, Idaho Department of Water Resources.
- Elderfield, H. and M. J. Greaves, 1982, "The Rare Earth Elements in Seawater," *Nature*, Vol. 296, March 1982, pp. 214–219, DOI: 10.1038/296214a0.
- EPA, *Geologic Sequestration of Carbon Dioxide: Underground Injection Control (UIC) Program Class VI Well Site Characterization Guidance*, <https://www.epa.gov/sites/production/files/2015-07/documents/epa816r13004.pdf>, published May 2013, website visited March 2017.
- Fiesinger, D. W., W. D. Perkins, and B. J. Puchy, 1982, "Mineralogy and Petrology of Tertiary-Quaternary Volcanic Rocks in Caribou County, Idaho," in *Cenozoic Geology of Idaho* (Bulletin 26 of the Idaho Bureau of Mines and Geology), edited by B. Bonnicksen and R. M. Breckenridge, pp. 465–488.
- Ford, M. T., 2005, *The Petrogenesis of Quaternary Rhyolite Domes in the Bimodal Blackfoot Volcanic Field, Southeastern Idaho*, M. S. Thesis: Idaho State University, Pocatello, Idaho.
- Fleet, A. J., 1984, "Aqueous and Sedimentary Geochemistry of the Rare Earth Elements," in *Developments in Geochemistry*, Rare Earth Element Geochemistry 2, edited by P. Henderson, pp. 343–373, Amsterdam, The Netherlands: Elsevier.
- Gislason, S. R., W. S. Broecker, E. H. Oelkers, E. Gunnlaugsson, H. Sigurdardottir, A. Stefansson, D. Wolff-Boenisch, J. Matter, M. Stute, and G. Axelsson, 2008, "The Carbfix Project: Mineral CO<sub>2</sub> Sequestration into Basalt," *Geochimica et Cosmochimica Acta*, Vol. 73, No. 13, Supplement, p. A440, DOI: 10.1016/j.gca.2009.05.025.
- Goldberg, D. S., D. V. Kent, and P. E. Olson, 2009, "Potential On-shore and Off-shore Reservoirs for CO<sub>2</sub> Sequestration in Central Atlantic Magmatic Province Basalts," *Proceedings of the National Academy of Sciences of the United States of America*, January 26, 2010, Vol. 107, No. 4, pp. 1327–1332, DOI: 10.1073/pnas.0913721107.
- Gosselin, D. C., M. R. Smith, E. A. Lepel, and J. C. Laul, 1992, "Rare Earth Elements in Chloride-Rich Groundwater, Palo Duro Basin, Texas, USA," *Geochimica et Cosmochimica Acta*, Vol. 56, No. 4, April 1992, pp. 1495–1505, DOI: 10.1016/0016-7037(92)90219-9.
- Gromet, L. P., R. F. Dymek, L. A. Haskin, and R. L. Korotev, 1984, "The 'North American Shale Composite': Its Compilation, Major and Trace Element Characteristics," *Geochimica et Cosmochimica Acta*, Vol. 48, No. 12, December 1984, pp. 2469–2482, DOI: 10.1016/0016-7037(84)90298-9.
- Haszeldine, S., O. Quinn, G. England, M. Wilkinson, Z. K. Shipton, J. P. Evans, J. Heath, L. Crossey, C. J. Ballentine, and C. M. Graham, 2005, "Natural Geochemical Analogues for Carbon Dioxide Storage in Deep Geological Porous Reservoirs," *Oil & Gas Science and Technology*, Vol. 60, No. 1, January/February 2005, pp. 33–49, DOI: 10.2516/ogst:2005004.
- Henderson, P., 1984, *Developments in Geochemistry*, Rare Earth Element Geochemistry 2, Amsterdam, The Netherlands: Elsevier.
- Hollings, P. and D. Wyman, 2005, "The Geochemistry of Trace Elements in Igneous Systems: Principles and Examples from Basaltic Systems," in *Rare-Element Geochemistry and Mineral Deposits* (Short Course Notes 17), edited by R. Linnen and I. Samson, pp. 1–16, St. John's, Newfoundland: Geological Association of Canada.
- Humphris, S. E., 1984, "The Mobility of the Rare Earth Elements in the Crust," in *Developments in Geochemistry*, Rare Earth Element Geochemistry 2, edited by P. Henderson, pp. 317–342, Amsterdam, The Netherlands: Elsevier.

- Hutsinpillar, A. and W. T. Parry, 1985, "Geochemistry and Geothermometry of Spring Water from the Blackfoot Reservoir Region, Southeastern Idaho," *Journal of Volcanology and Geothermal Research*, Vol. 26, Nos. 3–4, December 1985, pp. 275–296, DOI: 10.1016/0377-0273(85)90060-5.
- IPCC, 2007, *Climate Change 2007: The Physical Science Basis*, edited by S. Solomon, D. Qin, M. Manning, Z. Chen, M. Marquis, K. Averyt, M. M. B. Tignor, and H. L. Miller Jr., New York: Cambridge University Press.
- Jeandel, E., A. Battani, and P. Sarda, 2010, "Lessons Learned from Natural and Industrial Analogues for Storage of Carbon Dioxide," *International Journal of Greenhouse Gas Control*, Vol. 4, No. 6, December 2010, pp. 890–909, DOI: 10.1016/j.ijggc.2010.06.005.
- Johannesson, Karen H., C. D. Palmore, J. Fackrell, N. G. Prouty, P. W. Swarzenski, D. A. Chevis, K. Telfeyan, C. D. White, and D. J. Burdige, 2017, "Rare Earth Element Behavior During Groundwater-Seawater Mixing along the Kona Coast of Hawaii," *Geochimica et Cosmochimica Acta*, Vol. 198, February 2017, pp. 229–258, DOI: 10.1016/j.gca.2016.11.009.
- Johannesson, Karen H., D. A. Chevis, D. J. Burdige, J. E. Cable, J. B. Martin, and M. Roy, 2011, "Submarine Groundwater Discharge is an Important Net Source of Light and Middle REEs to Coastal Waters of the Indian River Lagoon, Florida, USA," *Geochimica et Cosmochimica Acta*, Vol. 75, No. 3, February 2011, pp. 825–843, DOI: 10.1016/j.gca.2010.11.005.
- Johannesson, Kevin H. and M. J. Hendry, 2000, "Rare Earth Element Geochemistry of Groundwaters from a Thick Till and Clay-Rich Aquitard Sequence, Saskatchewan, Canada," *Geochimica et Cosmochimica Acta*, Vol. 64, No. 9, May 2000, pp. 1493–1509, DOI: 10.1016/S0016-7037(99)00402-0.
- Johannesson, Kevin H. and X. Zhou, 1999, "Origin of Middle Rare Earth Element Enrichments in Acid Waters of a Canadian High Arctic Lake," *Geochimica et Cosmochimica Acta*, Vol. 63, No. 1, January 1999, pp. 153–165, DOI: 10.1016/S0016-7037(98)00291-9.
- Johannesson, Kevin H., K. J. Stetzenbach, and V. F. Hodge, 1997a, "Rare Earth Elements as Geochemical Tracers of Regional Groundwater Mixing," *Geochimica et Cosmochimica Acta*, Vol. 61, No. 17, September 1997, pp. 3605–3618, DOI: 10.1016/S0016-7037(97)00177-4.
- Johannesson, Kevin H., K. J. Stetzenbach, and V. F. Hodge, 1998, "Reply to the Comment by R. H. Byrne and J. Schijf On 'Rare Earth Elements as Geochemical Tracers of Regional Groundwater Mixing,'" *Geochimica et Cosmochimica Acta*, Vol. 62, No. 12, June 1998, pp. 2201–2206.
- Johannesson, Kevin H., K. J. Stetzenbach, V. F. Hodge, and W. B. Lyons, 1996, "Rare Earth Element Complexation Behavior in Circumneutral pH Groundwaters: Assessing the Role of Carbonate and Phosphate Ions," *Earth and Planetary Science Letters*, Vol. 139, Nos. 1–2, March 1996, pp. 305–319, DOI: 10.1016/0012-82X(96)00016-7.
- Johannesson, Kevin H., K. J. Stetzenbach, V. F. Hodge, D. K. Kremer, and X. Zhou, 1997b, "Delineation of Ground-Water Flow Systems in the Southern Great Basin Using Aqueous Rare Earth Element Distributions," *Groundwater*, Vol. 35, No. 5, September 1997, pp. 807–819, DOI: 10.1111/j.1745-6584.1997.tb00149.x.
- Kampman, N., N. M. Burnside, M. Bickle, Z. K. Shipton, R. M. Ellam, and H. Chapman, 2010, "Coupled CO<sub>2</sub>-Leakage and In-situ Fluid-Mineral Reactions in a Natural CO<sub>2</sub> Reservoir, Green River, Utah," *Geochimica et Cosmochimica Acta*, Vol. 74, No. 12, Supplement, June 2010, pp. A487–A552, DOI: 10.1016/j.gca.2010.04.036.

- Kampman, N., A. Busch, P. Bertier, J. Snippe, S. Hangx, V. Pipich, Z. Di, G. Rother, J. F. Harrington, J. P. Evans, A. Maskell, H. J. Chapman, and M. J. Bickle, 2016, "Observational Evidence Confirms Modelling of the Long-Term Integrity of CO<sub>2</sub>-Reservoir Caprocks," *Nature Communications*, Vol. 7, July 2016, DOI: 10.1038/ncomms12268.
- Keating, E. H., J. Fessenden, N. Kanjorski, D. J. Koning, and R. Pawar, 2010, "The Impact of CO<sub>2</sub> on Shallow Groundwater Chemistry: Observations at a Natural Analog Site and Implications for Carbon Sequestration," *Environmental Earth Sciences*, Vol. 60, No. 3, April 2010, pp. 521–536, DOI: 10.1007/s12665-009-0192-4.
- Kehew, A. E., 2001, *Applied Chemical Hydrogeology*, New Jersey: Prentice Hall.
- Kharaka, Y. K., J. J. Thordsen, E. Kakouros, G. Ambats, W. N. Herkelrath, S. R. Beers, J. T. Birkholzer, J. A. Apps, N. F. Spycher, L. Zheng, R. C. Trautz, H. W. Rauch, and K. S. Gullickson, 2010, "Changes in the Chemistry of Shallow Groundwater Related to the 2008 Injection of CO<sub>2</sub> at the ZERT field site, Bozeman, Montana," *Environmental Earth Sciences*, Vol. 60, No. 2, March 2010, pp. 273–284, DOI: 10.1007/s12665-009-0401-1.
- Klinkhammer, G., C. R. German, H. Elderfield, M. J. Greaves, and A. Mitra, 1994, "Rare Earth Elements in Hydrothermal Fluids and Plume Particulates by Inductively Coupled Plasma Mass Spectrometry," *Marine Chemistry*, Vol. 45, No. 3, February 1994, pp. 170–186, DOI: 10.1016/0304-4203(94)90001-9.
- Lewicki, J. L., G. E. Hilley, L. Dobeck, T. L. McLing, B. M. Kennedy, M. Bill, and B. D. V. Marino, 2013, "Geologic CO<sub>2</sub> Input into Groundwater and the Atmosphere, Soda Springs, ID, USA," *Chemical Geology*, Vol. 339, February 2013, pp. 61–70, DOI: 10.1016/j.chemgeo.2012.06.013.
- Lewis, R. S., P. K. Link, L. R. Stanford, and S. P. Long, 2012, *Geologic Map of Idaho*, Idaho Geological Survey Map M-9.
- Link, P. K., 2002, "Digital Atlas of Idaho, Nov. 2002," <http://imnh.isu.edu/digitalatlas/counties/caribou/geomapL.gif>, published November 2002, website visited March 2017.
- Link, P. K. and E. C. Phoenix, 1996, *Rocks, Rail, & Trails*, 2nd ed., Pocatello, Idaho: Idaho Museum of Natural History.
- Lokey-Aldrich, E., C. Koerner, J. C. Perkowski, and T. L. McLing, 2012, "Managing the Risks of Carbon Sequestration: Liability Concerns and Alternatives," in *Managing Climate Change Business Risks and Consequences: Leadership for Global Sustainability* (Global Sustainability through Business series), edited by J. A. F. Stoner and C. Wankel, pp. 183–205, New York: Palgrave Macmillan.
- Luedke, R. G., and R. L. Smith, 1983, *Map Showing Distribution, Composition, and Age of Late Cenozoic Volcanic Centers in Idaho, Western Montana, West-Central South Dakota, and Northwestern Wyoming*, U.S. Geological Survey, IMAP 1091-E.
- Mabey, D. R. and S. S. Oriel, 1970, *Gravity and Magnetic Anomalies in the Soda Springs Region, Southeastern Idaho*, U.S. Geological Survey, Professional Paper 646-E.
- Madhavaraju, J. and C. M. González-León, 2012, "Depositional Conditions and Source of Rare Earth Elements in Carbonate Strata of the Aptian-Albian Mural Formation, Pitaycachi Section, Northeastern Sonora, Mexico," *Revista Mexicana de Ciencias Geológicas*, Vol. 29, No. 2, pp. 478–491.

- Mansfield, G. R. and G. H. Girty, 1927, *Geography, Geology, and Mineral Resources of Part of Southeastern Idaho, with Descriptions of Carboniferous and Triassic Fossils*, U.S. Geological Survey, Professional Paper 152.
- Maskell, A., N. Kampman, H. Chapman, D. J. Condon, and M. Bickle, 2015, “Kinetics of CO<sub>2</sub>-Fluid-Rock Reactions in a Basalt Aquifer, Soda Springs, Idaho,” *Applied Geochemistry*, Vol. 61, October 2015, pp. 272–283, DOI: 10.1016/j.apgeochem.2015.06.010.
- Mayo, A. L., A. B. Muller, and D. R. Rolston, 1985, “Hydrogeochemistry of the Meade Thrust Allochthon, Southeastern Idaho, U.S.A., and Its Relevance to Stratigraphic and Structural Groundwater Flow Control,” *Journal of Hydrology*, Vol. 76, Nos. 1–2, January 1985, pp. 27–61, DOI: 10.1016/0022-1694(85)90089-7.
- McGrail, B. P., H. T. Schaef, A. M. Ho, Y. -J. Chien, J. J. Dooley, and C. L. Davidson, 2006, “Potential for Carbon Dioxide Sequestration in Flood Basalts,” *Journal of Geophysical Research: Solid Earth*, Vol. 111, No. B12, December 2006, DOI: 10.1029/2005JB004169.
- McLing, T. L., R. W. Smith, and T. M. Johnson, 2002, “Chemical Characteristics of Thermal Water beneath the Eastern Snake River Plain,” in *Geology, Hydrogeology, and Environmental Remediation: Idaho National Engineering and Environmental Laboratory, Eastern Snake River Plain, Idaho* (GSA Special Papers 353), edited by P. K. Link and L. L. Mink, pp. 205–211, DOI: 10.1130/0-8137-2353-1.205.
- McLing, T. L., W. W. Smith, and R. W. Smith, 2014, “Utilizing Rare Earth Elements as Tracers in High TDS Reservoir Brines in CCS Applications,” *Energy Procedia*, Vol. 63, pp. 3963–3974, DOI: 10.1016/j.egypro.2014.11.426.
- Mitchell, J. C., 1976, *Geothermal Investigations in Idaho, Part 6: Geochemistry and Geologic Setting of the Thermal and Mineral Waters of the Blackfoot Reservoir Area, Caribou County, Idaho*, Water Information Bulletin 30, Idaho Department of Water Resources.
- Moore, J., M. Adams, R. Allis, S. Lutz, and S. Rauzi, 2005, “Mineralogical and Geochemical Consequences of the Long-Term Presence of CO<sub>2</sub> in Natural Reservoirs: An Example from the Springerville-St. Johns Field, Arizona, and New Mexico, U.S.A.,” *Chemical Geology*, Vol. 217, Nos. 3–4, April 2005, pp. 365–385, DOI: 10.1016/j.chemgeo.2004.12.019.
- Muller, A. B. and A. L. Mayo, 1983, “Ground-Water Circulation in the Meade Thrust Allochthon Evaluated by Radiocarbon Techniques,” *Radiocarbon*, Vol. 25, No. 2, January 1983, pp. 357–372, DOI: 10.1017/S0033822200005646.
- Nance, W. B. and S. R. Taylor, 1976, “Rare Earth Element Patterns and Crustal Evolution—I. Australian Post-Archean Sedimentary Rocks,” *Geochimica et Cosmochimica Acta*, Vol. 40, No. 12, December 1976, pp. 1539–1551, DOI: 10.1016/0016-7037(76)90093-4.
- Nelson, B. J., S. A. Wood, and J. L. Osiensky, 2004, “Rare Earth Element Geochemistry of Ground Water in the Palouse Basin, Northern Idaho-Eastern Washington,” *Geochemistry: Exploration, Environment, Analysis*, Vol. 4, No. 3, August 2004, pp. 227–241, DOI: 10.1144/1467-7873/04-203.
- Nelson, D. T., 2005, *Rare Earth Elements as a Natural Tracer of Ground Water Flow in the Eastern Snake River Plain Aquifer, Idaho*, M. S. Thesis: University of Idaho, Moscow, Idaho.
- Noack, C. W., D. A. Dzombak, and A. K. Karamalidis, 2014, “Rare Earth Element Distributions and Trends in Natural Waters with a Focus on Groundwater,” *Environmental Science & Technology*, Vol. 48, No. 8, March 2014, pp. 4317–4326, DOI: 10.1021/es4053895.
- Oelkers, E. H., S. R. Gislason, and J. Matter, 2008, “Mineral Carbonation of CO<sub>2</sub>,” *Elements* Vol. 4, No. 5, October 2008, pp. 333–337, DOI: 10.2113/gselements.4.5.333.



- Ohly, S. R., 2016, *A Comparative Study of Geochemistry, Microfacies, and Depositional Processes of Travertine Deposits in the Blackfoot Volcanic Field: Implications for Potential Blind Geothermal Systems in Southeastern Idaho*, M. S. Thesis: Idaho State University, Pocatello, Idaho.
- Ojiambo, S. B., W. B. Lyons, K. A. Welch, R. J. Poreda, and K. H. Johannesson, 2003, "Strontium Isotopes and Rare Earth Elements as Tracers of Groundwater-Lake Water Interactions, Lake Naivasha, Kenya," *Applied Geochemistry*, Vol. 18, No. 11, November 2003, pp. 1789–1805, DOI: 10.1016/S0883-2927(03)00104-5.
- Oriel, S. S. and L. B. Platt, 1980, *Geologic Map of the Preston 1 Degree × 2 Degrees Quadrangle, Southeastern Idaho and Western Wyoming*, U.S. Geological Survey, Miscellaneous Investigations Series Map, I-1127.
- Peng, X. and E. D. Humphreys, 1998, "Crustal Velocity Structure across the Eastern Snake River Plain and the Yellowstone Swell," *Journal of Geophysical Research: Solid Earth*, Vol. 103, No. B4, April 1998, pp. 7171–7186, DOI: 10.1029/97JB03615.
- Pickett, K. E., 2004, *Physical Volcanology, Petrography, and Geochemistry of Basalts in the Bimodal Blackfoot Volcanic Field, Southeastern Idaho*, M. S. Thesis: Idaho State University, Pocatello, Idaho.
- Piper, A. M., 1944, "A Graphical Procedure in the Geochemical Interpretation of Water-Analyses," *EOS Transactions, American Geophysical Union*, Vol. 25, No. 6, pp. 914–928, DOI: 10.1029/TR025i006p00914.
- Polun, S. G., 2011, *Kinematic Analysis of Late Pleistocene Faulting in the Blackfoot Lava Field, Caribou County, Idaho*, M. S. Thesis: Idaho State University, Pocatello, Idaho.
- Prentice, I. C., G. D. Farquhar, M. J. R. Fasham, M. L. Goulden, M. Heimann, V. J. Jaramillo, H. S. Khesghi, C. Le Quéré, R. J. Scholes, and D. W. R. Wallace, 2002, "The Carbon Cycle and Atmospheric Carbon Dioxide," in *Climate Change 2001: The Scientific Basis*, edited by J. T. Houghton, Y. Ding, D. J. Griggs, N. Noguer, P. J. van der Linden, D. Xiaosu, K. Maskell, and C. A. Johnson, pp. 185–225. New York: Cambridge University Press.
- Ralston, D. R. and A. L. Mayo, 1983, *Thermal Ground Water Flow Systems in the Thrust Zone in Southeastern Idaho*, U.S. Department of Energy, DOE/ET/28407-4.
- Reilly, T. R., L. N. Plummer, P. J. Phillips, and E. Busenberg, 1994, "The Use of Simulation and Multiple Environmental Tracers to Quantify Groundwater Flow in a Shallow Aquifer," *Water Resources Research*, Vol. 30, No. 2, February 1994, pp. 421–433, DOI: 10.1029/93WR02655.
- Rollinson, H. R., 1993, *Using Geochemical Data: Evaluation, Presentation, Interpretation*, New York: John Wiley & Sons, Inc.
- Samson, I. M. and S. A. Wood, 2005, "The Rare Earth Elements: Behaviour in Hydrothermal Fluids and Concentration in Hydrothermal Mineral Deposits, Exclusive of Alkaline Settings," in *Rare-Element Geochemistry and Mineral Deposits: Geological Association of Canada, Short Course Notes 17*, edited by R. L. Linnen and I. M. Samson, pp. 269–297.
- Schaefer, H. T. and B. P. McGrail, 2009, "Dissolution of Columbia River Basalt under Mildly Acidic Conditions as a Function of Temperature: Experimental Results Relevant to the Geological Sequestration of Carbon Dioxide," *Applied Geochemistry*, Vol. 24, No. 5, May 2005, pp. 980–987, DOI: 10.1016/j.apgeochem.2009.02.025.
- Schaefer, H. T., B. P. McGrail, and A. T. Owen, 2009, "Basalt-CO<sub>2</sub>-H<sub>2</sub>O Interactions and Variability in Carbonate Mineralization Rates," *Energy Procedia*, Vol. 1, No. 1, February 2009, pp. 4899–4906, DOI: 10.1016/j.egypro.2009.02.320.

- Schaef, H. T., B. P. McGrail, and A. T. Owen, 2010, "Carbonate Mineralization of Volcanic Province Basalts," *International Journal of Greenhouse Gas Control*, Vol. 4, No. 2, March 2010, pp. 249-261, DOI: 10.1016/j.ijggc.2009.10.009.
- Shannon, W. M. and S. A. Wood, 2005, "The Analysis of Picogram Quantities of Rare Earth Elements in Natural Waters," in *Rare Earth Elements in Groundwater Flow Systems*, Water Science and Technology Library 51, edited by K. H. Johannesson, pp. 1-37, Dordrecht, The Netherlands: Springer Science+Business Media.
- Shibata, S. -N., T. Tanaka, and K. Yamamoto, 2006, "Crystal Structure Control of the Dissolution of Rare Earth Elements in Water-Mineral Interactions," *Geochemical Journal*, Vol. 40, No. 5, pp. 437-446, DOI: 10.2343/geochemj.40.437.
- Shinotsuka, K., H. Hidaka, and M. Ebihara, 1995, "Detailed Abundances of Rare Earth Elements, Thorium and Uranium in Chondritic Meteorites: an ICP-MS Study," *Meteoritics & Planetary Science*, Vol. 30, No. 6, November 1995, pp. 694-699, DOI: 10.1111/j.1945-5100.1995.tb01166.x.
- Siirila, E. R., A. K. Navarre-Sitchler, R. M. Maxwell, and J. E. McCray, 2012, "A Quantitative Methodology to Assess the Risks to Human Health from CO<sub>2</sub> Leakage into Groundwater," *Advances in Water Resources*, Vol. 36, February 2012, pp. 146-164, DOI: 10.1016/j.advwatres.2010.11.005.
- Smedley, P. L., 1991, "The Geochemistry of Rare Earth Elements in Groundwater from the Carnmenellis Area, Southwest England," *Geochimica et Cosmochimica Acta*, Vol. 55, No. 10, October 1991, pp. 2767-2779, DOI: 10.1016/0016-7037(91)90443-9.
- Smith, R. W., T. L. McLing, W. Barrash, W. P. Clement, and N. P. Erickson, 2005, "Geologic Sequestration of CO<sub>2</sub>: A Uniform Strategy for Assessing Mineralization Trapping Potential across Rock Types," *Big Sky Carbon Sequestration Partnership Third Annual Conference on Carbon Capture and Sequestration*.
- Solomon, S., R. T. Pierrehumbert, D. Matthews, J. S. Daniel, and P. Friedlingstein, 2013, "Atmospheric Composition, Irreversible Climate Change, and Mitigation Policy," in *Climate Science for Serving Society*, edited by G. R. Asrar and J. W. Hurrell, pp. 415-436, Dordrecht, The Netherlands: Springer Science+Business Media.
- Solomon, S., G. -K. Plattner, R. Knutti, and P. Friedlingstein, 2009, "Irreversible Climate Change due to Carbon Dioxide Emissions," *Proceedings of the National Academy of Sciences of the United States of America*, Vol. 106, No. 6, February 2009, pp. 1704-1709, DOI: 10.1073/pnas.0812721106.
- Sparlin, M. A., L. W. Braile, and R. B. Smith, 1982, "Crustal Structure of the Eastern Snake River Plain Determined from Ray Trace Modeling of Seismic Refraction Data," *Journal of Geophysical Research: Solid Earth*, Vol. 87, No. B4, April 1982, pp. 2619-2633, DOI: 10.1029/JB087iB04p02619.
- Spycher, N., K. Pruess, and J. Ennis-King, 2003, "CO<sub>2</sub>-H<sub>2</sub>O Mixtures in the Geological Sequestration of CO<sub>2</sub>. I. Assessment and Calculation of Mutual Solubilities from 12 to 100°C and up to 600 Bar," *Geochimica et Cosmochimica Acta*, Vol. 67, No. 16, August 2003, pp. 3015-3031, DOI: 10.1016/S0016-7037(03)00273-4.
- Stetzenbach, K. J., V. F. Hodge, C. Guo, I. M. Farnham, and K. H. Johannesson, 2001, "Geochemical and Statistical Evidence of Deep Carbonate Groundwater within Overlying Volcanic Rock Aquifers/Aquitards of Southern Nevada, USA," *Journal of Hydrology*, Vol. 243, Nos. 3-4, pp. 254-271, DOI: 10.1016/S0022-1694(00)00418-2.

- Stetzenbach, K. J., M. Amano, D. K. Kreamer, and V. F. Hodge, 1994, "Testing the Limits of ICP-MS: Determination of Trace Elements in Ground Water at the Part-Per-Trillion Level," *Groundwater*, Vol. 32, No. 6, November 1994, pp. 976–985, DOI: 10.1111/j.1745-6584.1994.tb00937.x.
- Strachan, D. M., S. Tymochowicz, P. Schubert, and H. M. Kingston, 1989, "Preconcentration of Trace Transition Metal and Rare Earth Elements from Highly Saline Solutions," *Analytica Chimica Acta*, Vol. 220, pp. 243–249, DOI: 10.1016/S0003-2670(00)80267-6.
- Sun, S. -S., 1982, "Chemical Composition and Origin of the Earth's Primitive Mantle," *Geochimica et Cosmochimica Acta*, Vol. 46, No. 2, February 1982, pp. 179–192, DOI: 10.1016/0016-7037(82)90245-9.
- Surdam, R. C., S. A. Quillinan, and Z. Jiao, 2013, "Displaced Fluid Management—The Key to Commercial-Scale Geologic CO<sub>2</sub> Storage," in *Geological CO<sub>2</sub> Storage Characterization: The Key to Deploying Clean Fossil Energy Technology*, edited by R. C. Surdam, pp. 233–244, New York: Springer Science+Business Media, DOI: 10.1007/978-1-4614-5788-6\_11.
- Taylor, S. R. and S. M. McLennan, 1995, "The Geochemical Evolution of the Continental Crust," *Reviews of Geophysics*, Vol. 33, No. 2, May 1995, pp. 241–265, DOI: 10.1029/95RG00262.
- Wakita, H., P. Rey, and R. A. Schmitt, 1971, "Abundances of the 14 Rare-Earth Elements and 12 Other Trace Elements in Apollo 12 Samples: Five Igneous and One Breccia Rocks and Four Soils," *Proceedings of the Second Lunar Science Conference, Houston, Texas, January 11–14, 1971*, Vol. 2, pp. 1319–1329.
- Wang, S. and P. R. Jaffe, 2004, "Dissolution of a Mineral Phase in Potable Aquifers due to CO<sub>2</sub> Releases from Deep Formations: Effect of Dissolution Kinetics," *Energy Conversion and Management*, Vol. 45, Nos. 18–19, November 2004, pp. 2833–2848, DOI: 10.1016/j.enconman.2004.01.002.
- Welhan, J. A., D. Garwood, and D. Feeney, 2013, "The Volcanic Field, Southeast Idaho: A Hidden High-T Geothermal Resource Revealed through Data Mining of the National Geothermal Data Repository," *Transactions (GRC)*, Vol. 37, January 2013, pp. 365–374.
- Welhan, J. A., C. M. Johannesen, K. S. Reeves, T. M. Clemo, J. A. Glover, and K. W. Bosworth, 2002, "Morphology of Inflated Pahoehoe Lavas and Spatial Architecture of their Porous and Permeable Zones, Eastern Snake River Plain, Idaho," in *Geology, Hydrogeology, and Environmental Remediation: Idaho National Engineering and Environmental Laboratory, Eastern Snake River Plain, Idaho* (GSA Special Papers 353), edited by P. K. Link and L. L. Mink, pp. 135–150, DOI: 10.1130/0-8137-2353-1.135.
- Wood, S. A., 1990, "The Aqueous Geochemistry of the Rare-Earth Elements and Yttrium. 1. Review of Available Low-Temperature Data for Inorganic Complexes and the Inorganic REE Speciation of Natural Waters," *Chemical Geology*, Vol. 82, pp. 159–186, DOI: 10.1016/0009-2541(90)90080-Q.
- Wood, S. A., 2006, "Rare Earth Element Systematics of Acidic Geothermal Waters from the Taupo Volcanic Zone, New Zealand," *Journal of Geochemical Exploration*, Vol. 89, Nos. 1–3, April–June 2006, pp. 424–427, DOI: 10.1016/j.gexplo.2005.11.023.
- Wood, S. A., C. H. Gammons, S. R. Parker, 2006, "The Behavior of Rare Earth Elements in Naturally and Anthropogenically Acidified Waters," *Journal of Alloys and Compounds*, Vol. 418, Nos. 1–2, July 2006, pp. 161–165, DOI: 10.1016/j.jallcom.2005.07.082.

- White, D. J., G. Burrowes, T. Davis, Z. Hajnal, K. Hirsche, I. Hutcheon, E. Majer, B. Rostron, and S. Whittaker, 2004, "Greenhouse Gas Sequestration in Abandoned Oil Reservoirs: The International Energy Agency Weyburn Pilot Project," *GSA Today*, Vol. 14, No. 7, July 2004, pp. 4–10, DOI: 10.1130/1052-5173(2004)0142.0.CO;2.
- Whitehead, P. G., R. L. Wilby, R. W. Battarbee, M. Kernan, and A. J. Wade, 2009, "A Review of the Potential Impacts of Climate Change on Surface Water Quality," *Hydrological Sciences Journal*, Vol. 54, No. 1, December 2009, pp. 101–123, DOI: 10.1623/hysj.54.1.101.
- Xu, T., J. A. Apps, and K. Pruess, 2003, "Reactive Geochemical Transport Simulation to Study Mineral Trapping for CO<sub>2</sub> Disposal in Deep Arenaceous Aquifers," *Journal of Geophysical Research: Solid Earth*, Vol. 108, No. B2, February 2003, pp. 3-1–3-13, DOI: 10.1029/2002JB001979.
- Young, H. W. and J. C. Mitchell, 1973, *Geothermal Investigations in Idaho, Part 1. Geochemistry and Geologic Setting of Selected Thermal Waters*, Water Information Bulletin No. 30, Idaho Department of Water Resources.
- Zheng, L., J. A. Apps, N. Spycher, J. T. Birkholzer, Y. K. Kharaka, J. Thordsen, S. R. Beers, W. N. Herkelrath, E. Kakouros, and R. C. Trautz, 2012, "Geochemical Modeling of Changes in Shallow Groundwater Chemistry Observed during the MSU-ZERT CO<sub>2</sub> Injection Experiment," *International Journal of Greenhouse Gas Control*, Vol. 7, March 2012, pp. 202–217, DOI: 10.1016/j.ijggc.2011.10.003.
- Zheng, L., J. A. Apps, Y. Zhang, T. Xu, and J. T. Birkholzer, 2009, "Reactive Transport Simulations to Study Groundwater Quality Changes in Response to CO<sub>2</sub> Leakage from Deep Geological Storage," *Energy Procedia*, Vol. 1, No. 1, February 2009, pp. 1887–1894, DOI: 10.1016/j.egypro.2009.01.246.
- Zhou, X., K. J. Stetzenbach, K. H. Johannesson, and I. M. Farnham, 2000, "Major Ion Geochemistry of Groundwaters from Southern Nevada and Eastern California, USA," *Chinese Journal of Geochemistry*, Vol. 19, No. 1, March 2000, pp. 1–22, DOI: 10.1007/BF03166646.

## Conclusion

Environmental tracers are natural or man-made substances that are widely distributed in the Earth's geologic and hydrologic systems. These substances may enter the systems of interest through the atmosphere by precipitation or by water-rock reactions as water moves through the vadose zones or aquifers. The suite of possible environmental tracers is large, and variations in their concentration and distribution can be used as tracers to determine the provenance, age, or fate and transport of constituents in systems of interest. One of the benefits of using natural tracers is their utility at a variety of scales. Presented in this dissertation are three studies using naturally existing tracers at three different sites at three different aquifer dimensions. In this dissertation, we used: enthalpy as a tracer to study the 27,900-km<sup>2</sup> Eastern Snake River Plain (ESRP); radon to characterize a 0.34-km<sup>2</sup> fractured-rock-hosted vadose zone at Fort Devens, Massachusetts; and rare earth elements (REEs) in groundwater as a tracer to track groundwater at a 65-km<sup>2</sup> natural carbon capture and storage (CCS) analogue site near Soda Springs, Idaho. The tracer examples presented in this dissertation are not an exhaustive list of tracers and their application to hydrogeologic systems. However, the three tracers enthalpy, <sup>222</sup>Rn, and REE are representative of a wide range of tracer types and their application to problems with societal impact. These impacts include:

- Using enthalpy to understand the water flow and aquifer dimensions for the ESRP, a sole-source aquifer, which is important to the 500,000 people who live in the region
- Using <sup>222</sup>Rn gas to understand potential pathways for water entering a contaminated landfill at Fort Devens, Massachusetts, where there is great concern that contaminants may migrate into the drinking water resources of the surrounding community
- Using REE and major element chemistry to delineate groundwater mixing at leaking CO<sub>2</sub> systems that serve as an analogue for a failed industrial CCS reservoir.

The use of natural tracers in hydrologic systems has the advantage of evaluating a system using existing infrastructure (e.g., production and monitoring wells, soil gas, lakes, streams). As an example, the ESRP deep wells that penetrate the upper productive portion of the aquifer can cost in excess of \$8M; therefore, drilling even one well is cost prohibitive. In addition to the cost of drilling expensive monitoring wells, some places like Fort Devens come with unacceptable liability. At the Fort Devens landfill, it is not possible to drill new wells due to the risk of penetrating the landfill or creating new leakage or recharge pathways. At Soda Springs, drilling new wells for monitoring is not only expensive, it can also be dangerous due to the pressurized CO<sub>2</sub> that can energetically erupt if

penetrated. Therefore, using naturally existing tracers and existing sampling opportunities represent a reasonable and responsible opportunity to evaluate a system.

Introduced trace tests often fail for a number of reasons, including but not limited to: tracers that react strongly with host rocks and don't break through at the observation points; tracers may degrade too quickly due to longer-than-predicted residence time; thermal breakdown of the tracer may result in concentrations that are too low to detect; or the background is so high it overwhelms the tracer signal (Davis et al. 1980). Natural tracers do not suffer from most of these limitations. After all, if the tracer did not occur in measurable concentrations, it would not have been chosen for the study in the first place. Although the interpretation of data from natural tracer studies requires a more nuanced approach compared to anthropogenic tracers, one common use of natural tracers is to provide supporting information to help in the design of more expensive and intrusive, introduced tracer studies. However, because the toolbox of natural tracers is very large, great care must be exercised when deciding what tracer(s) to use to ensure that the objectives of the study are consistent with what the tracer can provide.

The studies presented in this dissertation were carefully chosen to elucidate conditions in the system and at the scale needed for the stated objectives. We selected enthalpy as the tracer for the ESRP aquifer because we were looking for large-scale changes along the aquifer's 350-km flow path. Because the thermal flux entering the base of the aquifer is assumed constant at  $110 \text{ mw/m}^2$ , water characteristics should change at a predictable rate from recharge to discharge, 350 km downstream. Deviation from this predicted rate of change represents changing conditions in the aquifer, either due to changes in flow rate or changes in thermal input.

At Fort Devens, we chose  $^{222}\text{Rn}$  as the tracer because the study was being conducted in a vadose zone where saturated flow does not exist or is transient due to heavy precipitation events. Areas of high  $^{222}\text{Rn}$  flux may be correlated to areas that are able to preferentially transmit water through the vadose zone into the contaminated aquifer at the landfill.

Because of the presence of a shallow aquifer system at Soda Springs, we needed a tracer that was dissolved in groundwater. Also, because major element data is not particularly sensitive to subtle change in water chemistry, the 15 rare earth elements were chosen as the primary tracers. REEs are good tracers for these types of systems, as all 15 REEs possess very similar chemical characteristics. The small differences in chemical characteristics can be used to elucidate subtle changes in water chemistry due to the influence of upwelling  $\text{CO}_2$ .

### Reference

Davis, S. N., G. M. Thompson, H. W. Bentley, G. Stiles, 1980, "Ground-Water Tracers—A Short Review," *Groundwater*, Vol. 18, No. 1, January 1980, pp. 14–23, DOI: 10.1111/j.1745-6584.1980.tb03366.x.

**APPENDIX A: Reprint Permissions**

Chapter 2 The Application of Radon for Mapping Open Fracture Networks in a Thin Vadose Zone Underlain by Granite Rock, Fort Devens, Massachusetts, accepted by the Vadose Zone Journal and is reprinted with permission from the Soil Science Society of America.